

SYNTHESIS, CHARACTERIZATION AND ANALYTICAL APPLICATIONS OF TITANIA NANO HYBRIDS

*Thesis submitted
to the University of Calicut for the
award of*

DOCTOR OF PHILOSOPHY IN CHEMISTRY

JASEELA. P.K.



**DEPARTMENT OF CHEMISTRY
UNIVERSITY OF CALICUT
KERALA- 673635
JULY 2020**

CERTIFICATE

This is to certify that the thesis entitled “**Synthesis, Characterization and Analytical Applications of Titania Nano Hybrids**” submitted by **Jaseela. P.K.** to the University of Calicut for the award of the degree of Doctor of Philosophy in Chemistry, is a record of precise research work carried out at the Department of Chemistry, University of Calicut under my guidance and supervision. The contents of the thesis have been checked for plagiarism using the software ‘Urkund’ and similarity index falls under permissible limit. I further certify that the thesis or part has not previously formed the basis for the award of any degree, diploma or associateship of any other University or Institute.

As suggested by one of the adjudicator the size of certain figures have been increased in the revised thesis.

Calicut University

Prof. (Dr.) Abraham Joseph

DECLARATION

I, **Jaseela. P.K.**, hereby declare that the thesis entitled as **“Synthesis, Characterization and Analytical Applications of Titania Nano Hybrids ”** submitted to university of Calicut is a bonafide record of project done by me under the guidance and supervision of **Prof. Abraham Joseph**, Department of Chemistry, University of Calicut and it has not formed the basis for the award of any Degree/Diploma/Associateship/ Fellowship or other similar title of any other University or Institution.

University of Calicut

Jaseela. P.K

ACKNOWLEDGEMENT

I would like to express my sincere gratitude and affection to a number of important people who contributed immensely for making this Ph.D thesis a reality. First and foremost my deep gratitude goes to my supervisor Prof. Abraham Joseph, Department of Chemistry, University of Calicut for his decisive encouragement, inspiration and above all for his valuable immersive support during my research. Under his guidance I successfully overcame many difficulties and obstacles. His own zeal for perfection, passion, and conviction has always inspired me and I will be truly indebted to him throughout my life time. This dissertation would not have been complete without his guidance and persistent help.

I would like to express my sincere thanks to Dr.A.I. Yahya, Head of the Department of Chemistry, University of Calicut and also thankful to former HODs, Dr. P. Raveendran, Dr. K Muraleedharan, and Dr.V. M. Abdul Mujeeb for providing me basic facilities during my Ph.D. Programme. I express my sincere gratitude to all the faculty members of this department. I take this opportunity to thank the Librarian and office staffs, present and former of this department for their expeditious services.

It's my immense pleasure to thanks my research group colleagues, Dr.M.Prajila, Dr. P. Rugminiammal, Dr.K.K. Anupama, Dr.K.M.Shainy, Dr. Sabeel M Basheer, Anupama R Prasad, Shamsheera. K.O, Julia Garvasis, Sr.Asha Thomas, Jeeja Rani. A. T.,

P. Sowmya and Linda Williams, for their support and valuable suggestions.

I express my sincere thanks and gratitude to all other research scholars, ex research colleagues and MSc & M.Phil. students in our department for making pleasant working atmosphere, sharing valuable support and care. Thank you all, for standing by my side and supporting me when times get hard and making me laugh even I didn't want to smile.

I extend my gratitude to Dr. A. Sujith, Dr.P.S Suja, P. Sagitha, Vipin, and Dr. O.Manaf, NIT Calicut, Dr. Niveditha, and Dr. Sarada Karangadan ,SAIF Calicut university, Aneesa, MG university, Dr.Thara ,Department of Biotechnology ,Calicut university, and STIC Cochin (CUSAT), for helping with characterisation part.

I acknowledge authorities of MANF for the financial assistance to complete this work.

I wish to express my sincere thanks to faculties and friends of Sri Vyasa NSS College ,Wadakkanchery especially my teacher Smt.C.N. Sarala for her inspiration, support, care and influencing to take steps towards my dream.

The journey would have not been possible without the support of my family. Especially my ummachi: your love, care, warmth, and moral support have inspired me to achieve this position. The words fall short to express the affection and support shown by my husband, Mr. Baiju Pulikkal I salute you for the trust, love, care and sacrifice you

did to cherish my dream. None of my accomplishments would have been possible without his understanding and for that I am forever indebted to him. I would like to thank my father in law, mother in law and brother for their help to support all the decisions I have taken. Special thanks to my husband's cousins and relatives for treating me as family member and their unconditional support. I am greatly indebted to my "backbone" whose presence was a milestone : thank you my best friend, my stress reliever, my patience – listener, my correct-adviser, my mentor for making my dreams to reach its goal. Words are not enough to express my love and intimacy to my sweet little angel whose affection and smile helped me to conquer all the struggles and challenges that we had faced in the meantime. You have taught me another aspect of life than I could have ever imagined and continue to inspire me to be a better version of myself.

Finally I wish to express my deepest gratitude to everybody whose assistance was important to the successful realization of this thesis although my name appears on the cover of this dissertation.

Above all I thank the Almighty for giving me the strength and patience to overcome all the tests and trials in the past few years.

Jaseela.P.K.

To

My ummachi..

My soulmate..

My little angel.....

PREFACE

The environment pass through various threats/depreciations day by day due to various reasons including man made reasons. Metal degradation and water pollution are two major issues that have a direct impact on humanity and lead to huge problems. Due to rapid industrialization, the demand for metals and alloys is growing in construction, aerospace, containers, packaging, transport, etc. Corrosion is one of the extreme cause of depletion of our natural resources which get increased concern regarding environmental damage and other inconvenience to human being. The durability and efficiency of metals and alloys can be improved by applying anti-corrosion coatings has been an active area of materials science research for quite a long time. Environmental pollution, especially water resources has increased in the last few decades due to unscientific activities from agricultural, industrial, pharmaceutical and plastic industries. The unmanageable discharge of several hazardous contaminants and pollutants into aquatic streams troubles human health to a great extent. Adopting new waste management techniques is a necessity of the day in order to preserve the health of the globe. Research into the production of hybrid systems based on TiO_2 constitute a new group of compounds exhibiting strictly designed physicochemical properties have the potential applications in different fields. This study focussed on the management of different types of contaminants from water adopting different management strategies like adsorption, photocatalysis, superhydrophobic / non-

wettability control and the development of protective coatings on mild steel.

This thesis is organized into **six chapters** that provide comprehensive coverage of the major objectives and its results. **Chapter 1** accounts for the general introduction of Titania and its hybrids. It provides the requisite basic details on the history and structure of Titania. Different synthetic methods adopted for the preparation of Titania and hybrids are briefly discussed. It also includes a short overview of its applications for anticorrosion and remediation of wastewater. **Chapter 2** deals with experimental approaches, and this chapter gives a brief description of the various materials and methodologies used in this current research work. Various chemicals used in the study are shown here. A detailed outline of the experimental methodologies adopted for the study is also given. The most effective techniques for characterizing selected materials have been discussed. Application studies of the synthesized materials are given towards the end of the chapter. **Chapter 3** explains the development of titania, PVA-titania, thiourea loaded PVA-titania coatings on mild steel in hydrochloric acid and sodium chloride media. This is divided in to two parts, **Part A** deals with the discussion of characterization and application of titania, PVA titania and thiourea loaded titania PVA hybrid as anticorrosive protective coatings on mild steel in HCl media and **Part B** deals with the study of above mentioned coatings in NaCl media. The coatings on mild steel have been developed via sol-gel dip-coating method. To investigate structure and morphology of coating, Fourier Transform Infrared Spectroscopy (FTIR), Field Emission Scanning Electron

Microscopy (FESEM), Energy Dispersive X-ray Spectrometry (EDX) and Atomic Force Microscopy (AFM), Diffuse Reflectance Spectroscopy (DRS), X-ray Diffraction Spectroscopy (XRD) and Raman techniques were employed. Effects of different parameters on corrosion efficiency have investigated. In addition the modified coatings on metal offers attractive protection efficiency on extending the exposure period in HCl and NaCl media for several days, which is much higher than conventional sol-gel coating which losses efficiency day by day. The protective coating on the metal surface that provides a significant physical barrier against the attack of corrosive ions from acid solution and NaCl solution. This easy, fast and eco-friendly process has the potential to replace environmentally hazardous chromate conversion coatings. **Chapter 4** describes the selective adsorption nature of Titania (TiO₂) and Titania (TiO₂)–polyvinyl alcohol (PVA) nanocomposite to Methylene Blue dye from aqueous solution. The hybrid nanocomposite was characterized by X-ray diffraction (XRD), Fourier Transform Infrared Spectroscopy (FTIR), UV-Vis spectroscopy, Photoluminescence Spectroscopy (PL), Fourier Transform Raman Spectroscopy (FT Raman), Field Emission Scanning Electron Microscopy (FESEM) with (EDAX), and High-Resolution Transmission Electron Microscopy (HRTEM). The Surface charge of the nanocomposite was probed with Zeta potential (ζ) measurement by Dynamic Light Scattering (DLS) technique. This chapter addresses the characterization and application of inorganic–organic nanocomposite hybrids including TiO₂ and PVA. Using a simple and practical approach, we could achieve a very high surface area and a high pore volume hybrid. The composite has substantially improved adsorption

capacity for cationic methylene blue (MB) dye from methylene blue and methyl orange (MO) mixtures and is used as a selective adsorbent for cationic dyes. The selectivity of catalyst was confirmed with another cationic dye acridine orange (AO). Hybrid adsorption of MB was performed under various experimental conditions. Adsorption kinetics studies and isotherms were investigated. **Chapter 5** divided into **Part A** and **Part B**. Part A deal with the highly effective photocatalytic removal of endocrine disrupting Bisphenol- A (BPA) under visible light using mesoporous Titania – silica ($\text{TiO}_2 - \text{SiO}_2$) nanocomposite and Part B provides the details of HMDS/GPTMS modified Titania silica nanocomposite coated cotton fabric for Oil - water separation. Part A discusses on the characterization and application of titania and titania silica nanocomposites as photocatalysts for the degradation of BPA under visible light. The hybrids were characterized through technics such as XRD, FTIR, DRS, FESEM, HRTEM, BET and XPS. The radical intermediates formed during the degradation of BPA, the rate of mineralization and the degradation products in the solution have been identified. Part B focuses on the modification of titania silica nanocomposite with GPTMS and HMDS for the fabrication of super-hydrophobic coating on cotton fabric for the separation of oil from water. The fabric was characterized by using ATR and FESEM techniques. The durability of the coating was determined by the exposure of the specimen to harsh environments. Besides, the mechanical durability, abrasion test, tear test washing durability was also investigated. Environmentally friendly fluorine and chlorine-free fabrics can be successfully obtained by this

process. This coated fabric free of fluorine and chlorine can be effectively utilized in various fields.

Chapter 6 provides the conclusion of the work. It explains the relevance of the research work carried out and outlines of future scope and objectives to enhance the potential of Titania Hybrids for a number of applications.

TABLE OF CONTENTS

PREFACE

CHAPTER 1 1-36

INTRODUCTION

1.1 Metallic corrosion	1
1.2 Water pollution	4
1.3 Titania or Titanium dioxide	6
1.4 Application of Titania and hybrids – Present work	13
1.4.1 Titania hybrids - Sol -gel coatings	14
1.4.2 Titania hybrid - Adsorbents	15
1.4.3 Titania hybrids - Photocatalyst	17
1.4.4 Superhydrophobic Titania hybrid/ Wettability control	22
1.5 Objectives of the Present Study	24
References	26

CHAPTER II 37-60

MATERIALS AND METHODOLOGIES

2.1 Introduction	37
2.2 Materials	37
2.3 Experimental	38
2.4 Characterization Techniques	43
2.5 Applications of titania hybrid materials	52
2.5.1 Anticorrosion applications and electrochemical measurements	52
2.5.2 Water pollution remediation applications	54
References	60

CHAPTER III **61-110**
SYNTHESIS, CHARACTERIZATION AND CORROSION
STUDIES OF TITANIA NANO HYBRIDS

Part A

3.1 Introduction	61
3.2 Results and discussion	66
3.3 Corrosion inhibition of MS in HCl	74
3.3.1 Weight loss study	74
3.3.2 Electrochemical Impedance Spectroscopic (EIS) measurements	76
3.3.3 Potentiodynamic polarization study (PDS)	84
3.4 Conclusions	88

Part B

3.5 Corrosion inhibition of MS in NaCl	91
3.5.1 Electrochemical Impedance Spectroscopic (EIS) measurements	91
3.5.2 Potentiodynamic polarization study (PDS)	97
3.6 Corrosion protection mechanism	102
3.7 Conclusions	103
References	104

CHAPTER IV **111-136**
SYNTHESIS, CHARACTERIZATION AND DYE
REMOVAL PROPERTIES OF TITANIA-PVA NANO
HYBRID

4.1 Introduction	111
4.2 Results and discussion	114
4.2.1 Characterization of titania hybrid	114
4.2.2 Adsorption study	120
4.2.3 Adsorption isotherm and kinetic studies	124
4.2.4 Selective adsorption	127
4.3 Conclusions	130
References	132

CHAPTER V	137-178
SYNTHESIS, CHARACTERIZATION AND APPLICATIONS OF TITANIA NANO HYBRIDS IN PHOTOCATALYSIS AND WATER PURIFICATION	
5.1 Introduction	137
Part A	
5.2 Photocatalytic degradation of BPA with TiO ₂ - SiO ₂	144
5.2.1 Results and discussion	144
5.3 Photocatalytic activity analysis by HPLC	152
5.3.1 Measurement of hydroxyl radical content through fluorescence spectra	154
5.3.2 Photodegradation intermediates and pathways	156
5.3.3 TOC measurement	157
5.3.4 Kinetic study	158
5.4 Conclusions	159
Part B	
5.5 Superhydrophobic cotton fabric coated with GPTMS -HMDS modified Titania Silica nanocomposite for oil water separation	162
5.5.1 Results and discussion	163
5.5.2 Durability of the super-hydrophobic fabric	166
5.5.3 Separation of oil–water mixtures	168
5.6 Conclusions	169
References	170
CHAPTER VI	179-182
SUMMARY AND SCOPE OF FUTURE WORK	
6.1 Introduction	179
6.2 Summary	179
6.3 Scope of future work	181

Chapter 1

INTRODUCTION



Contents

1.1	Metallic corrosion
1.2	Water pollution
1.3	Titania or titanium dioxide
1.4	Application of Titania and hybrids – Present work
1.4.1.	Titania hybrids - Sol -gel coatings
1.4.2.	Titania hybrid - Adsorbents
1.4.3.	Titania hybrids - Photocatalyst
1.4.4.	Superhydrophobic Titania hybrid/Wettability control
1.5	Objectives of the Present Study

Titania has drawn considerable interest owing to its unique properties. A more general introduction to Titania and its hybrids provided in this chapter. The necessary basic information concerning the history and structure of Titania included in this chapter. Specific synthetic methodologies adopted for the preparation of Titania and hybrids are briefly discussed. This chapter also presents a brief outline regarding the applications of Titania based systems for anticorrosion and waste water remediation applications. Chapter 1 ends with the objectives and details of the present study.

Over recent decades, several issues affecting mankind directly or indirectly regarding environmental pollution, energy crisis, depletion of metals etc. are becoming an important research topic. Among these issues corrosion of metals and alloys are well documented. It is observed that, from everyday domestic applications to the construction of complex engineering structures for industrial purposes, metals are significantly deployed. Corrosion is the most important metal consumer known to man[1]. It is one of the oldest problems that have ever challenged the industrial world and remains as a challenging problem even in the 21st century. Another most alarming environmental problem affecting all living creatures is water pollution. It is the most serious ecological threat and thereby degrading the quality of public health and aquatic life[2]. New materials or strategies should be incorporated to reduce environmental contaminations and associated issues.

1.1. Metallic Corrosion

The costs of corrosion in commercial, residential and transportation has been estimated at a whopping trillion of dollars per year. The industrial requirement of metals and their alloys is growing steadily, making it one of the promising candidates for different applications. However, the use of this alloys and metals despite of its inherent advantages, is still not utilized fully for many applications due to its significant corrosion behaviour. Corrosion is defined as the degradation of material by reaction with its environment[3]. Corrosion of a given material can take place by two

major external components, namely the environment or the electrochemical system (eg. atmosphere, acid or corrosive media), and operating conditions (eg. stress or pressure, erosion and temperature etc.). The most significant is the electrochemical reaction, which involves the transfer of electrons between the participants. Electrochemical reactions can be divided into anodic and cathodic reactions. While anodic reaction involves anodic dissolution, all the electrons released at the anode are consumed by the cathode.

The three main concern of metal corrosion to the societal point of view are: the economic aspects, depletion of natural resources, and loss of life due to environmental damages[3-5].Metallic corrosion is a serious problem which affected a large portion of the government sector from infrastructure to manufacturing[6]. It causes safety and health issues other than the depletion of natural resources. In order to overcome these difficulties and making metals and alloys useful in various fields the metals should be protected from corrosion.

Although corrosion is a natural process, it can be controlled by using effective methods and strategies[7]. There are many ways to control corrosion, namely cathodic protection, anodic protection, use of inhibitors and protective coatings etc.(Figure 1).It is highly advantageous to improve the lifespan and performance of metals and alloys by applying different anti-corrosion coatings[8]. Anticorrosion coatings require the development of new surface materials such as nanomaterials that can impart various functional properties to the metal / component surfaces.The function of a protective coating is to provide a satisfactory barrier between the metal and its environment[1].

Corrosion behaviour of sol-gel coatings has been extensively studied on different metallic substrates[9]. The use of sol-gel coatings has been projected as a better substitute for the environmentally unacceptable chromium-based coatings[9-13].The nano sol gel coatings could be quite helpful to reduce or slow down the corrosion process. Due to their scratch-resistance, sound proofing, abrasive, or preventive properties, the coatings obtained by the sol-gel method could be used as protective coatings[14]. Compared to general coatings and traditional composite sol-gel coatings, the hybrid coatings have much improved properties due to the nanosize dispersion effect. Thus, the production of eco-friendly sol-gel coatings to prevent corrosion on metallic substrates was one of the emerging areas of research, competing with conventional chromate and phosphate coatings.[15]

Various methods available for monitoring the corrosion processes are pictorially represented in Figure 1



Figure 1. Pictorial representation of common methods of corrosion protection.

1.2. Water pollution

Another terrible environmental problem affecting mankind is water pollution which causes millions of deaths per year. Fresh water resources are continuously contaminated by pollutants due to various reasons including rapid industrialization[16-18]. Water is able to dissolve more substances than any other liquid on earth; hence it is easily polluted. According to the U.S. Environmental Protection Agency's most recent surveys of national water quality, nearly half of Indian rivers and streams and more than one-third of lakes are polluted and unfit for swimming, fishing and drinking. Pollution of fresh water may be due to soil erosion, inadequate sanitation, by algal blooms, detergents, dyes, fertilizers, pesticides, other chemicals, oils, heavy metals, etc as illustrated in Figure 2. These contaminants are either toxic or become toxic when being gradually decomposed in the eco system. These are degrading water quality and rendering it toxic to humans or the environment. The effect of these organic effluents in the waste water can be sensed by monitoring the change in the vital parameters of the discharged water such as COD, BOD, toxicity, unpleasant odour and colour. The presence of even a trace amount of coloured organic compounds in the aquatic systems can result in colouration of water. These undergo bioaccumulation in living organisms due to their slow degradation nature. As a consequence of this, water obstructs the sunlight access to aquatic organisms and plants, and diminishes the photosynthesis and affects the ecosystem[19, 20]. It is necessary to remove these contaminants to protect the water resources and to produce water of desired quality. Different physical, chemical and biological methods are developed

over the years. These are currently being employed to remove these contaminants or degrade them into non-toxic ones. Unfortunately, many types of organic pollutants in water are not removable by those conventional technologies. There is a need to modernize, update or modify the already existing methods to be more stable, economical and viable. These methods include adsorption, coagulation, oxidative-reductive degradation and membrane separation and so on. But each of these methodologies has its own advantages and limitations. In the current research we have chosen three different functionally modified materials as adsorbent, photocatalyst, and superhydrophobic material for the removal of contaminants. Among the group, organics, dyes and oil spills have invited serious concern and is chosen as our target contaminants. Variety of different fascinating materials has been used for the decontamination of water/ wastewater and in the present research work we have chosen titania as our base material whose functional properties have been modified and tuned to suite for different applications.



Figure 2. Common sources of water pollution

1.3. Titania or Titanium dioxide (TiO₂)

Titanium dioxide (TiO₂) or titania is one of the very interesting material used for different applications because of its unique optical and physical properties, availability, low cost and non-toxicity. It is found to be the most studied material especially in environmental and energy crisis management. TiO₂ is extensively studied as a photocatalysts, smart coatings, solar cells, etc. owing to its promising electronic and opto-electrochemical properties[2, 21-28].

Titanium is the world's fourth most abundant metal and ninth most abundant element which is not found in its free state. It is placed in the fourth group of the periodic table, and its chemistry shows similarities to that of silicon and zirconium. The outer electronic arrangement is 3d²4s², and the principal valence state is IV, though III, II states are also known. The metal has been detected in meteorites and stars. The element burns in air to give the oxide, TiO₂. It was discovered in 1791 in England by Reverend William Gregor, who recognised the presence of a new element in ilmenite[29]. A German chemist, Heinrich Klaporth, who named it after Titans, the mythological first sons of the goddess Ge (earth in Greek mythology), rediscovered it several years later in rutile ore. Titania occurs mainly in minerals like rutile, ilmenite, leucoxene, anatase, brookite, perovskite and spines and also found in titanates and many other iron ores.

1.3.1. Structure

TiO₂ is: i) insoluble in water, (ii) chemically and biologically inert, (iii) photo-stable, (iv) non-toxic, (v) cheap and (vi) readily available[30-32]. It crystallizes generally in to anatase, rutile and brookite morphologies. The band gap corresponding to these forms are 3.2 eV[33, 34] for anatase, 3.0 eV for rutile[35], and ~3.2 eV for brookite[36]. TiO₂ is an n-type semiconductor[37]. The valence band of TiO₂ consists of 2p orbitals of oxygen, whereas the conduction band is made up from 3d orbitals of titanium. The vacancies are formed upon the release of two electrons and molecular oxygen leaving a positive (+2) oxide ion vacancy[38].

Majority of research work has been carried out with either rutile or anatase phase. The primary source of titanium dioxide and the most stable form is rutile ore. It was discovered by Werner of Spain in 1803. Its name is derived from the Latin word, rutilus, means red, because of the deep colour observed in some specimens on exposure to light. In 1801 anatase was named by R. J. Haüy from the Greek word ‘anatisis’ meaning extension, and Brookite was discovered in 1825 by A. Levy and was named after an English mineralogist, H. J. Brooke. Anatase (a = b = 3.782, c = 9.502 Å), and rutile (a = b = 4.854, c = 2.953 Å) are both tetragonal in structure while the brookite structure is orthorhombic. Titania exists in the crystalline as well as amorphous forms. Titanium (Ti⁴⁺) atoms in all three forms are coordinated to six oxygen (O²⁻) atoms, forming octahedra TiO₆[39]. All the three forms differ only in the arrangement of these octahedra. In case of all the crystalline forms, each Ti⁴⁺ ions are surrounded by an irregular octahedron of oxide ions. Each octahedron is in contact with

10 and 8 neighbouring octahedrons in the rutile and anatase structure, respectively. Whereas in brookite structure three edges per octahedron are shared [40]. Such variations in terms of lattice structures cause difference in mass densities and electronic band structure between the two forms of titanium dioxide.

1.3.2. Anatase to rutile

The experimental conditions affect the transformation from amorphous to anatase or rutile morphology. According to the widely accepted theory of phase transformation of TiO_2 , the cleavage of two Ti–O bonds in anatase structure allows the Ti–O octahedral rearrangement and leads to a smaller volume, result in a dense rutile phase[41]. The cleavage of these bonds can be affected by parameters such as particle shape/ size, purity, source effects, atmosphere, reaction conditions, addition of dopants, method of synthesis and thermal treatment. Lattice vacancies are generated by the removal of oxygen ions, which accelerates the transformation. The heat treatment of amorphous titania converts it to a crystalline anatase structure at temperature below 300°C , which on further heating converted to rutile form. However, no unique phase transformation temperature is reported[42]. On heating concomitant with coarsening, one of the following transformations are observed; anatase to brookite to rutile, brookite to anatase to rutile, anatase to rutile and or brookite to rutile.

1.3.3. Titania hybrids

In fact, there is no clear borderline between the hybrid and nanocomposite materials. The term nano composite is widely used when discrete structural units are used in the respective size regime.

When inorganic units are formed in situ by molecular precursors, such as applying sol – gel reactions, the term hybrid material is used more frequently. This field is very creative, since it provides the opportunity to invent complex systems from simpler building blocks. The optical transparency of the resulting hybrid materials and nanocomposites is relatively high. It makes ideal candidates for many optical applications for these materials[43, 44]. Various strategies have been adopted for improving the properties of TiO₂ and to achieve outstanding performance in various fields. TiO₂-based hybrid systems form a new category of compounds with specifically engineered physicochemical properties. This is resulting from the effects of combining the characteristic behaviour of the individual compounds from which they are made. Modifications of TiO₂ can be achieved by the introduction of molecular species like metal, metal oxide, metal sulphides, metal selenides, metal nitrides, organic molecules, inorganic salts, polymers, dyes, non-metals, clays etc. generates unlimited set of new multifunctional materials. The physical properties like structural, textural, acid/base, catalytic properties of pure TiO₂ can be altered by the presence of foreign particles [45]. The production and potential applications of TiO₂ and its modified forms are effective when the final materials should have a strictly defined dispersive character, crystalline structure, morphology and porous structure.

1.3.4. Synthesis of titania and hybrids

In industry, TiO₂ is produced by older sulphate process or newer chloride process. On a laboratory scale, TiO₂ has been prepared mainly by use of titanium isopropoxide or alkoxides as precursors. A variety of chemical and physical methods of synthesis like solution

deposition, sol-gel processing, hydrothermal/solvothermal, gas-phase deposition, template method can be employed to synthesise effectively titania-hybrids at ambient conditions. The textural properties of hybrid materials, such as pore size distribution, surface area, etc., are strongly dependent on the conditions of synthesis, including precursor nature and structure, solvent, complexing / templating agent, hydrolysis and calcination state. In the present study we have selected sol gel method and hydrothermal method[46].

1.3.4.1. Sol-Gel method

Sol-Gel method is used for the synthesis of thin films, powders, and membranes. The major steps involving in sol-gel method are (i) hydrolysis of the metal precursor by using a suitable catalyst (generally an acid or a base), (ii) condensation of the hydrolyzed precursors, (iii) aging of the sol, (iv) processing or deposition of the coating on metal substrate generally by dip coating or spin coating, (v) cross linking of film by heat treatment which is known to a) drying and b) densification[47]. Successive steps like aging, drying and calcination are important for the formation of powders, glasses, ceramics etc. In Non-alkoxide route, the precursor used are TiOCl_2 , TiCl_4 , SiCl_4 , TiOSO_4 , [48-50] etc. and in alkoxide method, the precursors used are $\text{Ti}(\text{OC}_3\text{H}_7)_4$, $\text{Ti}(\text{OC}_4\text{H}_9)_4$ etc [51-53]. For the coordinative saturated metals such as the metal alkoxides, hydrolysis and condensation occur by nucleophilic substitution (SN) mechanisms, in which coordination and proton transfer are involved and followed by removal of either alcohol or water. The titanium precursor, can accept lone pair of electrons from water molecule through oxygen. It was reported that –OR group is a better leaving group, so which can be easily replaced by

an -OH group. The leaving alkoxide group can easily be protonated within the transition state from a water molecule and removed as alcohol. Condensation reaction can form large chains of molecules through polymerization. Condensation can proceed through either alcoxylation or oxolation reaction. In both these processes an oxo bridge (M-O-M) is formed in between the metals. Alcoxolation is the process of removal of an alcohol group and the site is occupied by water. Complete polymerization and solvent loss lead to the transformation of the liquid sol into a phase of solid gel. Thin films can be created by spin-coating or dip-coating on a piece of substrate. A wet gel will form when the sol is cast into a mold, and the wet gel is converted into a dense ceramic upon further drying and heat treatment. Organic matter, moisture and volatile impurities already present in the sample are driven out on calcination and get the pure oxide form of the metal. Because the precursors react quickly with water and appear to precipitate, several methods have been employed to regulate the reaction rate to obtain desired nanostructures. However, the main difficulty in binary metal systems is the control of the precursor hydrolysis rate. One way to alter the hydrolysis rate is by altering the precursors with an effective complexing agent. Interesting advantages in sol-gel method include 1) the method requires simple processing steps and simple equipment 2), cost effective method 3), sol-gel preparation needed only room temperature 4), chemical homogeneity of the sol-gel product is possible with high purity 5), able to get small sized materials having high surface area and porosity 6), sol-gel method can be used to make ceramic and glassy materials in the form of powders, fibres, or thin films 7), easily get variety of products such as fibres, films, powders with suitable properties 8), easy to do coatings for

films and 9), metal (inorganic) – organic nano composites can easily generate through sol-gel method[54-57]. Based on the above synthetic approach, oxides with different physical and chemical properties may be obtained. According to a report by Italian researchers, $\text{SiO}_2/\text{TiO}_2$ system can be obtained through the sol-gel method. Swinska-stefanska et al. studied the effect of doping of Fe and Co in nano- and microstructured TiO_2 , synthesised by the sol-gel method [58]. Fan et al. synthesised a mesoporous $\text{TiO}_2/\text{ZrO}_2$ nanocomposite from titanium tetrabutoxide, $\text{ZrOCl}_2 \cdot 8\text{H}_2\text{O}$, utilising the sol-gel method[59]. Shao et al. prepared pure TiO_2 and $\text{TiO}_2/\text{ZrO}_2$ system via simple sol gel method[60]. Similarly, in another study Kraveva and Ehrlich produced the $\text{TiO}_2/\text{Al}_2\text{O}_3$ system via simple sol-gel method[61].

1.3.4.2. Hydrothermal method

The hydrothermal process is one of the most widely used technique to produce several new hybrid materials with different morphologies and improved crystallinity. This route is often employed for the synthesis of powders, fibers, single crystals, monolithic ceramic bodies and metal, polymer and ceramic coatings [62]. The method is widely used in the ceramic industry for the production of small particles. It is a non-conventional method defined as crystal synthesis or crystal growth under high temperature and high pressure. Usually, this method is carried in steel pressure vessels called autoclaves under controlled temperature and/or pressure with reactions occurring in aqueous solution. The temperature can be increased above the boiling water level, which exceeds the saturation pressure of the vapor. The temperature and the amount of solution added to the autoclave mainly determine the internal pressure generated. During the synthesis, water

can work as a catalyst as well as a component of the continuous phase.

1.4. Application of titania and hybrids – present work

Titanium dioxide is widely accepted as an ideal candidate in the field of energy and other environmental crisis. Among the different applications of TiO_2 hybrids, we have aimed on anticorrosion, adsorption, photocatalysis and wettability control over various fields as represented in Figure 3.

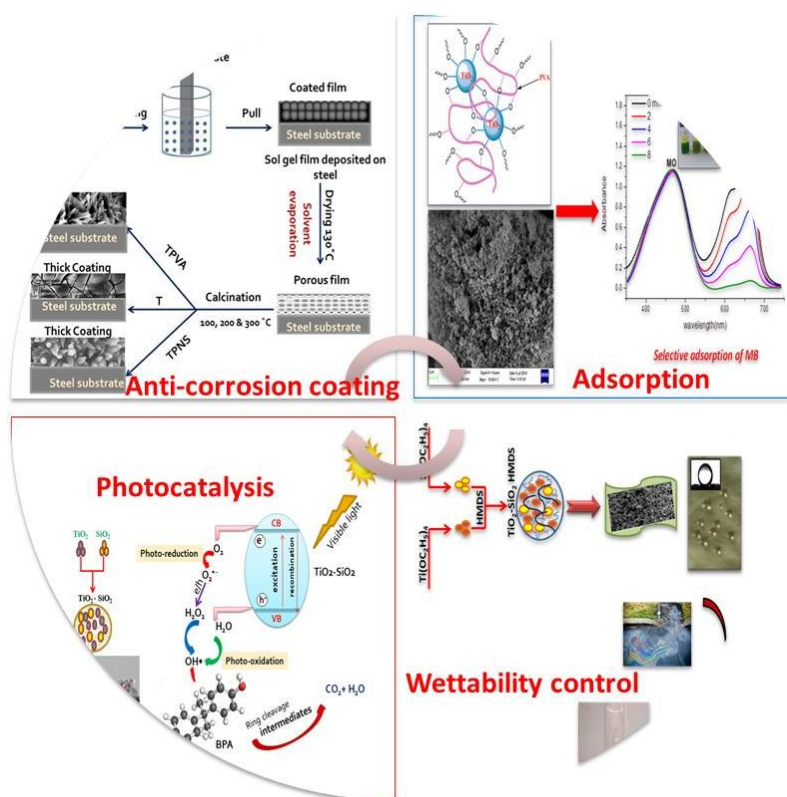


Figure 3. Pictorial representation of the applications of TiO_2 hybrids used in the present study.

1.4.1. Titania hybrids sol -gel coatings

Sol-gel inorganic coatings have been proposed as an alternative method for the protection of metallic materials. In the literature, some oxide coatings with very low electronic conductance such as TiO_2 , SiO_2 , Al_2O_3 , ZrO_2 , or mixed oxides composite coatings on metals to improve their surface properties have been reported as corrosion protection agents[63-65]. The major drawbacks of inorganic sol-gel coatings from the standpoint of corrosion resistant layers are 1).thick coatings are difficult to achieve without cracking, 2).brittle inorganic films have high crack-forming potential, 3). pure inorganic films have apertures[66, 67].Such drawbacks cause poor physical barriers to inorganic sol – gel films that cannot provide adequate protection for corrosion. The introduction of organic groups or polymers into inorganic sol-gel coatings eliminate the drawbacks of traditional inorganic coatings.The strong chemical interaction between organic and inorganic constituents improve anticorrosion properties of inorganic organic hybrid materials and this turned out to be an interesting areas of coating science in the last decade[68-73]. Guin et al. developed titania containing organic-inorganic hybrid sol-gel film using titanium isopropoxide as precursor and methyl hydrogen silicone as coupling agent[74]. Nowadays hybrid metal oxide sol-gel coatings are widely accepted materials to improve corrosion resistance on various metals like Al, Mg, Fe and other alloys. This is because of the fact that they have good adhesion to metallic substrates and good barrier effect to corrosion inducing substances. The application of sol-gel coatings, in fact has been projected as a better substitute for the

environmentally unacceptable chromate based coatings. The titania hybrid sol-gel coatings over metallic substrates act as adhesion promoters and are used to protect the metals against corrosion. The sol-gel derived titania organic-inorganic hybrid coatings have been demonstrated as promising conversion treatment for long term protection against atmospheric corrosion, but their corrosion protection performance is limited due to the presence of pores and cracks in the film. It was reported that a combination of different inhibiting species could provide a synergistic inhibition effect, and consequently confer a superior corrosion inhibition of alloys.

1.4.2. Titania hybrid- adsorbents (selective dye removal)

A plethora of research has been done for the remediation of waste water. Water pollutants include microorganism, pesticides, pathogens, and other organic materials. Dyes considered as a type of organic pollutants and represent one of the problematic groups. They are emitted into water from various industries exhibit toxic effects on microbials as well as mammals. Most of the dyes used in textile industries are photostable and non-biodegradable. A number of methods such as ozonisation, coagulation, precipitation, ion exchange, have been used for the removal of dyes from water. Each of these methods has inherent limitations[75]. These have been limited since they require high capital and operational costs. However, adsorption is considered as an effective and economical method. Many traditional adsorbents, such as active carbon, zeolites, and polymeric materials, have been used for removing pollutants. Activated carbon is an

effective material for the removal of pollutants from wastewater but in industrial processes, it was restricted due to its high operational and investment costs[76]. Due to low operating costs, the search for sorbents capable of selective removal of dyes is a challenge for scientists all over the world. Recently, mesoporous and microporous oxides as well as their mixtures have been developed to overcome these challenges. Its microstructure and superior morphological properties as well as mechanical strength and non-toxicity make them ideal adsorbents[77]. TiO_2 is reported to possess a high adsorption capacity. But due to its poor mechanical stability might limit their practical application in some fields. The literature reports that modification of TiO_2 enhances the surface area by controlling the growth of crystallites and gives higher porosity leading to high adsorption efficiency[78-80].

Apart from this the introduction of selective adsorbent is an important goal in the frontiers of research. The adsorbent can selectively adsorb one of the contaminants without any concentration change in the other from a mixture. Factors that influence the adsorption efficiency include adsorbate-adsorbent interaction, adsorbent surface area, adsorbent to adsorbate ratio, adsorbent particle size, temperature, pH etc[81, 82]. Numerous efforts have been taken for the preparation of environmentally benign hybrids to enhance and extend the application to selective dyes from contaminated water Lim et al. employed hydrothermal route to synthesize sodium titanate nanobelts and nanotubes using TiO_2 and TiS_2 as precursors, and showed that both nanostructures follow the Langmuir model regarding

the adsorption of methylene blue (MB) [83]. The dual phase anatase/titanate nanoparticles reported by Cheng et al. also follow the Langmuir model in the adsorption of MB with a capacity of 162.19 mg g⁻¹. It was also reported that the removal of MB by anatase-covered titanate nanotubes follow the Langmuir model.

1.4.3. Titania hybrid as photocatalyst

Photocatalysis is a promising, environmentally benign technology for the conversion of solar energy into chemical energy. It is the acceleration of a chemical transformation by the presence of a catalyst and light. Common photocatalyst are semiconductors such as ZnO, TiO₂, Fe₂O₃ etc. When a semiconductor metal oxide is illuminated by light with energy equal to or greater than band-gap energy, it can cause the formation of excitons and as a result the valence band having positive polarity and conduction band having negative polarity [84, 85]. Subsequent electron-hole recombination occurs when positive holes combine with promoted electrons to reverse the promotion process and releasing the input energy as heat, with no chemical effect. Nevertheless, if the electrons (and holes) migrate without recombination to the semiconductor surface, they may be involved in various oxidation and reduction reactions with adsorbed species such as water, oxygen and other organic or inorganic species other than the semiconductor itself. Photo-generated positive holes can react with electron donors to oxidize these molecules. Photo-generated electrons on the other hand tend to reduce electron donors exposed to the surface of the semiconductor [86]. Three factors mainly pertaining

to the band structure of semiconductors have greatest effect on photocatalytic reactions. Generally, the photocatalytic power of a semiconductor widely depends on, 1). light absorption characteristics; band gap energy determines which wavelength is more effective, 2). position of lowest point in the CB-determines the reducing power of catalyst and it should be negative with respect to the SHE potentials, 3). position of highest point in the VB determines the oxidizing power of catalyst and it should be positive with respect to the SHE potential, 4). rate of redox reaction by electron-hole pair on the surface of semiconductor, and 5). rate of e^-/h^+ recombination has greatest effect on photocatalytic reactions.

The wide band gap, high exciton binding energy, tuneable crystal structure (rutile, anatase, and brookite) and environmentally friendly nature of TiO_2 at nano scale have been employed to develop highly selective sorbents for the removal of contaminants from different fields by photocatalysis. Among the wide range of photocatalysts TiO_2 (band gap, $\text{BG} = 3.2 \text{ eV}$), WO_3 ($\text{BG} = 2.8 \text{ eV}$), SrTiO_3 ($\text{BG} = 3.2 \text{ eV}$), $\alpha\text{-Fe}_2\text{O}_3$ ($\text{BG} = 3.1 \text{ eV}$), ZnO ($\text{BG} = 3.2 \text{ eV}$), and ZnS ($\text{BG} = 3.6 \text{ eV}$) [87] in use, TiO_2 has been widely investigated due its high photochemical activity, and is considered as a bench mark material in the field of photocatalysis. The report entitled “Autooxidation by TiO_2 as a photocatalyst” might be the first study regarding photocatalysis with respect to TiO_2 developed by Kato and Masho in the year 1956. In 1972, the main breakthrough towards TiO_2 -based photocatalysis is reported by Honda and Fujishima by the

discovery of water photolysis on a TiO₂ electrode. This was considered as the land mark study which attracted much attention and contribution towards photocatalysis and hereafter the study using TiO₂ has become a hot subject in the area and the growth in publication was exponential. In general, photocatalytic reaction on TiO₂ consists of three steps 1).photo-excitation generates electrons (e⁻) and holes (h⁺), 2).the electrons and holes migrate to the TiO₂ surface and finally, 3). the electrons and holes react with adsorbed electron acceptors and donors, respectively, to complete the photocatalytic reaction. The redox potential of photo-generated holes is + 2.53V compared with the standard hydrogen electrode (SHE)[87]. After reaction with water, these holes can produce hydroxyl radicals (OH·), whose redox potential is only slightly decreased. Both are more positive than that for ozone. The redox potential of conduction band electron is -0.52 V, capable of reducing dioxygen to superoxide O₂^{•-}, or hydrogen peroxide H₂O₂. Depending upon the exact conditions, the holes, OH radicals, O₂^{•-}, H₂O₂ and O₂, all can play important role in the photocatalytic reaction mechanisms[88]. The mechanism of titania photocatalysis is shown in the Figure 4. Although the detailed mechanism of photocatalysis reactions of TiO₂ differs from one pollutant to another, it has been widely recognized that O₂^{•-} and, in particular, OH radicals act as active reagents for the degradation of organic compounds.

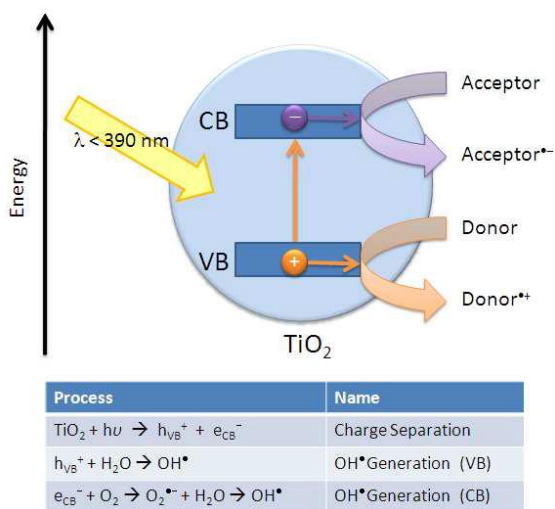


Figure 4. Mechanism of Titania photocatalysis

The extensive availability of visible light makes interest for the development of visible light active photo-catalysts. A small band gap is strongly desirable for an effective visible light photocatalyst. Much effort is currently focused on to meet these criteria and to harvest visible light (43% of the solar spectrum) for better solar energy conversion. A limitation of TiO_2 is its wide band gap of 3.2 eV which allows only UV light to be absorbed that covers limited area of solar spectrum ($< 387 \text{ nm}$, accounting for 5% of the solar spectrum)[89-91]. So, in order to achieve outstanding photocatalytic performance advances must be made to improve the light absorption, charge separation, and surface reactivity of TiO_2 . Different strategies have been adopted to achieve the modification of the above-mentioned factors either by altering morphology or by developing composite using foreign components into the TiO_2 structure using chemical modifications. Figure 5 a) gives titania photocatalysis under visible light and b) gives the influence of additional components. Important

photocatalytic modifications can be obtained by surface modification of TiO_2 . It include, 1). the incorporation of transition metal ions (such as Cu, Mo, Zr, Mn, Fe etc.) [92-94], 2).developing reduced form TiO_{2-x} , 3) Dye sensitisation, 4). non-metal doping (such as N, P,C, S) [95-97],5).use of hybrid semiconductors (such as $\text{TiO}_2 / \text{SiO}_2$, $\text{TiO}_2 / \text{Al}_2\text{O}_3$)[98-100], etc. Fabrication of mesoporous and microporous titania hybrids is one of the most promising ways to achieve excellent photo-catalytic performance of TiO_2 . In order to study the photocatalytic properties, $\text{TiO}_2 / \text{ZrO}_2$ composite was developed by Zhou et. al using sol-gel method. The obtained anatase crystalline structure confirmed from different physicochemical analysis. The specific surface areas of the resulting composites (for all variant methods of synthesis) lay in the range 187.0–219.2 m^2 / g [101]. Similarly Cheng et al. studied the photocatalytic properties of a hybrid material (UTZ) consisting of 3D nano spherical TiO_2 with a “hedgehog” shape and one-dimensional ZnO in the form of “nano spindles”. The composite was highly homogeneous with crystalline structure of anatase (TiO_2) and the hexagonal wurtzite structure (ZnO) [102]. The wrapping of TiO_2 hollow microspheres with rGO sheets via a facile solvothermal route using poly(L-lysine) (PLL) and ethylene glycol (EG) as coupling agents by Yan et al leads the formation of a 3-dimensional reduced graphene oxide/ TiO_2 (rGO/ TiO_2) hybrid composite [103]. Modifying the electron structure of titanium dioxide in the formation of hybrid oxide systems shown to have, 1).modify the surface properties such as surface area of TiO_2 , 2).enhance thermal stability of the anatase phase, 3). enhance the electron–hole separation, and 4). extend the light absorption into the visible range.

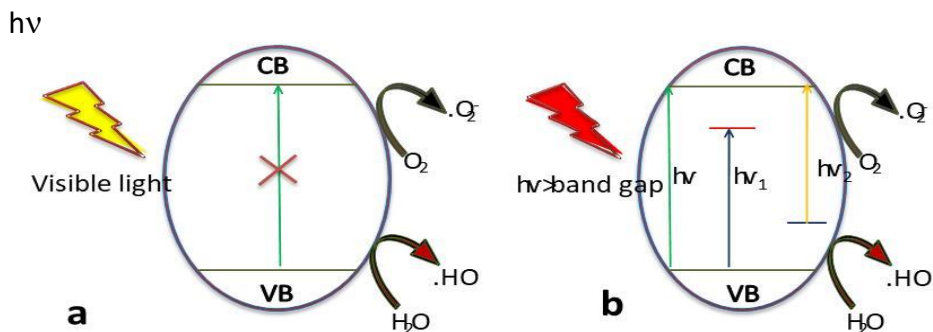


Figure 5 a) Titania photocatalysis under visible light and b) effect of additional components on titania.

1.4.4. Superhydrophobic titania hybrid wettability control – (oil – water separation)

A solid surface that strongly repels water drops is called a superhydrophobic surface. Based on the contact angle and the wetting behaviour, the solid surfaces are classified into four categories, 1).super hydrophilic if the contact angle is less than 10, 2).hydrophilic, if the contact angle is between 10 and 90, 3).hydrophobic, if the contact angle is between 90 and 150, and 4).super hydrophobic, if the contact angle is above 150 . Contact angle is usually used as a measure of hydrophobicity or wettability. It is the angle made by the water drop with the contacting solid surface at the contact line. Understanding the wetting behaviour of a water drop on a solid surface is the basis for designing a superhydrophobic surface. Numerous super-hydrophobic artificial surfaces have been created inspired by living creatures with unique wettability that possesses super-hydrophobic properties. Nearly all methods for achieving super hydrophobicity consist of two steps: first, making a hierarchical surface roughness, and then surface modification of some materials such as fatty acids, fluoroalkylsilanes,

etc. by means of a low surface energy solution. Superhydrophobic surfaces and coatings have a unique behaviour against water droplets. This unique behaviour results into a new set of applications including self-cleaning, antibacterial, oil-water separation, corrosion resistance etc[104]. To date, various strategies have been proposed for imparting superhydrophobic surfaces to substrates, such as template methods, colloidal self-assembly, sol-gel processing electro-spinning, layer-by-layer deposition, lithography and others[105-107].

There have been many reports of oil contaminants in sea waters and rivers due to the leakage and sudden accidents [108-113]. It has always been challenging and expensive to remove oil contaminants from water. Special wetting membranes with simultaneous super hydrophobicity and super oleophilicity making it a promising candidate for water purification[114, 115]. Different methods have been introduced by scientists and the use of super hydrophobic cotton as filter material has been reported recently. The development of bio-inspired special wettability in textile industries concerned with cloths/paper for oil (or organic solvents)-water separation. Many findings have also been reported for the preparation of super-hydrophobic surfaces and the oil-water separation efficiency by using super-hydrophobic cotton fabric. Indranee et.al reported fluorinated silyl functionalized zirconia synthesized using the Sol-Gel process to create an extremely durable superhydrophobic coating on cotton fabrics. The photocatalytic activity and chemical stability of TiO_2 material facilitates the easy removal of the pollutants by ultraviolet irradiation, and allows facile separation ability, enables it a robust and

highly effective material for oil-water separation .The electrochemical anodizing method for making porous TiO₂.

Fluorinated compounds are expensive, toxic, non-biodegradable and can easily be reacting with other materials and harmful to human health. Therefore, superhydrophobic and superoleophilic coated fabrics must be manufactured using fluorine and chlorine-free precursors[117]. The wetting ability control on the TiO₂ nanostructure, the rate of change of wetting properties, mechanical strength and UV stability should be carefully studied. The durability of the coating under severe environmental conditions is also an essential requirement for suitable application in oil–water separation. In the present work we have focussed on the treatment of water contaminated by oil which results from some industrial activities such as oil production, oil delivery, oil refining and petrochemical operation.

1.5. Objectives of the study

The aim of this research work is to investigate the efficacy of titania hybrids for environmental applications, especially for removing contaminants from water through various techniques and as protective coatings on mild steel.

- To fabricate facile, low cost and environmentally benign anti-corrosion Titania, PVA modified titania, and thiourea loaded PVA titania coatings on mild steel, by dip-coating technique. This is followed by characterization by Fourier Transform Infrared Spectroscopy (FTIR), Field Emission Scanning Electron Microscopy (FESEM), Energy Dispersive X-ray Spectrometry (EDX) and Atomic Force Microscopy (AFM),

Diffuse Reflectance Spectroscopy (DRS), X- ray Diffraction (XRD) and Raman techniques.

- Investigation of corrosion protection behaviour of these coatings on mild steel in HCl and NaCl by using weight loss study, EIS and polarization study, surface screening and kinetic studies.
- To synthesise titania and PVA modified titania and characterize by various techniques.
- Application of the prepared hybrids for adsorptive removal of Methyl Orange and Methylene Blue dye and utilization as a selective adsorbent for cationic dyes.
- Synthesis of titania and titania silica nanocomposites through modified sol-gel hydrothermal route. The structure, optical and photo-catalytic properties were characterized by XRD, UV–Vis spectra, FTIR, FESEM, Raman, TEM, XPS and BET and to conduct photocatalytic degradation of BPA under visible light, HPLC method LCMS method are also employed.
- Modification of titania and titania-silica by HMDS (hexamethyldinesilazane) and GPTMS and coating on fabric through dip coating method characterized by FTIR, FESEM, UV. To study oil-water separation experiment using as prepared fabric.

Life's most persistent and urgent question is, 'What are you doing for others?'

Martin Luther King Jr.

References

- [1] A. Popoola, O. Olorunniwo, O. Ige, Corrosion resistance through the application of anti-corrosion coatings, *Developments in corrosion protection*, 2 (2014) 241-270.
- [2] Y. Zhang, Z. Jiang, J. Huang, L.Y. Lim, W. Li, J. Deng, D. Gong, Y. Tang, Y. Lai, Z. Chen, Titanate and titania nanostructured materials for environmental and energy applications: a review, *RSC Advances*, 5 (2015) 79479-79510.
- [3] K.R. Trethewey, J. Chamberlain, *Corrosion for students of science and engineering*, 1988.
- [4] M. Aliofkhazraei, *Developments in corrosion protection*, BoD-Books on Demand 2014.
- [5] L. Umoru, O. Ige, Effects of Tin on Aluminum–Zinc–Magnesium Alloy as Sacrificial Anode in Seawater, *Journal of Minerals & Materials Characterization & Engineering*, 7 (2007) 105-113.
- [6] R.W. Revie, *Uhlig's corrosion handbook*, John Wiley & Sons 2011.
- [7] G.P. Bierwagen, L. He, J. Li, L. Ellingson, D. Tallman, Studies of a new accelerated evaluation method for coating corrosion resistance—thermal cycling testing, *Progress in organic coatings*, 39 (2000) 67-78.
- [8] O. Fayomi, M. Popoola, Comparative studies of microstructural, tribological and corrosion properties of plated Zn and Zn-alloy coatings, *International Journal of electrochemical science*, 7 (2012) 4860-4870.
- [9] R.B. Figueira, C.J. Silva, E.V. Pereira, Influence of experimental parameters using the dip-coating method on the barrier performance of hybrid sol-gel coatings in strong alkaline environments, *Coatings*, 5 (2015) 124-141.
- [10] S.K. Jayaseelan, W.J. Van Ooij, Rubber-to-metal bonding by silanes, *Journal of adhesion science and technology*, 15 (2001) 967-991.
- [11] M. Ferreira, R. Duarte, M. Montemor, A. Simões, Silanes and rare earth salts as chromate replacers for pre-treatments on galvanised steel, *Electrochimica acta*, 49 (2004) 2927-2935.

-
- [12] K. Mittal, *Silanes and Other Coupling Agents*, Vol. 4. VSP, Brill, Leiden, 2007.
- [13] K.L. Mittal, *Silanes and other coupling agents*, vol. 2, VSP, Utrecht, DOI (2000).
- [14] M. Jasiorski, B. Borak, A. Baszczuk, J. Krzak-Ros, A. Łukowiak, Active oxide materials obtained by the sol-gel method: synthesis, identification, and application, *Ceramics*, 101 (2008) 175-182.
- [15] M. Zheludkevich, J. Tedim, M. Ferreira, "Smart" coatings for active corrosion protection based on multi-functional micro and nanocontainers, *Electrochimica Acta*, 82 (2012) 314-323.
- [16] R.P. Schwarzenbach, B.I. Escher, K. Fenner, T.B. Hofstetter, C.A. Johnson, U. Von Gunten, B. Wehrli, The challenge of micropollutants in aquatic systems, *Science*, 313 (2006) 1072-1077.
- [17] C.B. Ong, L.Y. Ng, A.W. Mohammad, A review of ZnO nanoparticles as solar photocatalysts: synthesis, mechanisms and applications, *Renewable and Sustainable Energy Reviews*, 81 (2018) 536-551.
- [18] N. Ferroudj, J. Nzimoto, A. Davidson, D. Talbot, E. Briot, V. Dupuis, A. Bée, M.S. Medjram, S. Abramson, Maghemite nanoparticles and maghemite/silica nanocomposite microspheres as magnetic Fenton catalysts for the removal of water pollutants, *Applied Catalysis B: Environmental*, 136 (2013) 9-18.
- [19] J. Chang, M. Jin, F. Yao, T.H. Kim, V.T. Le, H. Yue, F. Gunes, B. Li, A. Ghosh, S. Xie, Asymmetric supercapacitors based on graphene/MnO₂ nanospheres and graphene/MoO₃ nanosheets with high energy density, *Advanced Functional Materials*, 23 (2013) 5074-5083.
- [20] P. Jain, T. Pradeep, Potential of silver nanoparticle - coated polyurethane foam as an antibacterial water filter, *Biotechnology and bioengineering*, 90 (2005) 59-63.
- [21] X. Lang, X. Chen, J. Zhao, Heterogeneous visible light photocatalysis for selective organic transformations, *Chemical Society Reviews*, 43 (2014) 473-486.
- [22] D. Fattakhova-Rohlfing, A. Zaleska, T. Bein, Three-dimensional titanium dioxide nanomaterials, *Chemical reviews*, 114 (2014) 9487-9558.
-

-
- [23] X. Wang, Z. Li, J. Shi, Y. Yu, One-dimensional titanium dioxide nanomaterials: nanowires, nanorods, and nanobelts, *Chemical reviews*, 114 (2014) 9346-9384.
- [24] A.K. Chandiran, A. Yella, M.T. Mayer, P. Gao, M.K. Nazeeruddin, M. Grätzel, Sub - Nanometer Conformal TiO₂ Blocking Layer for High Efficiency Solid - State Perovskite Absorber Solar Cells, *Advanced Materials*, 26 (2014) 4309-4312.
- [25] J. Kim, H. Lee, D.Y. Kim, Y. Seo, Resonant multiple light scattering for enhanced photon harvesting in dye-sensitized solar cells, *Advanced materials (Deerfield Beach, Fla.)*, 26 (2014) 5192.
- [26] Y. Tang, Y. Zhang, J. Deng, J. Wei, H.L. Tam, B.K. Chandran, Z. Dong, Z. Chen, X. Chen, Mechanical force - driven growth of elongated bending TiO₂ - based nanotubular materials for ultrafast rechargeable lithium ion batteries, *Advanced Materials*, 26 (2014) 6111-6118.
- [27] J. Fei, J. Li, Controlled preparation of porous TiO₂ - Ag nanostructures through supramolecular assembly for plasmon - enhanced photocatalysis, *Advanced Materials*, 27 (2015) 314-319.
- [28] S. Xiong, Y. Tang, H.S. Ng, X. Zhao, Z. Jiang, Z. Chen, K.W. Ng, S.C.J. Loo, Specific surface area of titanium dioxide (TiO₂) particles influences cyto-and photo-toxicity, *Toxicology*, 304 (2013) 132-140.
- [29] O. Carp, C.L. Huisman, A. Reller, Photoinduced reactivity of titanium dioxide, *Progress in solid state chemistry*, 32 (2004) 33-177.
- [30] K.R. Reddy, K. Nakata, T. Ochiai, T. Murakami, D.A. Tryk, A. Fujishima, Facile fabrication and photocatalytic application of Ag nanoparticles-TiO₂ nanofiber composites, *Journal of nanoscience and nanotechnology*, 11 (2011) 3692-3695.
- [31] A. Fujishima, K. Honda, Electrochemical photolysis of water at a semiconductor electrode, *nature*, 238 (1972) 37-38.
- [32] T. Xia, Y. Zhang, J. Murowchick, X. Chen, Vacuum-treated titanium dioxide nanocrystals: Optical properties, surface disorder, oxygen vacancy, and photocatalytic activities, *Catalysis Today*, 225 (2014) 2-9.

-
- [33] R. Asahi, Y. Taga, W. Mannstadt, A.J. Freeman, Electronic and optical properties of anatase TiO₂, *Physical Review B*, 61 (2000) 7459.
- [34] N. Hosaka, T. Sekiya, C. Satoko, S. Kurita, Optical properties of single-crystal anatase TiO₂, *Journal of the Physical Society of Japan*, 66 (1997) 877-880.
- [35] A. Amtout, R. Leonelli, Optical properties of rutile near its fundamental band gap, *Physical Review B*, 51 (1995) 6842.
- [36] M. Koelsch, S. Cassaignon, C.T.T. Minh, J.-F. Guillemoles, J.-P. Jolivet, Electrochemical comparative study of titania (anatase, brookite and rutile) nanoparticles synthesized in aqueous medium, *Thin Solid Films*, 451 (2004) 86-92.
- [37] A. Wisitsoraat, A. Tuantranont, E. Comini, G. Sberveglieri, W. Wlodarski, Characterization of n-type and p-type semiconductor gas sensors based on NiOx doped TiO₂ thin films, *Thin Solid Films*, 517 (2009) 2775-2780.
- [38] Y. Hu, H.-L. Tsai, C.-L. Huang, Effect of brookite phase on the anatase–rutile transition in titania nanoparticles, *Journal of the European Ceramic Society*, 23 (2003) 691-696.
- [39] D. Nicholls, *Complexes and first-row transition elements*, Macmillan International Higher Education 2017.
- [40] J.K. Burdett, T. Hughbanks, G.J. Miller, J.W. Richardson Jr, J.V. Smith, Structural-electronic relationships in inorganic solids: powder neutron diffraction studies of the rutile and anatase polymorphs of titanium dioxide at 15 and 295 K, *Journal of the American Chemical Society*, 109 (1987) 3639-3646.
- [41] S. Yoganarasimhan, C.R. Rao, Mechanism of crystal structure transformations. Part 3.—factors affecting the anatase-rutile transformation, *Transactions of the Faraday Society*, 58 (1962) 1579-1589.
- [42] J. Zhao, Z. Wang, L. Wang, H. Yang, M. Zhao, Effect of nuclei on the formation of rutile titania, *Journal of materials science letters*, 17 (1998) 1867-1869.
- [43] A.Y. Nazzal, L. Qu, X. Peng, M. Xiao, Photoactivated CdSe nanocrystals as nanosensors for gases, *Nano letters*, 3 (2003) 819-822.

-
- [44] V. Lee, J. Sundar, M. Heine, Bawendi, and KF Jensen, *Adv. Mater.*, 12 (2000) 1102.
- [45] B. Azambre, L. Zenboury, J. Weber, P. Burg, Surface characterization of acidic ceria–zirconia prepared by direct sulfation, *Applied surface science*, 256 (2010) 4570-4581.
- [46] J.M. Miller, L.J. Lakshmi, Spectroscopic characterization of sol–gel-derived mixed oxides, *The Journal of Physical Chemistry B*, 102 (1998) 6465-6470.
- [47] S. Bera, G. Udayabhanu, R. Narayan, T. Rout, Sol–gel process for anticorrosion coatings, *J. Res. Updates Polym. Sci*, 2 (2013) 209.
- [48] M. Iwasaki, M. Hara, S. Ito, Facile synthesis of nanocrystalline anatase particles from titanyl sulfate, *Journal of materials science letters*, 17 (1998) 1769-1772.
- [49] P. Periyat, P. Saeed, S. Ullattil, Anatase titania nanorods by pseudo-inorganic templating, *Materials Science in Semiconductor Processing*, 31 (2015) 658-665.
- [50] S. Sivakumar, C. Siby, P. Mukundan, P.K. Pillai, K. Warriar, Nanoporous titania–alumina mixed oxides—an alkoxide free sol–gel synthesis, *Materials Letters*, 58 (2004) 2664-2669.
- [51] J. Yu, L. Zhang, B. Cheng, Y. Su, Hydrothermal preparation and photocatalytic activity of hierarchically sponge-like macro-/mesoporous titania, *The Journal of Physical Chemistry C*, 111 (2007) 10582-10589.
- [52] N. Wetchakun, S. Chaiwichain, B. Inceesungvorn, K. Pingmuang, S. Phanichphant, A.I. Minett, J. Chen, BiVO₄/CeO₂ nanocomposites with high visible-light-induced photocatalytic activity, *ACS applied materials & interfaces*, 4 (2012) 3718-3723.
- [53] S.C. Pillai, P. Periyat, R. George, D.E. McCormack, M.K. Seery, H. Hayden, J. Colreavy, D. Corr, S.J. Hinder, Synthesis of high-temperature stable anatase TiO₂ photocatalyst, *The Journal of Physical Chemistry C*, 111 (2007) 1605-1611.
- [54] D. Tsukamoto, M. Ikeda, Y. Shiraishi, T. Hara, N. Ichikuni, S. Tanaka, T. Hirai, Selective photocatalytic oxidation of alcohols to aldehydes in water by TiO₂ partially coated with WO₃, *Chemistry–A European Journal*, 17 (2011) 9816-9824.
-

-
- [55] J.-P. Jolivet, S. Cassaignon, C. Chanéac, D. Chiche, E. Tronc, Design of oxide nanoparticles by aqueous chemistry, *Journal of Sol-Gel Science and Technology*, 46 (2008) 299-305.
- [56] K. Okada, N. Yamamoto, Y. Kameshima, A. Yasumori, K.J. MacKenzie, Effect of silica additive on the anatase - to - rutile phase transition, *Journal of the American Ceramic Society*, 84 (2001) 1591-1596.
- [57] D. Napper, A. Netschey, Studies of the steric stabilization of colloidal particles, *Journal of Colloid and Interface Science*, 37 (1971) 528-535.
- [58] K. Siwinska-Stefanska, D. Paukszta, A. Piasecki, T. Jesionowski, Synthesis and physicochemical characteristics of titanium dioxide doped with selected metals, *Physicochemical Problems of Mineral Processing*, 50 (2014).
- [59] M. Fan, S. Hu, B. Ren, J. Wang, X. Jing, Synthesis of nanocomposite TiO₂/ZrO₂ prepared by different templates and photocatalytic properties for the photodegradation of Rhodamine B, *Powder technology*, 235 (2013) 27-32.
- [60] G.N. Shao, Y. Kim, S. Imran, S.J. Jeon, P.B. Sarawade, A. Hilonga, J.-K. Kim, H.T. Kim, Enhancement of porosity of sodium silicate and titanium oxychloride based TiO₂-SiO₂ systems synthesized by sol-gel process and their photocatalytic activity, *Microporous and mesoporous materials*, 179 (2013) 111-121.
- [61] E. Krалева, M.L. Saladino, R. Matassa, E. Caponetti, S. Enzo, A. Spojakina, Phase formation in mixed TiO₂-ZrO₂ oxides prepared by sol-gel method, *Journal of Structural Chemistry*, 52 (2011) 330-339.
- [62] K. Byrappa, M. Yoshimura, *Handbook of hydrothermal technology*, William Andrew 2012.
- [63] H.M.A. El-Lateef, M.M. Khalaf, Corrosion resistance of ZrO₂-TiO₂ nanocomposite multilayer thin films coated on carbon steel in hydrochloric acid solution, *Materials Characterization*, 108 (2015) 29-41.
- [64] H. Cheraghi, M. Shahmiri, Z. Sadeghian, Corrosion behavior of TiO₂-NiO nanocomposite thin films on AISI 316L stainless steel prepared by sol-gel method, *Thin Solid Films*, 522 (2012) 289-296.

-
- [65] L. Ćurković, H.O. Ćurković, S. Salopek, M.M. Renjo, S. Šegota, Enhancement of corrosion protection of AISI 304 stainless steel by nanostructured sol–gel TiO₂ films, *Corrosion science*, 77 (2013) 176-184.
- [66] C.J. Brinker, G.W. Scherer, *Sol-gel science: the physics and chemistry of sol-gel processing*, Academic press 2013.
- [67] J. De Damborenea, N. Pellegrini, O. De Sanctis, A. Durán, Electrochemical behaviour of SiO₂ sol-gel coatings on stainless steel, *Journal of Sol-Gel Science and Technology*, 4 (1995) 239-244.
- [68] Y. Castro, B. Ferrari, R. Moreno, A. Duran, Silica sol-gel coatings on metals produced by EPD, *Journal of sol-gel science and technology*, 26 (2003) 735-739.
- [69] S. Messaddeq, S.H. Pulcinelli, C.V. Santilli, A.C. Guastaldi, Y. Messaddeq, Microstructure and corrosion resistance of inorganic–organic (ZrO₂–PMMA) hybrid coating on stainless steel, *Journal of Non-Crystalline Solids*, 247 (1999) 164-170.
- [70] H. Sayilkan, Ş. Şener, E. Şener, M. Sülü, The sol-gel synthesis and application of some anticorrosive coating materials, *Materials Science*, 39 (2003) 733-739.
- [71] T. Sugama, K. Gawlik, D. Jung, Polyaminopropylsiloxane coatings for geothermal air-cooled condensers, *Recent Res. Devel. Mat. Sci*, 4 (2003) 695.
- [72] S. Ono, H. Tsuge, Y. Nishi, S.-i. Hirano, Improvement of corrosion resistance of metals by an environmentally friendly silica coating method, *Journal of sol-gel science and technology*, 29 (2004) 147-153.
- [73] T. Sasaki, K. Kamitani, Preparation of thick and hard coating films via sol–gel process with a low temperature treatment, *Journal of sol-gel science and technology*, 46 (2008) 180-189.
- [74] A.K. Guin, S. Nayak, T.K. Rout, N. Bandyopadhyay, D.K. Sengupta, Corrosion resistance nano-hybrid sol–gel coating on steel sheet, *ISIJ international*, 51 (2011) 435-440.
- [75] H. Wang, H. Gao, M. Chen, X. Xu, X. Wang, C. Pan, J. Gao, Microwave-assisted synthesis of reduced graphene oxide/titania nanocomposites as an adsorbent for methylene blue adsorption, *Applied Surface Science*, 360 (2016) 840-848.

-
- [76] Y. Zhou, J. Lu, Y. Zhou, Y. Liu, Recent advances for dyes removal using novel adsorbents: a review, *Environmental pollution*, DOI (2019).
- [77] M. Tauqeer, M. Ahmad, M. Siraj, A. Mohammad, O. Ansari, M. Baig, *Nanocomposite Materials for Wastewater Decontamination*, *Modern Age Waste Water Problems*, Springer2020, pp. 23-46.
- [78] Z.-l. Shi, H. Lai, S.-h. Yao, S.-f. Wang, Preparation, characterization and photocatalytic activity of lanthanum doped mesoporous titanium dioxide, *Chinese Journal of Chemical Physics*, 25 (2012) 96.
- [79] R. Shwetharani, M. Jyothi, P. Laveena, R. Geetha Balakrishna, Photoactive titania float for disinfection of water; evaluation of cell damage by bioanalytical techniques, *Photochemistry and photobiology*, 90 (2014) 1099-1107.
- [80] L.P. D'Souza, R. Shwetharani, V. Amoli, C. Fernando, A.K. Sinha, R.G. Balakrishna, Photoexcitation of neodymium doped TiO₂ for improved performance in dye-sensitized solar cells, *Materials & Design*, 104 (2016) 346-354.
- [81] G. Crini, Non-conventional low-cost adsorbents for dye removal: a review, *Bioresource technology*, 97 (2006) 1061-1085.
- [82] S. Allen, B. Koumanova, Decolourisation of water/wastewater using adsorption, *Journal of the University of Chemical Technology and Metallurgy*, 40 (2005) 175-192.
- [83] Y.W.L. Lim, Y. Tang, Y.H. Cheng, Z. Chen, Morphology, crystal structure and adsorption performance of hydrothermally synthesized titania and titanate nanostructures, *Nanoscale*, 2 (2010) 2751-2757.
- [84] A. Fujishima, T.N. Rao, D.A. Tryk, Titanium dioxide photocatalysis, *Journal of photochemistry and photobiology C: Photochemistry reviews*, 1 (2000) 1-21.
- [85] C. Guillard, H. Lachheb, A. Houas, M. Ksibi, E. Elaloui, J.-M. Herrmann, Influence of chemical structure of dyes, of pH and of inorganic salts on their photocatalytic degradation by TiO₂ comparison of the efficiency of powder and supported TiO₂, *Journal of Photochemistry and Photobiology A: Chemistry*, 158 (2003) 27-36.
- [86] K. Siwińska-Stefańska, T. Jesionowski, *Advanced Hybrid Materials Based on Titanium Dioxide for Environmental and Electrochemical Applications*, *Titanium Dioxide*, DOI (2017) 143.
-

-
- [87] M. Grätzel, Photoelectrochemical cells, *nature*, 414 (2001) 338-344.
- [88] A. Dodd, A. McKinley, T. Tsuzuki, M. Saunders, Optical and photocatalytic properties of nanocrystalline TiO₂ synthesised by solid-state chemical reaction, *Journal of physics and chemistry of solids*, 68 (2007) 2341-2348.
- [89] Y. Wang, Q. Wang, X. Zhan, F. Wang, M. Safdar, J. He, Visible light driven type II heterostructures and their enhanced photocatalysis properties: a review, *Nanoscale*, 5 (2013) 8326-8339.
- [90] J. Ran, J. Zhang, J. Yu, M. Jaroniecc, S.Z. Qiao, Earth-abundant Q1 Q2 cocatalysts for semiconductor-based photocatalytic water splitting, DOI.
- [91] X. Pan, M.-Q. Yang, X. Fu, N. Zhang, Y.-J. Xu, Defective TiO₂ with oxygen vacancies: synthesis, properties and photocatalytic applications, *Nanoscale*, 5 (2013) 3601-3614.
- [92] A. Di Paola, E. Garcia-López, S. Ikeda, G. Marci, B. Ohtani, L. Palmisano, Photocatalytic degradation of organic compounds in aqueous systems by transition metal doped polycrystalline TiO₂, *Catalysis Today*, 75 (2002) 87-93.
- [93] R.C. Lam, M.K. Leung, D.Y. Leung, L.L. Vrijmoed, W. Yam, S. Ng, Visible-light-assisted photocatalytic degradation of gaseous formaldehyde by parallel-plate reactor coated with Cr ion-implanted TiO₂ thin film, *Solar energy materials and solar cells*, 91 (2007) 54-61.
- [94] N. Venkatachalam, M. Palanichamy, B. Arabindoo, V. Murugesan, Enhanced photocatalytic degradation of 4-chlorophenol by Zr⁴⁺ doped nano TiO₂, *Journal of Molecular Catalysis A: Chemical*, 266 (2007) 158-165.
- [95] A. Fujishima, T. Rao, D. Tryk, P-Doped titania xerogels as efficient UV-visible photocatalysts, *J. Photochem. Photobiol., C*, 1 (2000) 1-21.
- [96] H. Irie, Y. Watanabe, K. Hashimoto, Carbon-doped anatase TiO₂ powders as a visible-light sensitive photocatalyst, *Chemistry Letters*, 32 (2003) 772-773.
- [97] E. Kociolek-Balawejder, M. Szymczyk, Titanium dioxide as pigment and photocatalyst, *Przemysl Chemiczny*, 86 (2007) 1179-1188.

-
- [98] D.M. Tobaldi, A. Tucci, A.S. Škapin, L. Esposito, Effects of SiO₂ addition on TiO₂ crystal structure and photocatalytic activity, *Journal of the European Ceramic Society*, 30 (2010) 2481-2490.
- [99] M. Hirano, K. Ota, M. Inagaki, H. Iwata, Hydrothermal synthesis of TiO₂/SiO₂ composite nanoparticles and their photocatalytic performances, *Journal of the Ceramic Society of Japan*, 112 (2004) 143-148.
- [100] J. Ren, Z. Li, S. Liu, Y. Xing, K. Xie, Silica–titania mixed oxides: Si–O–Ti connectivity, coordination of titanium, and surface acidic properties, *Catalysis Letters*, 124 (2008) 185-194.
- [101] W. Zhou, K. Liu, H. Fu, K. Pan, L. Zhang, L. Wang, C.-c. Sun, Multi-modal mesoporous TiO₂–ZrO₂ composites with high photocatalytic activity and hydrophilicity, *Nanotechnology*, 19 (2007) 035610.
- [102] P. Cheng, Y. Wang, L. Xu, P. Sun, Z. Su, F. Jin, F. Liu, Y. Sun, G. Lu, High specific surface area urchin-like hierarchical ZnO–TiO₂ architectures: hydrothermal synthesis and photocatalytic properties, *Materials Letters*, 175 (2016) 52-55.
- [103] W. Yan, F. He, S. Gai, P. Gao, Y. Chen, P. Yang, A novel 3D structured reduced graphene oxide/TiO₂ composite: synthesis and photocatalytic performance, *Journal of Materials Chemistry A*, 2 (2014) 3605-3612.
- [104] M. Khodaei, Introductory Chapter: Superhydrophobic Surfaces-Introduction and Applications, *Superhydrophobic Surfaces-Fabrications to Practical Applications*, IntechOpen2019.
- [105] J. Hong, W.K. Bae, H. Lee, S. Oh, K. Char, F. Caruso, J. Cho, Tunable superhydrophobic and optical properties of colloidal films coated with block - copolymer - micelles/micelle - multilayers, *Advanced materials*, 19 (2007) 4364-4369.
- [106] S. Yang, S. Chen, Y. Tian, C. Feng, L. Chen, Facile transformation of a native polystyrene (PS) film into a stable superhydrophobic surface via sol–gel process, *Chemistry of Materials*, 20 (2008) 1233-1235.
- [107] X.X. Zhang, S. Cai, D. You, L.H. Yan, H.B. Lv, X.D. Yuan, B. Jiang, Template - free sol - gel preparation of superhydrophobic ORMOSIL films for double - wavelength broadband antireflective coatings, *Advanced Functional Materials*, 23 (2013) 4361-4365.

-
- [108] J. Zhu, B. Liu, L. Li, Z. Zeng, W. Zhao, G. Wang, X. Guan, Simple and green fabrication of a superhydrophobic surface by one-step immersion for continuous oil/water separation, *The Journal of Physical Chemistry A*, 120 (2016) 5617-5623.
- [109] Y. Yu, H. Chen, Y. Liu, V.S. Craig, Z. Lai, Selective separation of oil and water with mesh membranes by capillarity, *Advances in colloid and interface science*, 235 (2016) 46-55.
- [110] J. Wang, Y. Chen, Oil - water separation capability of superhydrophobic fabrics fabricated via combining polydopamine adhesion with lotus - leaf - like structure, *Journal of Applied Polymer Science*, 132 (2015).
- [111] G. Wang, Z. Zeng, H. Wang, L. Zhang, X. Sun, Y. He, L. Li, X. Wu, T. Ren, Q. Xue, Low drag porous ship with superhydrophobic and superoleophilic surface for oil spills cleanup, *ACS applied materials & interfaces*, 7 (2015) 26184-26194.
- [112] B. Dubansky, A. Whitehead, J.T. Miller, C.D. Rice, F. Galvez, Multitissue molecular, genomic, and developmental effects of the Deepwater Horizon oil spill on resident Gulf killifish (*Fundulus grandis*), *Environmental Science & Technology*, 47 (2013) 5074-5082.
- [113] Z. Xue, Y. Cao, N. Liu, L. Feng, L. Jiang, Special wettable materials for oil/water separation, *Journal of Materials Chemistry A*, 2 (2014) 2445-2460.
- [114] L. Li, Z. Liu, Q. Zhang, C. Meng, T. Zhang, J. Zhai, Underwater superoleophobic porous membrane based on hierarchical TiO₂ nanotubes: multifunctional integration of oil-water separation, flow-through photocatalysis and self-cleaning, *Journal of Materials Chemistry A*, 3 (2015) 1279-1286.
- [115] C. Gao, Z. Sun, K. Li, Y. Chen, Y. Cao, S. Zhang, L. Feng, Integrated oil separation and water purification by a double-layer TiO₂-based mesh, *Energy & Environmental Science*, 6 (2013) 1147-1151.
- [116] I. Das, G. De, Zirconia based superhydrophobic coatings on cotton fabrics exhibiting excellent durability for versatile use, *Scientific reports*, 5 (2015) 18503.
- [117] K. Sasaki, M. Tenjimbayashi, K. Manabe, S. Shiratori, Asymmetric superhydrophobic/superhydrophilic cotton fabrics designed by spraying polymer and nanoparticles, *ACS applied materials & interfaces*, 8 (2016) 651-659.
-

Chapter 2

MATERIALS AND METHODOLOGIES



Contents

2.1	Introduction
2.2	Materials
2.3	Experimental
2.4	Characterization Techniques
2.5	Applications of titania hybrid materials
2.5.1	Anticorrosion applications and electrochemical measurements
2.5.2	Water pollution remediation applications

Chapter 2 offers a brief overview of the different materials and methodologies used for this research work. Various chemicals used in the analysis are tabulated in this chapter. A detailed description of the experimental methodologies adopted for the study is also outlined in this section. The most important techniques used to characterize the selected materials have also been included in this section. Application studies of the synthesized materials aimed at are given towards the end of the chapter.

2.1. Introduction

The selection of appropriate materials and adopted experimental conditions significantly contributes in deciding the extent of solution to a research problem. The synthesis and characterization of various nanomaterials is one of the major concerns of scientific community. In order to solve various environmental issues, different experimental procedures can be selectively opted. This chapter describes the detailed experimental methods and characterization techniques used for the present research work.

2.2. Materials

The list of chemicals used for the present work is listed in the Table 2.1. All the chemicals used are analytical grade and are used as received without any further purification.

Table 2. 1. List of chemicals used for the synthesis and application studies

SI. No.	Chemicals	Formula	Manufacturer
1	Titanium Tetra Ethoxide	Ti (OC ₂ H ₆) ₄	Spectrochem. India Pvt.Ltd
2	Ethanol	C ₂ H ₅ OH	Alfa Aesar
3	Triethanolamine	C ₆ H ₁₅ NO ₃	Merck, India
4	Poly Vinyl Alcohol	(C ₂ H ₄ O) _x	Loba Chemie Pvt.Ltd, India
5	Thiourea	SC (NH ₂) ₂	Merck, India
6	Hydrochloric acid	HCl	Merck, India
7	Sodium Chloride	NaCl	Merck, India
8	Tetraethylorthosilicate	Si (OC ₂ H ₅) ₄	Spectrochem. India Pvt.Ltd

9	Ammonia	NH ₃	Merck, India
10	acetic acid	CH ₃ COOH	Merck, India
11	BPA	(CH ₃) ₂ C(C ₆ H ₄ OH) ₂	Alfa Aesar
12	Acetonitrile	C ₂ H ₃ N	Merck, India
13	Terephthalic acid	C ₈ H ₆ O ₄	Merck, India
14	HMDS	HN[Si(CH ₃) ₃] ₂	Merck, India
15	GPTMS	C ₉ H ₂₀ O ₅ Si	Merck, India
16	Methylene blue	C ₁₆ H ₁₈ ClN ₃ S	Merck, India
17	Methyl Orange	C ₁₄ H ₁₄ N ₃ NaO ₃ S	Qualigens, AR grade
18	Other organic solvents		Merck, India,

2.3 Experimental

2.3.1 Synthesis of titania hybrid materials

2.3.1.1 Synthesis of titania sol

Titania sol was prepared using titanium ethoxide as precursor. 6 mL of titanium ethoxide was mixed with 50 mL of ethanol in a beaker. 6 mL of triethanolamine was added drop wise into the beaker followed by 15 minutes stirring using a magnetic stirrer. To this reaction mixture 8 mL of distilled water was added drop wise and the solution was further stirred for 2.5 hours at room temperature. Finally, solution was left to react under stirring at room temperature for another 1 hour to obtain a homogeneous titania sol. The obtained sol was aged for 1 day before coating on mild steel.

2.3.1.2 Synthesis of titania –PVA sol

0.3 g of PVA is dissolved in 25 mL of water with stirring to prepare homogenous solution at 70 °C. The cooled solution was added

drop wise into titania sol followed by 1.5 hour of stirring at room temperature in order to obtain titania-PVA hybrid. Then, 0.2 g and 0.4 g PVA was added to obtain different concentrations of titania–PVA hybrid.

2.3.1.3 Synthesis of thiourea loaded titania-PVA sol

Thiourea doped titania-PVA nanocomposite was prepared using the controllable sol–gel route by mixing two different solutions. To incorporate thiourea in the matrix, 1 weight % of thiourea added into the Titania–PVA composite. The mixture was then stirred for 1 hour at room temperature to obtain TPNS sol. Then, 1.4 weight % and 1.8 weight % of thiourea was added to obtain different concentrations of thiourea loaded titania–PVA nanocomposites.

2.3.1.4 Fabrication of sol-gel coatings on mild steel

Mild steel specimens of composition (atom %): C (0.2%), Mn (1%), P (0.03%), S (0.02%), and Fe (98.75%) were used as the test specimens. The metal samples were cut in to $2 \times 1.8 \text{ cm}^2$ coupons. Before the measurements, the samples were rubbed with different grades of emery papers (600–1200 grades) and cleaned as per ASTM recommendations by washing with ethanol and distilled water. The cleaned and dried specimen, was then coated by dip-coating technique using a dip coater with a withdrawal speed of 10 mm / min and after air – drying, the specimens were dried in an oven at 130 °C for 1 hour. Then, the specimens were heat-treated in a muffle furnace from room

temperature to 200 °C (5 °C /min) for 2hours. The fabrication procedure of coatings on mild steel is shown in figure 2.1.

Coating fabrication

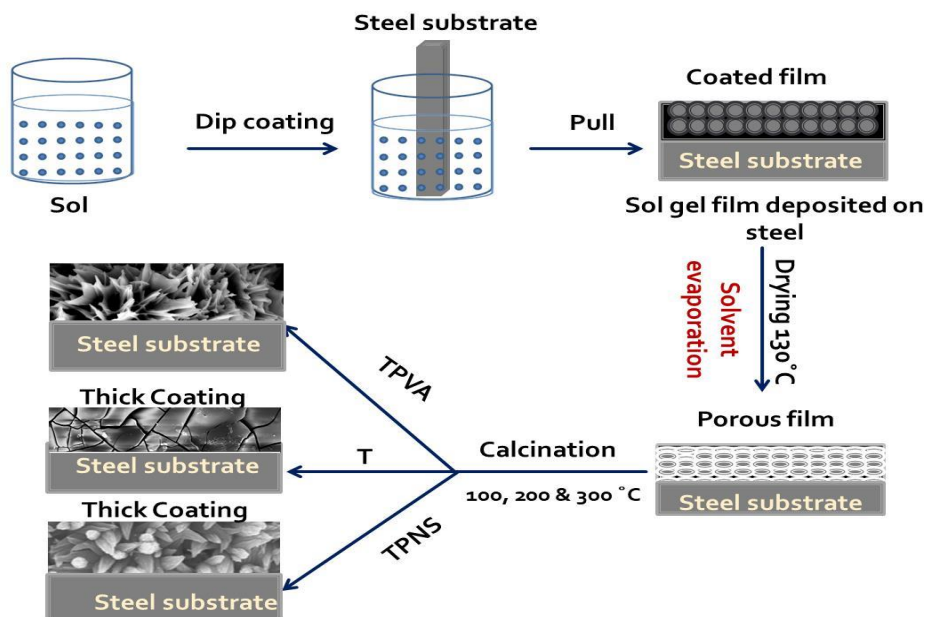


Figure 2.1. fabrication procedure of coatings on mild steel

2.3.1.5. Synthesis of titania-PVA adsorbent

The TiO₂ sol was obtained by hydrolysing titanium ethoxide in presence of triethanolamine and anhydrous ethanol for 2.5 hours to obtain homogeneous sol. The composition was [TEO]: [EtOH]: [TEA]: [H₂O] 1:30:1.5:16. After that 20 wt % PVA was added in the above sol and the solution stirred for 1.5 h at room temperature in order to obtain TiO₂-PVA nanocomposite. After repeated washing with ethanol-water mixture, the final product was dried in air oven at 130°C. Then, the

nanocomposite was heat-treated in a muffle from room temperature to 200 °C (5 °C /min) for 2 hour.

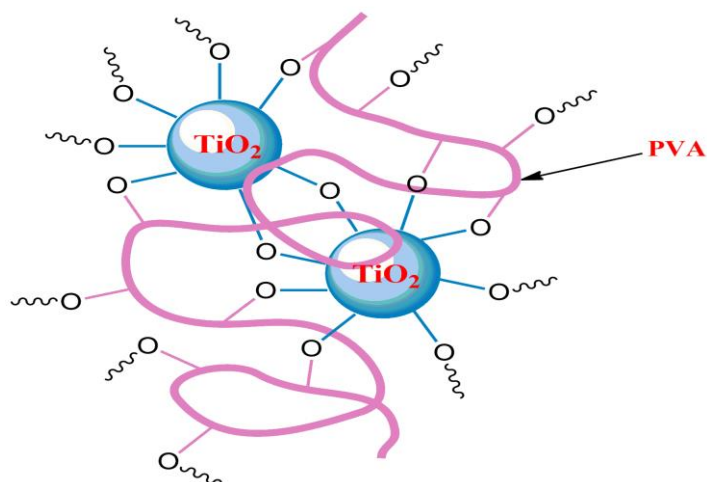


Figure 2.2. Titania-PVA nanocomposite

2.3.1.6. Synthesis of TiO₂ and TiO₂-SiO₂ hybrid

Initially, the TiO₂ sol was prepared using titanium ethoxide as the precursor. Definite volume of titanium ethoxide was mixed with absolute ethanol and acetic acid followed by 3 hours stirring in a magnetic stirrer. The volume ratio was [titanium ethoxide]: [CH₃COOH]: [EtOH] = 1: 1.87: 7.87. The obtained sol was subjected to hydrothermal treatment at 150°C for 24 hours. The resultant mixture was cooled in air and allowed to dry. Finally, mixture was subjected to calcination (5 °C /min for 2 h) at 500 °C (T5), 600 °C (T6) and 700 °C (T7).

To synthesize TiO₂-SiO₂ nanocomposite

The SiO₂ sol was obtained by hydrolysing tetraethylorthosilicate (TEOS) in the presence of acetic acid and anhydrous ethanol. The ratio fixed at [TEOS]: [EtOH]: [CH₃COOH]: [H₂O] = 1: 9.47: 0.3: 4.

TiO₂ sol was prepared as above said procedure. TiO₂ and SiO₂ sols have then mixed in a beaker by constant stirring at room temperature for 1 h and subjected to hydrothermal treatment at 150 °C for 24 h. The molar ratio of [TiO₂] : [SiO₂] was maintained as 1: 0.35. The composite thus obtained was then allowed to dry and subjected to calcination in a muffle furnace at temperatures 500 °C (TS5), 600 °C (TS6), and 700 °C (TS7) for 2 h at heating rate 5 °C /min.

2.3.1.7. Preparation of HMDS-GPTMS modified TiO₂-SiO₂ coating solution and fabrication of coating on cotton fabric

The synthesized TiO₂-SiO₂ hybrids were cooled and allowed to dry followed by the addition of aq.NH₃ and mixed using magnetic stirrer at room temperature for 1 hour, and allowed to change into gel. To prepare the superhydrophobic hybrid of TiO₂-SiO₂ gels, about 0.8g of hybrid was mixed with 2.5g of HMDS in ethanol (1: 8 wt/wt ratio), and the mixture was kept at 70° C for 20 hours in a closed container. After that, the obtained hybrid gel was washed with ethanol to remove excess free HMDS and dried at 70° C for 2 hours. HMDS-modified hybrid TiO₂-SiO₂ gels (0.6 g) were dispersed in 1- propanol (8 mL) for

about 20 min in an ultrasonic bath and to the mixture 0.1 g of GPTMS was added and stirred for 30 min.

The cotton fabric used for coating was (cut in to a size of 5 cm x 5 cm) washed several times with acetone, ethanol, and finally with distilled water and dried before the dip-coating process. Cotton fabric immersed in the solution using a dip-coater at a speed of 10 mm/sec, dried at room temperature, and then cured at 120° C for 40 min.

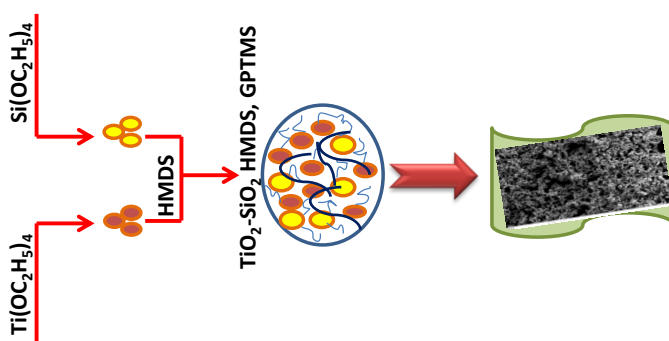


Figure 2.3. fabrication of superhydrophobic coating on cotton fabric

2.4 Characterization Techniques

2. 4. 1. X-ray Diffraction Studies (XRD)

X-ray diffraction is a powerful non-destructive technique used to study surface nanostructure, nanotexture, plane orientation and size of the particles for a crystalline material. A crystal is a periodic three-dimensional arrangement of particles. The distance between the particles comes in the order of wavelength of X-rays. When X-rays

falls on the sample they will be transmitted, absorbed, refracted, scattered, and diffracted by the samples. The diffraction will occur from the crystalline planes satisfying Bragg's law ($n\lambda = 2d\sin\theta$). Bragg's law is used to explain the interference pattern created by the X-rays by interacting with the nanomaterial[1]. The plane orientation and the phase composition were determined by comparing the XRD data with JCPDS data. By knowing the angle of diffraction and wavelength of X-rays the crystalline properties of the material can be studied. RIGAKU MINIFLEX-600 diffractometer with Cu $K\alpha$ ($\lambda = 1.5418 \text{ \AA}$) scanned in the range at 2θ 10° to 80° at room temperature.

2.4.2 Fourier Transform Infrared Spectroscopy (FTIR)

FT-IR spectrometer is used for quantitative and qualitative analysis. Infrared (IR) region of electromagnetic spectrum is used in FT-IR techniques to identify functional groups and other molecular properties. When IR radiation is passed through the sample, some of the IR radiations absorbed, transmitted and reflected by the sample. The instrument records the transmitted and absorbed radiations as a function of their intensity. The resulting spectrum reflects the molecular finger print of the sample and there by different properties of the sample can be studied[2]. JASCO FTIR-4100 spectrometer was used to record FTIR spectra in the range of $4000\text{-}400 \text{ cm}^{-1}$. Attenuated total reflectance mode is used to record FTIR spectrum using JASCO FTIR- 4700 spectrometer equipped with ATR cell in the range of $4000\text{-}400 \text{ cm}^{-1}$. ATR-FTIR technique is a widely used technique to

eliminate complex sample preparation and it can be used to measure infrared spectrum of wide variety of solids and liquids directly.

2.4.3 UV-Visible Spectroscopy

UV-Visible spectroscopy highly recognized for the study of the interaction of UV-Visible radiation with molecules. Depending on the functional group present, different wavelength of UV-Visible radiations are absorbed or transmitted. The absorbance is proportional to the concentration and path length of the cuvette used. In UV-Visible absorption spectra the intensity of absorbed radiation is recorded as a function of wavelength absorbed. Jasco-V 500 UV-Visible spectrophotometer in the range of 200-800 nm is used for studying the optical properties of developed composites.

2.4.4 Photoluminescence Spectroscopy (PL)

Photoluminescence spectroscopy is a non-destructive method to study the electronic structure of materials. When electromagnetic radiation directed onto a sample, photoexcitation can occur. As a result, high energy states become more populated. Eventually reemission of absorbed radiation from the excited state to ground state is occurred through photoluminescence process. By monitoring the intensity and wavelength of reemitted radiation, valuable information regarding the electronic structure of the molecule is obtained[3]. Fluorescence study was done using Agilent Technologies model Cary Eclipse Fluorescence Spectrophotometer.

2.4.5 Dynamic Light scattering (DLS)

Dynamic light scattering (DLS) is a common technique used to study particle size, particle size distribution and zeta potential of particles in colloidal suspension. In DLS the Brownian motion of suspended particle relates to the size of the particles. There exist an inverse relationship between size of the particle and Brownian motion. Zeta potential measure the stability of colloidal system. HORIBA, Zeta Sizer nano series was used to measure the zeta potential (ζ) at room temperature.

2.4.6 Field Emission Scanning Electron Microscopy (FE-SEM)

FE-SEM is used for high resolution imaging of material surface in nano scale dimension. High energetic electron (100 eV to 50 KeV) is focused into a beam is used for the scanning of material surface. Electron beam undergo different effect on interaction with the sample. The different interaction and effects are monitored and transformed in to an image using back scattered electron. The surface morphology of the samples were examined by field emission scanning electron microscopy (FESEM, Zeiss, Germany,)

2.4.7 Energy dispersive X-ray spectroscopy (EDS)

EDS analysis is used for the study of elemental composition of a material imaged in a FE-SEM. Most of the elements are detected at concentration on the order of 0.1%. X- rays will be generated when high energetic electrons are passing through the surface of the specimen. The energy of X-rays will be a characteristic of the element.

The EDS detector collects the X-rays and identifies the element from the known or computer generated standard to produce quantitative analysis. The elemental analysis was performed with an Energy Dispersive Spectroscopy (FESEM, Zeiss, Germany,)

2.4.8 Transmission electron microscopy (TEM)

Transmission electron microscopy (TEM) is used to study morphology, size, size distribution etc. of nanomaterials. TEM uses very high energetic electrons (100KeV-1MeV). These energetic electrons are passed through the sample by means of condenser lens system. Electrons will penetrate through the sample and get scattered. The scattering of electron from the specimen determine the kind of information generated. TEM has the ability to provide both image and diffraction information of the sample. TEM images were recorded with JEOL JEM-2100 transmission electron microscope. Very dilute suspension of the sample is drop casted on carbon coated copper grid, which was dried and used for imaging.

2.4.9 Atomic force microscopy (AFM)

AFM is an emerging technique used for imaging materials on nanoscale. The surface images of the sample obtained by studying the interactions between cantilever tip and sample surface. When the AFM tip touches the sample, it can record the force between the probe and the surface. The force can be measured using Hook's law. AFM analysis utilise three primary imaging modes: contact AFM, tapping mode AFM and non-contact AFM. Atomic force microscopy (AFM)

study of the samples was made by using APER-A-100 SPM in contact mode.

2.4.10 X-ray photoelectron spectroscopic (XPS)

X-ray photoelectron spectroscopy (XPS) is a powerful method of analysis for quantitative atomic composition study. The emission of photoelectron from the sample is observed when it interacts with monochromatic X-rays. The energies of photoelectron are characteristic of the element present in the sample. XPS spectra is obtained by plotting number of electrons versus binding energy. XPS measurements were performed using Ultra axis Kratos Analytical, U.K, XPS instrument with an Al K α X-ray source.

2.4.11 BET Surface area analysis

The study of adsorption of gas molecules on the surface of solid substrate is used for the determination of surface properties of solid substrate. Surface area, surface energy, pore size, pore size distribution etc. can be studied using BET theory of adsorption. BET theory is an extension of Langmuir model of adsorption by considering multilayer adsorption. BET equation can be written as

$$\frac{P}{V_{total}}(P_0 - P) = \left[\frac{1}{V_{mono}} C \right] + \left[\frac{C-1}{V_{mono}} C \right] \left(\frac{P}{P_0} \right) \quad (9)$$

where v_{total} the volume of the gas adsorbed at pressure P and v_{mono} is the volume of the gas adsorbed when monolayer adsorption is completed. P_0 the saturation pressure of the gas molecule and C is a constant related to the enthalpy of adsorption in the monolayer. The

plot of $\frac{P}{V_{total}}(P_0 - P)$ against $\frac{P}{P_0}$ should be a straight line with intercept $I = \frac{1}{V_{mono}}C$ and slope $S = \frac{C-1}{V_{mono}}C$. Thus from the slope and intercept the value of v_{mono} and C can be evaluated and from this the specific surface area of the solid adsorbent can be calculated by the equation $S = V_{mono} N_A/m \times 22400 \text{ m}^2\text{g}^{-1}$. Where N_A is Avogadro constant, m is the mass of test powder in grams, 22400 is the volume capacity occupied by 1 mole of gas at STP. The surface area and average pore size were measured at -195.80°C Bel SORP Max by adsorption automatic analyser after degassing at 150°C .

2.4.12 Water Contact Angle

The angle formed between the outline tangent of the water drop deposited on the substrate and the surface of the substrate is known as water contact angle (WCA). Depending on the value of contact angle, substrate can be categorized into four, hydrophobic ($> 90^\circ$), superhydrophobic ($> 150^\circ$), hydrophilic ($< 90^\circ$) and superhydrophilic ($< 30^\circ$). Surface contact angle Goniometer is the common instrument used for measuring the contact angle. The WCA measurement is quite helpful for evaluating the super-hydrophobicity of cotton fabric using a static water contact angle Goniometer (DIGIDROP) instrument.

2.4.13 TOC

TOC analysis is a common method used for quantitative determination of organic carbon content in a sample. TOC of the

degraded solution at different time interval was analysed through TOC analyser Shimadzu TOC-L CPH

2.4.14 HPLC

High-performance liquid chromatography (HPLC) is an analytical method commonly used to separate and quantify components of liquid samples. Concentration of BPA solution was monitored by using Shimadzu Prominence HPLC system with binary pump, PDA detector 25 x 5 mm C18 column.

2.4.15 Liquid Chromatography- Mass spectrometry (LC/MS)

LC-MS is an analytical technique which combines the physical separation capability of liquid chromatography (or HPLC) with the mass analysis capability of mass spectrometry (MS). The combination of liquid chromatography with mass spectrometry (LC-MS) enables the separation of nonvolatile, thermally unstable and polar dyes for introduction into the mass spectrometer for identification. Intermediate product analysis of BPA degradation was done by using LC/MS method using ESI negative mode with instrument Waters (UPLC-TQD) mass spectrometer.

2.4.16 Electrochemical Impedance Spectroscopy (EIS)

Electrochemical impedance spectroscopy is one of the powerful techniques used for the investigation and prediction of the corrosion process. EIS does not cause damage of the sample in comparison to other electrochemical techniques; therefore it can be used in situ for

long term evaluations[4]. EIS ordinarily works by applying an AC potential to the sample by means of reference electrode, and then measuring the current passing through the specimen using a counter electrode. A potentiostat is used for applying the potential and measuring the current. The impedance calculation is done with a Frequency Response Analyzer (FRA), and the procedure is controlled by Zimp win software in a computer. The EIS spectra can be displayed in different ways. In a Nyquist plot, the imaginary part of the impedance, Z'' , is plotted against the real part of the impedance, Z' . The change in impedance spectrum due to the immersion in the corrosive environment helps to understand the protective ability of the developed coatings.[5] It is one of the most intensively used techniques which can be used to model the physicochemical behavior of coated substrates during corrosion test. AC impedance measurements were carried out at E_{corr} values in the range from 0.1 Hz–10 kHz with amplitude of 10 mV using Gill AC potentiostat (model number 1475).

2.4.17 Potentiodynamic polarization study (PDP)

Polarization curves have been widely used to predict the ability of the metallic substrates to withstand harsh corrosive environments[6, 7]. Tafel studies are mainly involved in changing the potential of the working electrode and monitoring the current that is produced as a function of potential. In these measurements, both anodic and cathodic polarizations are performed in a cyclic manner[8].For anodic polarization, the working electrode becomes the anode by changing the potential in the anodic direction forcing electrons to be withdrawn from the metal being tested. But in cathodic polarization, electrons are

added to the metal. As a result, the working electrode becomes more negative. The variation of current with potential of a corroding electrode is analysed by a plot of potential of standard calomel electrode (SCE) vs $\log i$ whose slopes give the Tafel constants (β_a or β_c) and the intercept gives the corrosion current (i_{corr}). The corrosion potential (E_{corr}) and corrosion current (i_{corr}) values are calculated using Tafel extrapolation method.

2.5 Applications of titania hybrid materials

2.5.1. Anticorrosion applications and electrochemical measurements

Corrosion resistance properties of titania (T_1 T_2 T_3), titania – PVA (TP_1 , TP_2 , TP_3), and thiourea loaded titania-PVA ($TPNS_1$, $TPNS_2$, $TPNS_3$) coating on mild steel were evaluated using, weight loss study, electrochemical impedance spectroscopy (EIS) and potentiodynamic polarization studies (PDP). EIS and PDS were performed in HCl and 3.5wt % NaCl solution using Gill AC Potentiostat (model number 1475). A three-electrode cell assembly was used for electrochemical measurements, with platinum as a counter electrode and saturated calomel as the reference electrode. Either bare metal or coated metal was used as a working electrode.

2.5.1.1. Weight loss study

Previously weighed coated mild steel samples were immersed in 1M HCl for 24, 48, 72 and 98 hours. After exposure, the metal was taken out from the acid and the corrosion products were removed by rubbing and cleaned as per ASTM recommendations, by washing with

ethanol and distilled water, and dried, cooled and weighed. The same procedure was repeated with bare mild steel sample and the inhibition efficiency (IE) was calculated using the equation (1)

$$\text{The percentage efficiency, IE} = \frac{W_0 - W}{W_0} \times 100 \quad (1)$$

where W_0 and W represents the weight loss corresponding to uncoated and coated MS. The coated samples immersed in 1M HCl solution for 70 days and at a regular interval. The weight loss was measured.

2.5.1.2 Electrochemical Impedance Spectroscopy and Polarization Study

A conventional three-electrode electrochemical cell consists of a working electrode, a saturated calomel electrode (SCE) as a reference electrode and a platinum electrode as a counter electrode was used. Electrochemical impedance spectroscopy (EIS) and polarization measurements were performed using a Gill AC computer controlled work station (model no. 1475) in a frequency range from 10 kHz to 0.1 Hz. The coated mild steel or bare mild steel specimens were used as a working electrode, and the exposed area was approximately 1.0 cm². EIS measurements were performed at an open-circuit potential (OCP) using a sine wave of 10 mV amplitude peak to peak. The impedance data have been fitted to an appropriate equivalent circuit. The Tafel plots were obtained by changing the electrode potential automatically from -250 mV to +250 mV at the OCP at a scan rate of 60 mV/min. Inhibition efficiencies were determined from corrosion currents calculated by the Tafel extrapolation method. Corrosion parameters were measured after reaching steady state.

All the experiments were repeated thrice so as to confirm the accuracy of the attained results. The percentage of protection efficiency (PE) was calculated from charge transfer resistance using equation (2)

$$\text{PE \%} = \frac{R_{\text{Ct}}^* - R_{\text{Ct}}}{R_{\text{Ct}}^*} \times 100 \quad (2)$$

where R_{Ct} and R_{Ct}^* represents the charge transfer resistance for the bare and coated mild steel samples.

The polarization behaviour was studied at a scan rate of 1 mVs^{-1} and a scan range of -250 mV to $+250$ mV. The percentage of protection efficiency (PE) was calculated from corrosion current density using equation (3)

$$\text{PE (\%)} = \frac{I_{\text{Corr}}^* - I_{\text{Corr}}}{I_{\text{Corr}}^*} \times 100 \quad (3)$$

where I_{Corr}^* and I_{Corr} represents the corrosion current density of the blank and coated mild steel.

2. 5. 2 Water pollution remediation applications

The synthesized hybrid systems such as titania, titania-PVA (T, TPVA), TiO_2 ; TiO_2 - SiO_2 (T_5, T_6, T_7, T_8 ; TS_5, TS_6, TS_7, TS_8) and HMDS-GPTMS modified TiO_2 - SiO_2 (HGTS) were employed as remediation materials for effective removal of contaminants from water resources. A detailed procedure of dye removal (adsorption), organic pollutant removal (photocatalysis) and oil-water separation (superhydrophobic cotton fabric) were explained as follows.

2.5.2.1. Dye removal through adsorption

The dye removal experiment was conducted at room temperature in a batch system. In a typical experiment, 35 ppm 50 ml of MB solution was used. Adsorption parameters like temperature, dye concentration, pH, and adsorbent dosage were investigated. Solution pH is varied over a range from 3-9 by adding NaOH and HCl. The required amount of nanocomposite was added to the solution and was stirred for a particular period of time. The composite was separated from the MB solution through centrifugation (750 rpm). The concentration of dye solution was determined using JASCO UV - Vis spectrometer at 670 nm in a definite time interval. The amount of methylene blue adsorbed per unit mass of the adsorbent at equilibrium, q_e (mg g^{-1}) and the amount of dye adsorbed per unit mass of the composite, q_t (mg g^{-1}) at time t , were measured by the following equations,

$$q_e = (C_0 - C_e) \frac{V}{W} \quad (4)$$

$$q_t = (C_0 - C_t) \frac{V}{W} \quad (5)$$

The percentage dye removal and adsorption capacity of hybrid nanocomposite was calculated using the equation

$$\% \text{ removal} = \frac{(C_0 - C_t)}{C_0} \times 100 \quad (6)$$

$$\text{Adsorption capacity} = (C_0 - C_t) \frac{V}{W} \times 100 \quad (7)$$

where C_0 is the initial dye concentration (mg L^{-1}), C_t is the dye concentration at time t (mg L^{-1}), C_e is the equilibrium dye concentrations in the solution, V is the volume of dye solution used (L), and W is the weight of the polymer composite used (g). All

experiments were performed in triplicate, and the mean value was reported.

2.5.2.2. Selective Adsorption of Cationic Dye from Dye Mixture

The selective adsorption experiments were performed in the mixture of MO and MB. Typically, 0.075g of TPVA nanocomposite was added to 30 mL of dye mixture at room temperature. The initial concentrations of MB and MO are both 35 ppm. The residual dye concentration in the solution was determined by UV–Vis spectrophotometry.

2.5.3. Photocatalytic removal of Bisphenol A (BPA)

2.5.3.1 Evaluation of photocatalytic activity

Photocatalytic activity of the nanocomposite was assessed by the photodegradation of BPA under visible light irradiation. 0.05g of catalyst immersed in 35 ppm BPA solution. The solution was maintained in the dark to reach adsorption-desorption equilibrium. BPA solution was irradiated by 500 W halogen lamp at a distance of 11 cm from lamp. The intensity of light was measured using Lutron LX-107- HA lux meter and was found to be 85000-95000 Lux. In order to maintain a constant temperature throughout the progress of reaction a constant supply of ice-cold water was provided. The samples were withdrawn at regular intervals of time, and the concentration of the remaining BPA was measured by recording its concentration using HPLC analyser after filtering the solution through a 0.22 μm nylon membrane.

$$\% \text{ degradation efficiency} = \frac{(C_0 - C_x)}{C_0} \times 100 \quad (8)$$

where C_0 is the initial concentration and C_x is the final concentration of BPA.

2.5.3.2. Monitoring BPA concentration

High performance liquid chromatography (Shimadzu Prominence HPLC) was employed to monitor the concentration of BPA. Separation was achieved on a 25 x 5 mm C18 column. The mobile phase consisting of 80:20 acetonitrile: UPW the flow rate was set to 1 mL/min, and the injection volume was 20 μ L. Detection was achieved through PDA detector. The wavelength of the excitation was 280 nm and the emission wavelength was 305 nm. The solution was subjected to TOC (TOC analyser TOC-L CPH, Shimadzu) and LC/MS (Waters UPLC-TQD mass spectrometer) using negative ESI mode to determine intermediate degradation products and mineralization rates in the solution at definite time intervals.

2.5.3.3. Intermediate reactive species determination

The radical trapping agents added to the solution before degradation experiment to evaluate the contribution of h^+ , \bullet OH, O_2 and $O_2^{\bullet-}$ produced during the visible-light irradiation process. Potassium iodide (KI) was added to determine the participation of holes (h^+), tert.butanol (tBuOH), was added to recognize hydroxyl radical (\bullet OH) influence, sodium azide (NaN_3) and benzoquinone (BQ) as oxygen (O_2) and super oxide radical ($O_2^{\bullet-}$) scavengers. The concentration of scavengers maintained as constant (0.5 mol/L).

2.5.3.4 Measurement of hydroxyl radical content using fluorescence spectra

50 mL of 0.1 M terephthalic acid solution (dissolved in NaOH) and 0.05g of the photocatalyst was added to the solution in a 100 mL beaker. The reaction mixture was stirred continuously under visible

light. Samples were collected at regular time interval and were analysed by fluorescence spectrophotometer at 432 nm to measure the hydroxyl radical produced during reaction. Photocatalytic activity of the nanocomposite was assessed by the photodegradation of Bisphenol A under visible light as mentioned in 2.5.3.1.

2.5.4 Superhydrophobic cotton fabric for wettability control- Application in oil–water separation

2.4.4.1 Oil–water separation

We have conducted oil water separation experiment to investigate the oil separation property of the coated fabric using simple filtration experiment. In this study n-hexane/water, toluene/water, chloroform/water, hexadecane/water, dichloromethane/water and some other oils like coconut oil, olive oil, sunflower oil were taken and to identify water from the mixture colored with methyl orange dye. The coated cotton fabric was placed in a funnel as a filter membrane. Oil–water mixture (1:1 v/v) was taken in a beaker and the mixture was poured slowly onto the cotton fabric. The experiment was repeated for all oil-water mixtures up to 15 cycles. The WCA measured after filtration process and further the oil–water separation efficiency was calculated in each case.

2.5.4.2. Durability and stability of the as-prepared superhydrophobic fabric

The mechanical durability such as tensile strength, abrasion resistance and washing durability of the coated fabric (CF) were examined. The repeated tear test assessed with an adhesive tape. In this test, the cotton surface was pasted onto an adhesive tape, and then it

was peeled off. The test on a coated sample was repeated 10 times and corresponding WCA after test was measured. Abrasion resistance was investigated by the sand paper abrasion test. A 600-800 grade sand paper was used. The coated fabric was placed on the sand paper facing on the surface and dragged forward along one direction maintained 20 cm distance and repeated several times. The stability was analysed by WCA measurement. The durability of the coated fabric against washing was done in 0.38 % soap water with magnetic stirring with a rotation speed of 850 rpm for 10 min at 40°C. The fabric was rinsed with pure water and dried under atmospheric conditions, durability assessed by measuring WCA after repeated wash cycle. The tensile strength of the coated fabric (CF) and uncoated fabric (UF) were done. Chemical stability of the super-hydrophobic coatings, under harsh environmental conditions like exposure to acidic, alkaline, salty solutions have also done. The ultraviolet irradiation stability was done by placing in an UV chamber, equipped with four 16 W ultraviolet lamps. The distance between the UV light source and the sample was approximately 8 cm. Chemical and UV stability experiments were done up to 72 hours and the contact angle of the CF was measured every 24 hours

Living is worthwhile if one can contribute in some small way to this endless chain of progress.

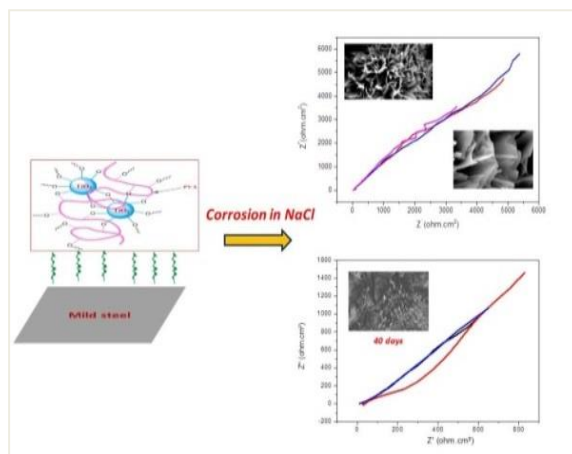
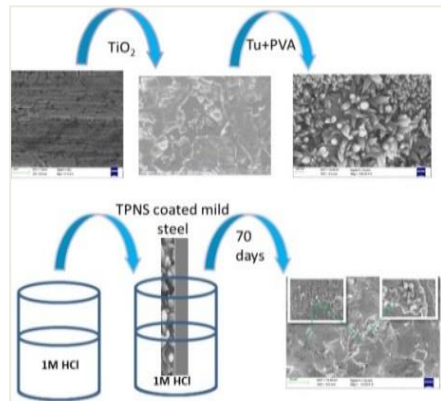
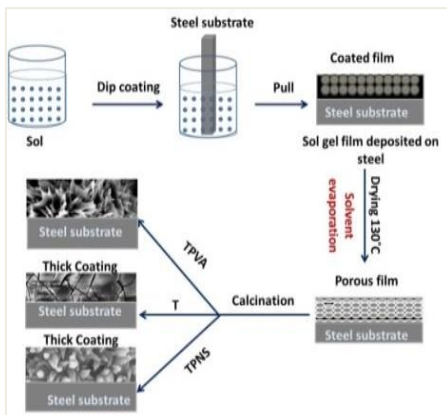
Paul Dirac

REFERENCES

- [1] A. Monshi, M.R. Foroughi, M.R. Monshi, Modified Scherrer equation to estimate more accurately nano-crystallite size using XRD, *World journal of nano science and engineering*, 2 (2012) 154-160.
- [2] L. Barbeş, C. Rădulescu, C. Stihi, ATR-FTIR spectrometry characterisation of polymeric materials, *Romanian Reports in Physics*, 66 (2014) 765-777.
- [3] P. Nandakumar, C. Vijayan, Y. Murti, Optical absorption and photoluminescence studies on CdS quantum dots in Nafion, *Journal of applied physics*, 91 (2002) 1509-1514.
- [4] S. Amand, M. Musiani, M. Orazem, N. PØb re, B. Tribollet, V. Vivier, *Electrochim. Acta*, 87 (2013) 693-700.
- [5] F. Mansfeld, Concerning the Display of Impedance Data, *Corrosion*, 44 (1988) 558-559.
- [6] N. Karthik, V. Arunkumar, M. Sethuraman, Enhancement of protection of aluminum through dopamine impregnation into hybrid sol-gel monolayers, *Journal of Materials Science*, 49 (2014) 7970-7978.
- [7] M. Zheludkevich, R. Serra, M. Montemor, I.M. Salvado, M. Ferreira, Corrosion protective properties of nanostructured sol-gel hybrid coatings to AA2024-T3, *Surface and Coatings Technology*, 200 (2006) 3084-3094.
- [8] N. Laethaisong, Carbide formation on carbon steels in CO₂ corrosion by use of applied anodic current, University of Stavanger, Norway, 2011.

Chapter 3

SYNTHESIS, CHARACTERIZATION AND CORROSION STUDIES OF TITANIA NANO HYBRIDS



CONTENTS

Part A	
3.1	Introduction
3.2	Results and discussion
3.3	Corrosion inhibition of MS in HCl
3.3.1	Weight loss study
3.3.2	Electrochemical Impedance Spectroscopic (EIS) measurements
3.3.3	Potentiodynamic polarization study (PDS)
3.4	Conclusions
Part B	
3.5	Corrosion inhibition of MS in NaCl
3.5.1	Electrochemical Impedance Spectroscopic (EIS) measurements
3.5.2	Potentiodynamic polarization study (PDS)
3.6	Corrosion protection mechanism
3.7	Conclusions

This chapter is divided in to two parts; Part A deals with the discussion of characterization and application of titania, PVA titania and thiourea loaded titania PVA hybrid as anticorrosive protective coatings on mild steel in HCl media and Part B deals with the study of above mentioned coatings in NaCl media. The coatings on mild steel have been developed via sol-gel dip-coating method. This simple, facile and eco-friendly method has great potential to replace environmentally hazardous chromate conversion coatings. Moreover, the modified coatings on metal offers attractive protection efficiency on extending the exposure period in HCl and NaCl media for several days, which is far superior to the conventional sol-gel coating which losses efficiency day by day. The protective layer on the surface of the metal offering significant physical barrier against the attack of corrosive species from HCl and NaCl.

PART A

3.1. Introduction

Many disasters have resulted from the corrosion of metallic surfaces and usually, corrosion of metals occurs in an environment that can be considered as an electrolyte. Electrolytes encountered in corrosion are usually liquids containing dissolved ionic species [1, 2]. Acid solutions are generally used for removal of undesirable scale and rust on the metals, cleaning of boilers and heat exchangers, oil-well acidizing in oil recover and so on. The rate of metal dissolution caused by the acidic media is quite high [3]. The World Corrosion Organization evaluated an annual cost of around \$2.4 trillion expenditure worldwide [4]. Considering the safety of human life, environment, for many decades, protection of metal was undertaken using hexavalent chromate species and the same is being replaced widely with more environmentally benign materials [5-7]. But it is essential to find most economical and feasible method to be applied for practical uses. Mild steel is one of the most commonly used materials in various chemical industries owing to its low cost, good tensile strength and availability, but corrosion of steel is a fundamental academic and industrial concern [8, 9]. It is estimated that 20% of world steel production is lost each year in the form of rust. The application of coatings is the most common strategy to protect metals from corrosion [10]. Corrosion behavior of sol-gel coatings has been extensively studied on mild steel substrates [11, 12]. The design and fabrication of flexible nontoxic materials are urgently needed to meet

the demands of industry specially to protect the corrosion prone materials from aggressive environments. Development of these materials in a convenient and inexpensive manner together with their potential utilization in various fields is very much desired. Due to their scratch-resistance, sound proofing, abrasive, or preventive properties, the coatings obtained by the sol-gel method could be used as protective coatings [13]. Thus the production of eco-friendly sol-gel coatings to prevent corrosion on metallic substrates was one of the emerging areas of application, competing with conventional chromate and phosphate coatings [10].

In the literature, some oxide coatings with very low electronic conductance such as TiO_2 , SiO_2 , Al_2O_3 , ZrO_2 , or mixed oxides composite coatings on metals to improve their surface properties have been reported as corrosion protection agents [11, 14, 15]. Metal oxide sol gel coatings are very attractive because they possess good thermal and electrical properties and they are more resistant to wear, erosion, corrosion and oxidation in aggressive environments. TiO_2 and its modifications have attracted scientists as an excellent anti-corrosion material due to its fascinating properties. They can be used as functional materials such as protective layers on metals surface to improve the wear and corrosion resistance [16, 17]. The application of sol-gel based titania and hybrid coatings over the metallic surface, is a promising method [18, 19] to protect the metal and has the potential to replace the hexavalent chromate coating. Sol-gel process allows the introduction of organic moiety like polymers into the TiO_2 matrix easily. Recently Hongjun Kan et.al was fabricated a novel

nanostructured TiO₂ mesh membrane by a simple electrochemical anodization and heating process which showed anticorrosive ability [20]. Normally sol-gel pure titania coatings develop surface defects on prolonged exposure which may lead to decreased efficiency of protection [21]. However, because of changes in the mechanical properties, pure inorganic sol-gel coatings during their service of life are susceptible to undergo cracks deep within the structure. The cracks propagate and expose the substrate to atmospheric moisture and oxygen, finally leading to the failure of the coatings. The inorganic-organic hybrid materials forming a set of composites in which the organic part improves the adhesion of coating on metal surface, while inorganic part increases the hardness and the scratch resistance property of the coating [22]. The surface treatment based on sol-gel technology forms a promising strategy of fabricating a coating with the ability to tailor the metal oxide-polymer interface, which is capable of protecting the surface [23-30]. Also, the physical, chemical, and thermal properties of the hybrid material are superior to pure polymeric or inorganic oxide. Recently many studies have focused on eco-friendly titania based organic/inorganic nanocomposite films [29]. Researchers applied numerous measures to enhance the barrier performance and corrosion protection properties of titania using inorganic organic hybrid materials, however, most of these methods are cumbersome.

Due to the outstanding properties of polymers like epoxy, polypropylene, polyethylene etc for protecting metal substrates from environmental and corrosion attacks they have been widely

used[31]. Yongxing Zhang et.al developed epoxy composite coatings filled with silane functionalized silicon nitride and applied to protect Q235 carbon steel from corrosion. The main constituent of majority of works reported using epoxy coatings are based on Bisphenol A. However, due to toxic and carcinogenic nature of the bisphenol-based epoxy coatings, the use of these coatings has been extremely restricted. PVA[32, 33] being a green inhibitor with excellent properties such as film forming, emulsifying and adhesion can be utilized as eco-friendly material for corrosion protection of mild steel. Moreover, mixed titania - PVA layers deposited on mild steel substrate via sol-gel technique increase the bridge effect between organic-inorganic phases. Many experiments revealed the proper corrosion inhibition properties of PVA on the steel surface [34]. Strawhecker and Manias have identified the corrosion inhibitive performances of the poly vinyl alcohol [35]. Recently novel multifunctional catalysts of PVA based nanocomposite membranes have been developed via an ecofriendly and self-assembled process for catalytic applications in waste water treatment[36]. Luo et al reported that the design of poly vinyl alcohol have been utilized to functionalize graphene oxide (GO), shows potential to improve the mechanical and chemical properties of GO[37].

Due to the prolonged exposure, or change of pH, defects occur often in the hybrid sol-gel coatings. To solve this problem, corrosion inhibitors as healing agent have been introduced into sol-gel coatings. Sol-gel hybrid coatings permit the impregnation of additives such as corrosion inhibitors because of their porous nature [38, 39]. The

combining effect of polymer and corrosion inhibitor executes long term protection of metal from corrosion. To date, many corrosion inhibitors have been introduced sol–gel coatings to increase the corrosion resistances of the coatings [40-43]. In addition to inorganic inhibitors, organic corrosion inhibitors are also added into the sol–gel matrix. Thiourea and its derivatives, with two nitrogen atoms and a sulphur atom, serve as potential corrosion inhibitors [43, 44]. These are mainly used as addition agents in industrial operations such as pickling, descaling, cleaning etc. The efficacy of thiourea and its derivatives in preventing the corrosion of aluminium, steel and copper has been reported [45-47].

Many Studies carried out to use polymer/TiO₂ composites as corrosion resistant material for many metals other than mild steel substrates. Xiaokun Cui et.al investigated the anticorrosion ability of the PDMS/TiO₂ composite coating on the AA 2024 (An alloy of aluminium). Long-term immersion tests on the coating have been performed and the findings have shown that the coating still has a protective effect on aluminum after 40 days of immersion[48]. Balaji et.al have made attempts to form smart/intelligent, corrosion resistant nanocomposite coatings through sol-gel process by self-assembly method. Chitosan-doped-hybrid/TiO₂ nanocomposite based sol-gel coating exhibited better protection for the corrosion resistance of aluminum metal in 3.5% NaCl[49]. Based on these concepts herein we develop titania, by an in-expensive green modifier PVA, eco-friendly corrosion resistant titania- PVA nanocomposite, thiourea doped titania-PVA flower like hierarchical nanocomposite protective coatings on mild steel. The protecting ability of as prepared coating on mild steel

in 1M HCl and in 3.5 wt% NaCl solution was determined. Usually, the pH of 3.5wt% NaCl is around 5.8 at room temperature [50]. The presence of chloride ions promotes rapid attack of metallic substrate in neutral aqueous solutions and even higher in acidic solution due to the extensive localized attack.

3.2. Results and discussion

3.2.1. Characterization of T, TPVA and TPNS coatings

3.2.1.1 Fourier Transform Infrared Analysis (FTIR)

Figure. 1 shows the FTIR spectra of T₂, TPVA₂ and TPNS₃ coated on mild steel at 200 °C. Pure T consists number of peaks and shows a broad peak in the range of 500-900 cm⁻¹ assigned to the stretching vibration of Ti-O and bending vibration of O-Ti-O and Ti-O-Ti [51]. The peak at 487 cm⁻¹ is attributed to Ti-O stretching [52]. This peak is shifted to the range 400-700 cm⁻¹ for TPVA₂ and TPNS₃ coated samples vouched for the introduction of PVA in the TiO₂, and confirmed the cross-linked structure of the hybrid nanocomposite. The band at 570 cm⁻¹ in three samples could be due to Fe-O-Ti stretching [53]. This showed the excellent adhesion of sol-gel coating on mild steel substrate through Fe-O-Ti bond. The broad band at 1070 cm⁻¹ was assigned for C-O-H bond and the absorption band at 1629 cm⁻¹ could be due to the bending vibration of H-O-H in the samples [52, 54]. The bands near 778 & 508 cm⁻¹ corresponding to C-N and NCN stretching [45]. The additional bands at 3274, 3360 cm⁻¹ corresponding to NH₂, N-H stretching appeared in TPNS₃ coating [36]. The peak at 620 cm⁻¹ due to Fe-N (NCS) stretching vibration and 702 cm⁻¹ attributed to C-S stretching vibration for TPNS₃ coated sample [45]. This confirmed that

thiourea doped in to the coating. The peak in the range 1300-1460 cm^{-1} was observed due to the C-H deformation and the anti-symmetric and symmetric C-H stretching of methylene groups are observed respectively at 2931 cm^{-1} and 2860 cm^{-1} [55-57]. This clearly indicates the presence of a remarkable number of organic groups on the surface of the TPVA₂ and TPNS₃ sample. These observations clearly indicated the presence of hybrid sol-gel coating on mild steel. The spectra consist of a broad band at 3380 cm^{-1} corresponds to O-H stretching vibration of hydroxyl group of PVA and titania.

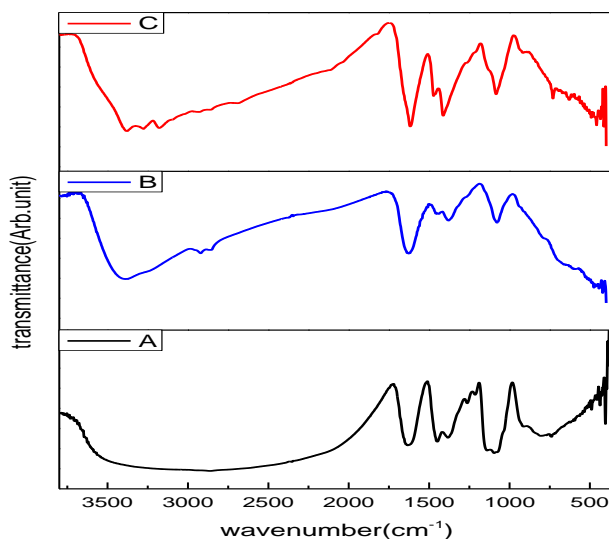


Figure 1. FTIR spectra of A) T₂, B) TPVA₂ C) TPNS₃ dried at 200 °C

3.1.2.2. X-ray diffraction (XRD) Studies

The X-ray diffraction (XRD) is a powerful method for the investigation of coatings. XRD patterns of T₂, TPVA₂ as well and TPNS₃ coatings on mild steel and corresponding dried washed powder are shown in Figure 2. The major peaks obtained for T₂ coating

on mild steel at 2θ equal to 25.53° , 38.07° , 48.36° , 54.59° , 62.88° from the planes (101), (103), (200), (105), and (213) respectively. The major peaks obtained for TPVA₂ coating on mild steel at 2θ equal to 25.45° , 38.25° , 48.23° , 54.59° , 62.88° from the planes (101), (103), (200), (105), and (213) respectively. TPNS₃ possess peaks at 2θ equal to 25.68° , 38.11° , 48.40° , 54.54° and 62.87° from the planes (101), (103), (200), (105) and (213) respectively. These results are in accordance with the data base (JCPDS No 75-1537) showing the presence of complete anatase phase of titania in the coating on mild steel for both samples.

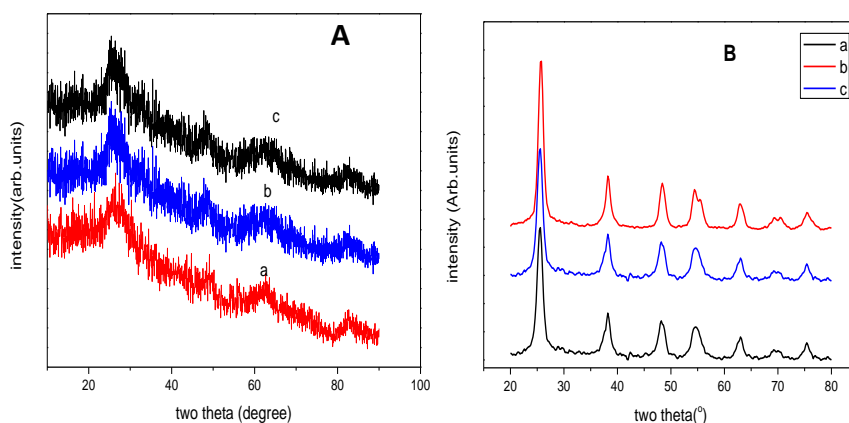


Figure 2. XRD spectra of A) a) T₂ and b) TPVA₂ c) TPNS₃ coating on mild steel dried at 200 °C and B) corresponding powder sample.

3.1.3.3. UV absorbance spectra

The diffuse reflectance spectra of the prepared samples are shown in Figure 3. The strong absorption in the 200–400 nm region is the characteristic peak of TiO₂ which confirms the presence of TiO₂ in the coating. Although all samples have broad absorption in the UV/Vis

range, the absorption edge of TPVA₂ and TPNS₃ sample in figure clearly exhibits a red shift and the same indicates the reduction of band gap of the material due to the presence of PVA and thiourea in the coating. The bandgap energy of T₂,TPVA₂ and TPNS₃ coatings calculated from Tauc plot are 2.4 eV, 2.1 eV and 1.8 eV respectively. The mixing of p orbital of non- metal elements in thiourea molecule with the 2p orbital of O in titania could reduce the band gap energy of TiO₂ [54]. The lower value of band gap energy would render good inhibition efficiencies since the energy to remove an electron from the highest occupied orbital(HOMO) will be minimized [57].

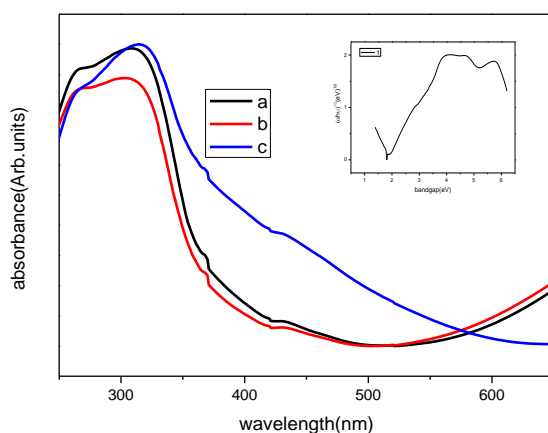


Figure 3.UV-Vis spectra of a) T₂ and b) TPVA₂ c) TPNS₃ dried at 200 °C inset Tauc plot of TPNS sample

3.1.3.4. FT Raman Analysis

Raman spectroscopic technique also used to confirm further the formation of titania and its phase transformations. The Raman spectra of the T₂,TPVA₂ and TPNS₃ powders are shown in Figure 4.The anatase phase and the rutile phase have different Raman active modes

[58]. The four peaks shown by each sample are due to the anatase phase. Anatase peaks were identified at values of 144, 395, 514 and 639 cm^{-1} [59]. The results of Raman spectroscopy are consistent with XRD data.

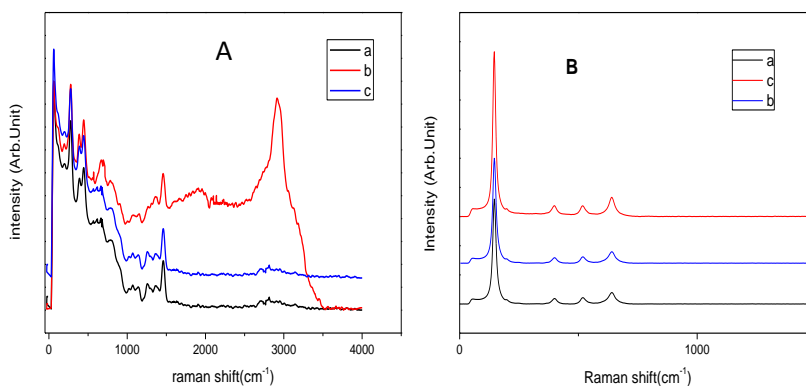


Figure 4. FT Raman spectra of a) T₂ and b) TPVA₂ c) TPNS₃ coating on mild steel dried at 200 °C and B) corresponding powder sample.

3.1.3.5. SEM /EDAX Analysis

Figure 5 shows FESEM image of T₂, TPVA₂ and TPNS₃ coated mild steel. It is clear that there are visible cracks for T₂ coating which results for the corrosion of mild steel on prolonged use. There were no cracks on the TPVA₂ and TPNS₃ coated mild steel surface. The TPVA₂, TPNS₃ nanocomposite exhibit flower like hierarchical distribution and are uniformly covered over the entire surface. The coated surface is more homogeneous and there are no pores and it is difficult to enter water or other ions responsible for corrosion of mild steel. These types of compact arrangement of particles results in better surface coverage, strength and toughness which resist nucleation, extension of micro cracks, and other corrosive ingredients through coating which was delayed. The self-healing ability developed by the

incorporation of thiourea inhibitor in toTPVA₂ and reduces penetrable damage of localized corrosion. Rough morphology of particles ensures their good adherent nature to the coating matrix and their shape guarantees stable storage of thiourea inhibitor. The stable adherent nature of the coating contributed to a large extent in the protection of mild steel from corrosion. Although the EDAX spectra don't supply information about chemical state of these elements, we can expect that Ti present as oxides and some additional peaks of C and N are also present which could be due to the presence of organic part in the reagents; oxygen is also present in organic polymers as hydroxyl (–OH) groups or oxides from TiO₂. The basic coating contains Ti along with Fe peaks which show that the steel specimen covered with titanium oxide. The presence of N and S along with Ti in TPNS₃ coated sample indicates the presence of thiourea in the coating as shown in Figure 5.

3.1.3.6. Surface Characterizations after Corrosion test

To observe the morphological changes on the mild steel surface during the corrosion process, FESEM/EDAX studies were carried out. Mild steel specimens were screened after 70 days of exposure in 1M HCl. FESEM micrographs of TPNS₃ coated mild steel samples after 70 days immersion in 1M HCl solution is shown in Figure 5. The results of % weight loss obtained during this period for TPNS₃ coating is shown in the Figure 8. The enhanced corrosion protection of TPNS₃ coating on mild steel was mainly due to the presence of hybrid PVA-titania and electron donating nature of thiourea molecule. This forms stable protective layer on the metal surface and offer significant physical barrier against the attack of corrosive ions.

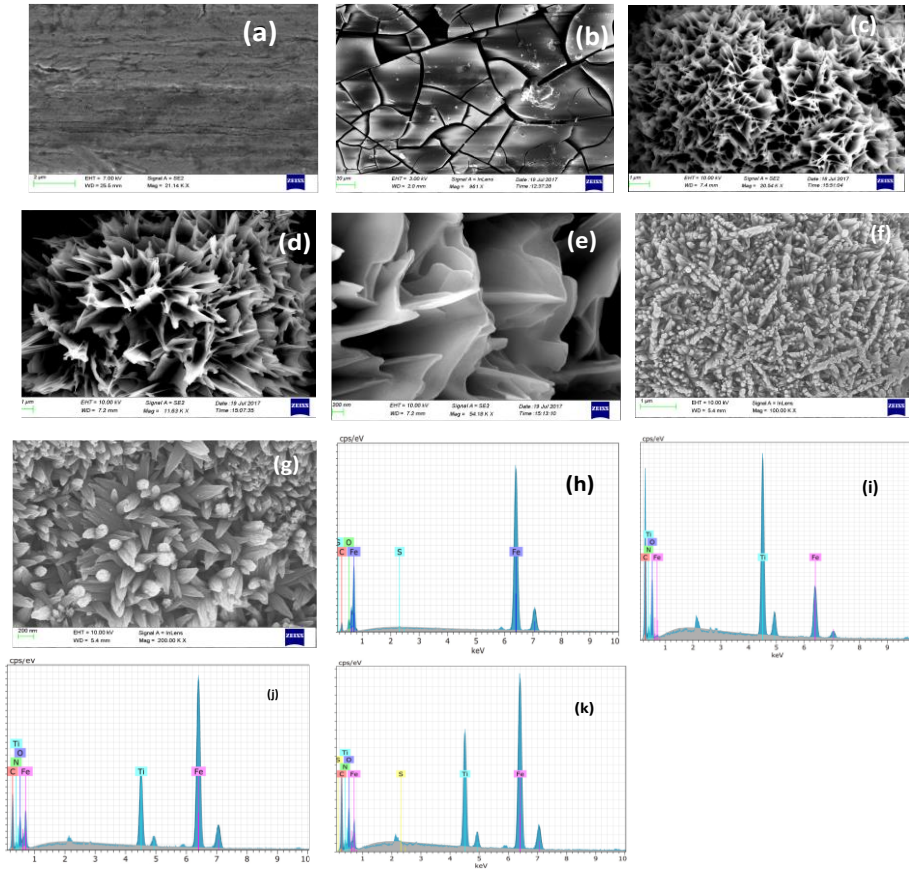


Figure 5.FESEM image of a) b are b)T₂, c - e)TPVA₂ f-g)TPNS₃ coated on mild steel at different magnification and EDAX image of h) bare and i) T₂ and j) TPVA₂ and k) TPNS₃ coated on mild steel

As evident from FESEM in Figure 5, before coating the mild steel surface shows cracks and the surface was self-healed after TPNS₃ coating even after it is immersed in 1M HCl for many days. Although the coating was exposed in acid solution for long period of immersion, the protective layer is intact. Corresponding EDAX spectra after long term immersion are shown in the Figure 6. The spectrum shows additional lines, demonstrating the existence of Ti and N for samples.

It is clearly seen that even after 70 days of exposure, mild steel surface get protected with the titania coating.

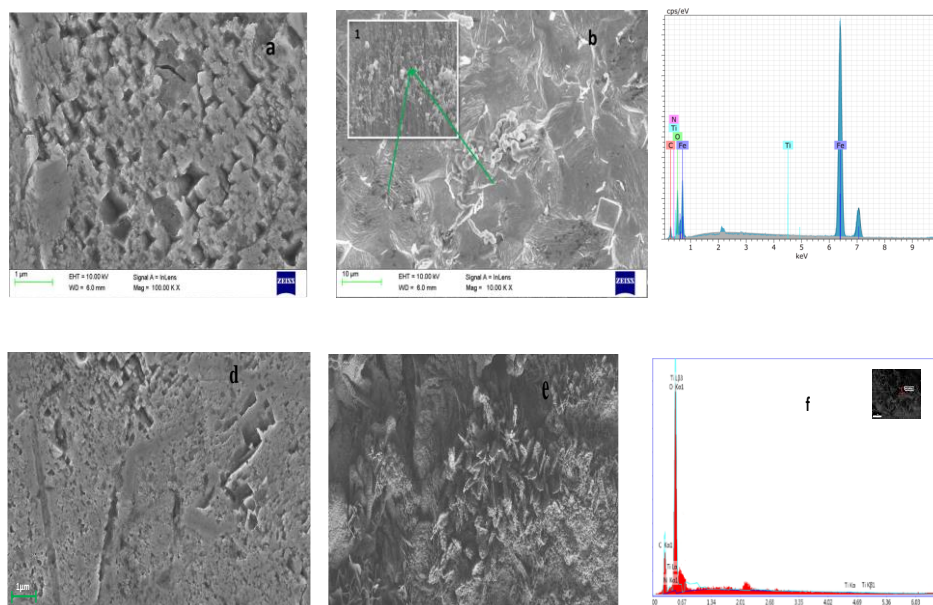


Figure 6.FESEM image of a) the damaged mid steel surface b) TPNS₃ coating on mild steel and c) EDAX spectra immersed in 1M HCl after 70 days d)The damaged mid steel surface e) TPVA₂ coating on mild steel and f) EDAX spectra immersed in 3.5wt % NaCl after40 days

3.1.3.7. AFM Analysis

The 3D AFM images showing the surface topography of coatings are represented in Figure 7. The root mean square (rms) surface roughness value obtained from the images for bare mild steel, T₂, TPVA₂, and TPNS₃ coated samples are 0.23 μm, 0.4 μm, 0.28 μm, and 0.33 μm respectively. The AFM surface analysis of coatings compared to bare mild steel reveals that the addition of nanoparticles into the matrix leads to increase in surface roughness. This is

understood as the existence of nanoparticles into mild steel matrix hinders the free movement of the AFM tip [60]. The TPNS₃ and TPVA₂ coated mild steel surface was found to be spiky in nature favors the flower like surface obtained from FESEM image.

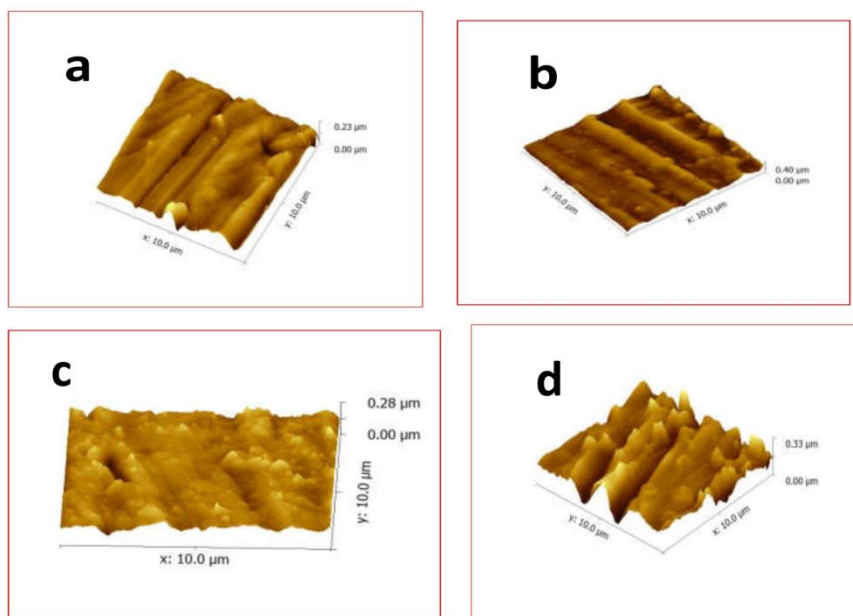


Figure 7 AFM image showing the surface topography a) bare mild steel b) T₂ and c) TPVA₂ d) TPNS₃ coatings on mild steel

3.3. Corrosion studies in HCl media

3.3.1. Weight loss study results

Weight loss technique being the oldest, easiest and most reliable method is considered as the “gold standard” corrosion testing. After each regular intervals of time, 1, 4, 8, 12, 16, upto 70 days the metal was taken out from the acid, rubbed and cleaned as per ASTM recommendations, washed with ethanol and distilled water, cleaned, dried and weight loss was measured. Weight loss results of TPVA₂ and

TPNS₃ coatings to 70 days with T₂ coating is given in Figure. 8 A. The TPVA₂ and TPNS₃ coating on metal surface do offer attractive protection efficiency on extending the exposure period in 1M HCl to 70 days, as evident from the weight loss studies, which is far superior to the conventional sol-gel coatings which losses efficiency day by day. The percentage weight loss of TPVA₂ coating from 5 to 40 days is below 30% and reaches upto 50% after 70 days. For TPNS₃ coatingthe weight loss is below 10% up to 40 days and increased up to 25% weight loss is after 70 days. The EDAX of TPNS₃ coated specimen immersed in 1M HCl for 70 days is given in figure 8 B.

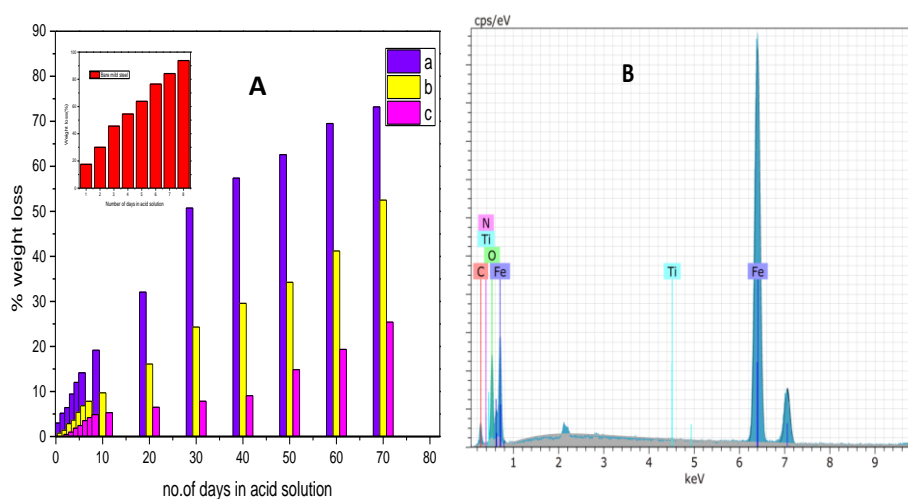


Figure 8.A) Weight loss results of a)T₂ b) TPVA₂ and c)TPNS₃ (inset: bare mild steel in 8 days) and B) EDAX of TPNS immersed in 1M HCl for a period of 70 days

3.3.2. Electrochemical Impedance Spectroscopic (EIS) measurements

The electrochemical method is an efficient and convincing tool for analyzing the corrosion behavior of metals. While EIS techniques are used to estimate the electrochemical interactions between the metal surface and electrolyte solution, DC techniques are used to provide details on corrosion rate and pitting susceptibility and to determine the electrochemical process of the cell [61].

The coating resistance or impedance varies according to applied frequency and the responses are presented as Nyquist and Bode plots. To determine the impedance parameters for bare and modified samples the corresponding equivalent patterns in HCl are fitted with Zsimp Win software. The experimental EIS data for bare samples are well fitted by the equivalent circuit pattern in Figure 9. In this R_{sol} , Q_1 , and R_{ct} respectively denotes the electrolyte resistance, electric double layer capacitance, and charge transfer resistance, and the equivalent circuit pattern for modified samples are well fitted in Figure 9 b. Among them, R_{sol} , R_c , Q_2, C_{dl} , and R_{ct2} represents the electrolyte resistance, coating resistance, coating capacitance, double layer capacitance and charge transfer resistance at the substrate/coating interface in corrosion regions respectively. The pictorial representation of corrosion mechanisms is shown in the Figure 9 c and Figure 9 d.

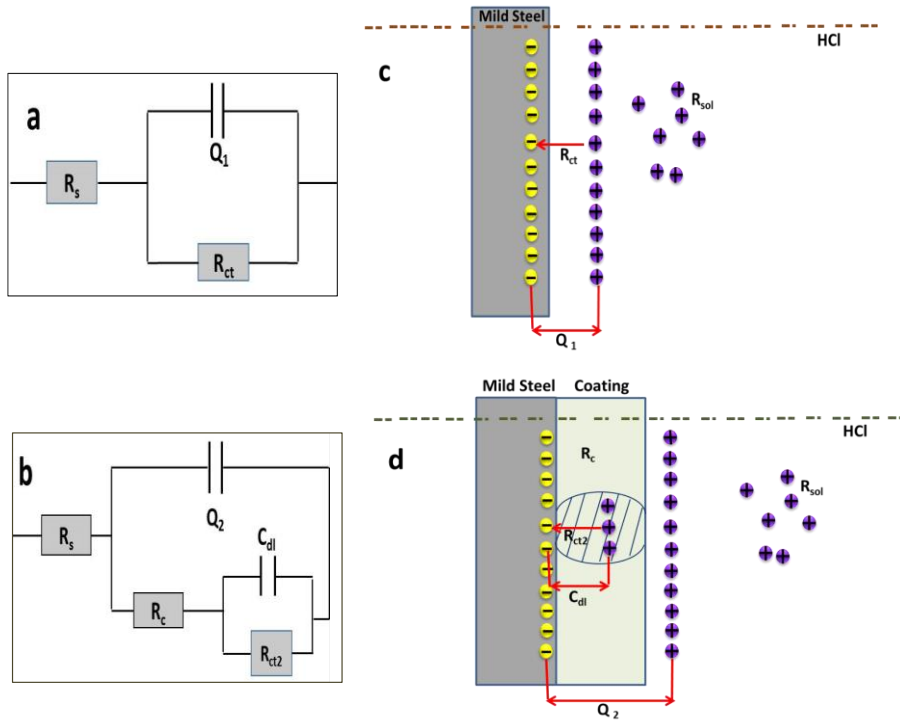


Figure 9. Proposed Equivalent circuit model and corrosion mechanisms for a) &c) bare b) &d) modified samples.

After data fittings, the obtained impedance parameters and corresponding plots are presented in Tables (1,2,3) and Figure (10,11,12). The general shape of the curves is very similar for all samples and only one capacitive loop appears for each of the samples. The shape of the capacitive loops suggests that the charge transfer controls the corrosion of mild steel at E_{corr} [62]. Larger capacitive loops are observed for the coated samples compared to the bare mild steel substrate. The capacitive loop is supposedly linked to the EIS response of the corrosion process occurring at the titania or titania-PVA-

thiourea mild steel interface. From the charge transfer resistance obtained by fitting an equivalent circuit, inhibition efficiency was calculated by the equation

$$IE \% = \frac{R_{Ct}^* - R_{Ct}}{R_{Ct}^*} \times 100 \quad (1)$$

where R_{Ct} and R_{Ct}^* represents the charge transfer resistance for the bare and coated mild steel samples.

The charge transfer resistance (R_{ct}) is able to yield information regarding the rate of the corrosion process occurring at the metal substrate beneath the coating. An analysis of the data presented in Table(1,2,3) shows that, the values of Q decreased while the values of protection efficiency increased. Further inspection of the data shows that the values of C_{dl} decreased while inhibition efficiency increased. Usually, the uniform and thick coatings behave as an insulator with high resistances and low capacitances, the C_{dl} values were decreased, this decrease in C_{dl} values could be resulted from a decrease in local dielectric constant and/or an increase in the thickness of the electrical double layer. The presence of a single semicircle in the Nyquist plots indicates that the corrosion process of T_2 , $TPVA_2$ and $TPNS_3$ coatings include a single time constant.

3.3.2.1. Effect of electrolyte concentration on corrosion behavior

The effect of electrolyte concentration 0.5M, 1M, 1.5M of HCl solution on coated samples were investigated. From the data in Table 1 and Figure. 10, it can be concluded that coated sample in 1M solution exhibits better corrosion resistance than others. It is really expected that the efficiency decreases on increasing acid concentration. But in

1M HCl solution the inhibition efficiency is higher compared to 0.5 M solution and thereafter decreases towards 1.5M as shown in Table.

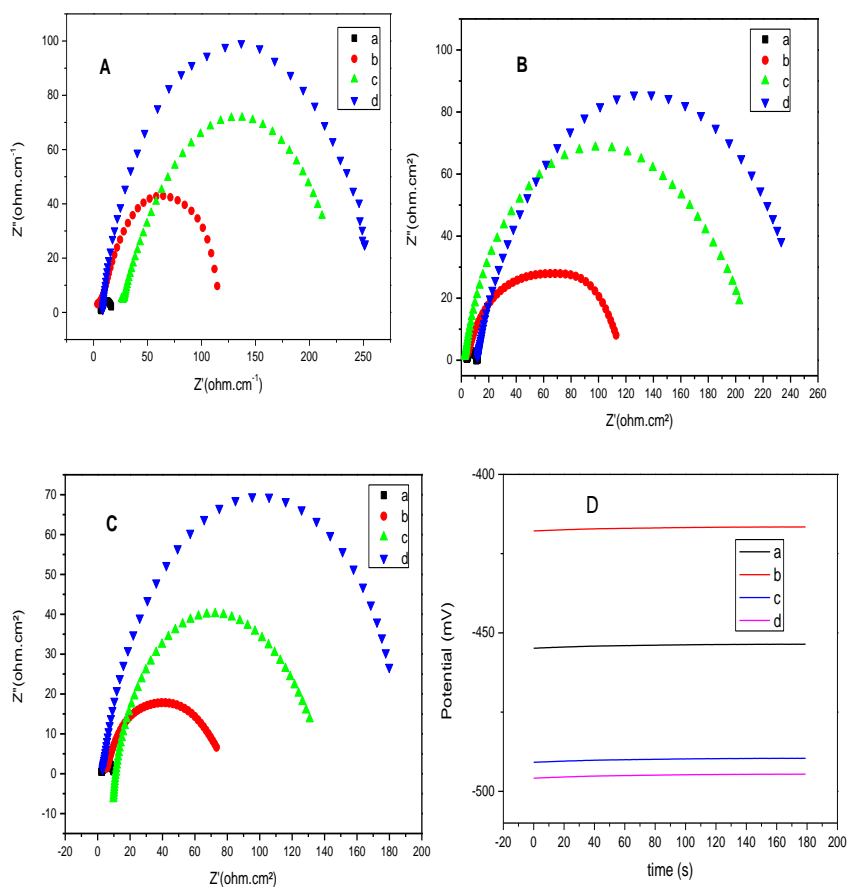


Figure 10. Nyquist plots for a) bare mild steel b) T_2 c) $TPVA_2$ d) $TPNS_3$ in A) 0.5 M HCl B) 1M HCl and C) 1.5M HCl D) Open circuit potential (OCP) against time curves a) bare mild steel b) T_2 c) $TPVA_2$ d) $TPNS_3$ coating in 1M HCl solution on mild steel at 35°C .

Table 1 Electrochemical impedance parameters for T₂, TPVA₂ and TPNS₃ coatings on mild steel for different concentration of electrolyte

Sample code	Concentration of acid(M)	Rs(Ωcm^2)	Q($\mu\text{F}/\text{cm}^2$)	Rc(Ωcm^2)	Cdl($\mu\text{F}/\text{cm}^2$)	Rct(Ωcm^2)	IE %
Bare mild steel	0.5	1.8	695	-	-	15.7	
	1	3.85	876.74		-	7.77	
	1.5	0.92	1258	-	-	6.8	
T ₂	0.5	1.9	267.3	29.88	49.52	130	88.53
	1	3.24	311.5	26.17	68.35	102.9	92.44
	1.5	2.9	342.2	8.9		60.9	88.80
TPVA ₂	0.5	21.9	296.9	23.2	15.4	222.7	91.60
	1	1.8	167	22.5	5.4	191.5	95.94
	1.5	11.6	373.8	17.5	6.57	121.1	94.30
TPNS ₃	0.5	3.99	119.6	50.5	6.8	266.3	94.10
	1	3.81	113.15	78.12	7.31	254.3	97.00
	1.5	2.5	137	20.5	3.66	173.3	96.10

3.3.2.2. Effect of drying temperature of coatings on corrosion behavior

For comparison, the effect of drying temperature at 100°C, 200°C and 300 °C of coated samples were investigated in 1 M HCl solution. From the data in Table 2 and Figure 11, it is clear that coated sample dried at 200°C shows better corrosion resistance than others. The R_{ct} values obtained for coated samples first increases from temperature 100°C to 200°C thereafter decreases towards 300°C as in Figure 11. The decrease in R_{ct} as well as efficiency above 300°C may be due to the degradation of organic part from the surface.

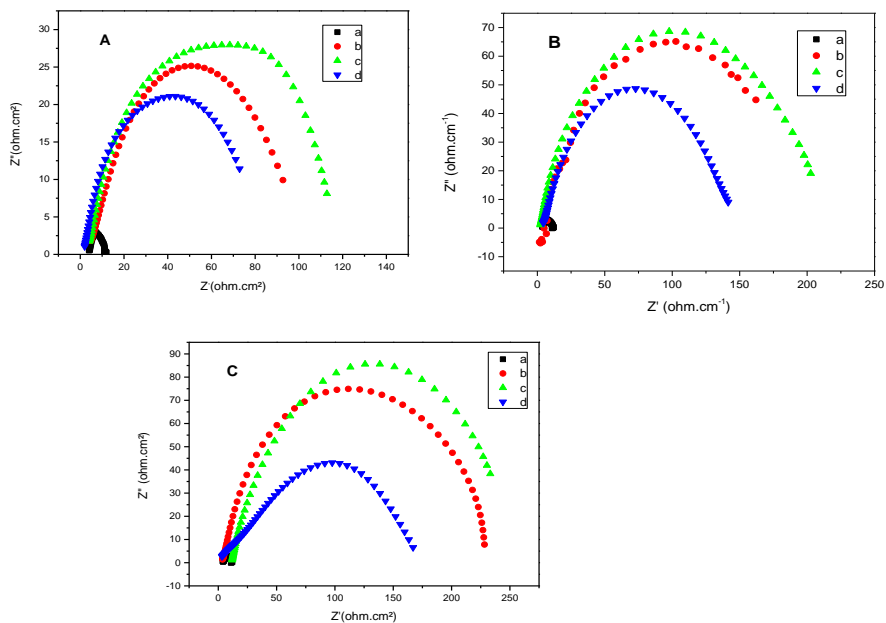


Figure 11 Nyquist plots of a) bare mild steel b) 100 °C c) 200 °C d) 300 °C A) T₂; B) TPVA₂ C) TPNS₃ coated on mild steel in 1M HCl

Table 2 Electrochemical impedance parameters for T₂, TPVA₂ and TPNS₃ coatings on mild steel for different drying temperature

Sample code	Calcination temperature(°C)	R _s (Ωcm ²)	Q(μF/cm ²)	R _c (Ωcm ²)	Cdl(μF/cm ²)	R _{ct} (Ωcm ²)	IE %
Bare mild steel		3.85	876.4	-	-	7.77	
T ₂	100	3.85	450.2	12.32	73.8	96.8	92.04
	200	3.24	311.5	26.17	68.35	102.9	92.44
	300	1.91	581.3	4.15	105.8	81.7	90.50
TPVA ₂	100	1.82	110	42.4	25.52	183.5	95.40
	200	1.8	167	12.5	22.4	191.5	95.94
	300	3.42	216.3	16.1	26.96	127.4	93.90
TPNS ₃	100	3.44	197.0	39.61	9.46	230.4	96.66
	200	3.81	113.15	78.12	7.31	254.3	97.00
	300	4.32	237.1	28.81	29.22	177.5	95.62

3.3.2.3. Effect of PVA loading in TiO₂ coatings on corrosion behavior

From the Figure 12, it was found that as the weight of PVA increases from 0.2 g to 0.3 g an increasing tendency of Rct value was observed while further addition of 0.4 g leads to decrease in Rct value. It can be inferred that there is an optimum amount for beneficial effects of loading PVA on corrosion resistance, while higher loading percentage of PVA in the sol-gel coating leads to the formation of a fragile film with poor barrier properties. It can be concluded that, the increasing of defects and cracks will be negatively affected on the formed sol– gel layer[11]. So that an optimum amount (0.3 g) of PVA in titania has chosen for thiourea loading.

3.3.2.4. Effect of thiourea loading on corrosion behavior

The data in Table 3 and Figure 12 B also showed that, protection efficiency was increased with increasing the thiourea loading whereas, C_{dl} values were decreased. From Figure 12 it is clear that the inhibitor thiourea in titania-PVA enhances the efficiency to a great extent. As the amount of inhibitor in the nanocomposite increases, the efficiency also increases. At a concentration of 1 w % thiourea efficiency is 96 % and increases to 96.8% at 1.4 w% and further addition of thiourea (1.8 w%) will not increase the efficiency significantly (97%) and the inhibitor limit is reached in the composite. Corrosion inhibition efficiency for different coatings is in the order TPNS₁ < TPNS₂ ≈ TPNS. This means the corrosion protection property is depend on the composition of coatings. It can be inferred that there is an optimum percent of thiourea loading for beneficial effects on the corrosion resistance. Thus, the results of the study reveal that the

addition of thiourea causes considerable increase in the corrosion inhibition potential of titania -PVA sol-gel coating by preventing the electrolytic diffusion. Ordinarily, the coating materials have to save the metal substrate from the corrosive medium by forming a complete separation barrier and no electrochemical reaction occurs at the coating – mild steel interface. These results were affirmed by SEM studies which discussed earlier. Bode plots (frequency vs phase angle) of coated samples having different drying temperatures and compositions are shown in Figure 12 C. The plots of all coated samples show onetime constants indicating the formation of a dense and uniform coating on the mild steel surface. Hence it is evident that the T and TPNS coatings offer substantive charge transfer resistance in 1M HCl.

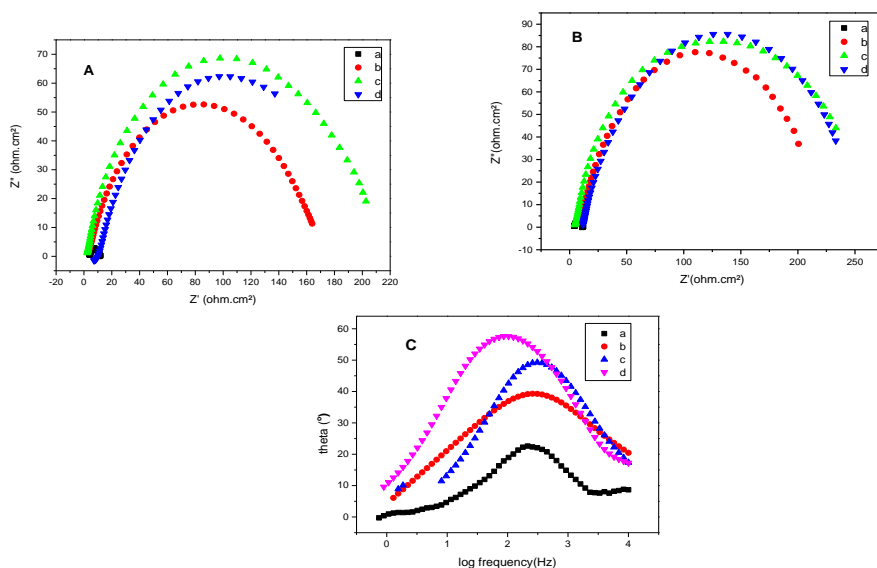


Figure 12. Nyquist plots for A) a) bare mild steel b) TPVA₁ c) TPVA₂ d) TPVA₃ B) a) bare mild steel b) TPNS₁ c) TPNS₂ d) TPNS₃ C) Frequency vs phase angle plots for a) bare mild steel b) T₂ c) TPVA₂ d) TPNS₃ coated on mild steel dried at 200°C in 1M HCl

Table 3 Electrochemical impedance parameters for T₂, TPVA₂ and TPNS₃ coatings on mild steel for different PVA and thiourea loading

Sample code	Rs(Ωcm^2)	Q($\mu\text{F}/\text{cm}^2$)	Rc(Ωcm^2)	Cdl($\mu\text{F}/\text{cm}^2$)	Rct(Ωcm^2)	IE %
Bare mild steel	3.850	876.4	-	-	7.77	
T	3.24	311.5	26.17	68.35	102.9	92.4
TPVA ₁	1.2	218	11	26.9	128	93.9
TPVA ₂	1.8	167	12.5	22.4	191.5	95.9
TPNS ₃	7.8	198	14.06	25.7	130.4	93.5
TPNS ₁	5.37	148	43.02	13.64	197	96.0
TPNS ₂	4.25	143	53.24	7.12	246.3	96.8
TPNS ₃	3.81	113	78.12	7.31	254.3	97.0

3.3.3. Potentiodynamic polarization study (PDS)

PDS gives useful information on various corrosion parameters such as corrosion current densities (I_{corr}), Tafel constants (β_a and β_c) and corrosion potential (E_{corr}) [63]. Figures 11&12 shows the results of potentiodynamic polarization parameters calculated by the Tafel extrapolation method and Table 4&5 gives the corresponding electrochemical parameters.

As can be seen from the Table 4& 5, the Tafel constant β_a is related to the dissolution of metal which occurs at the anodic region and β_c is associated with the reduction of oxygen taking place at the cathodic region [64]. The random change in both β_a and β_c values indicates the blocking of anodic and cathodic active sites by the coating of nanocomposite over the mild steel surface. There is a drastic decrease in I_{corr} value for TPVA₂ and TPNS₃ coatings, when compared to those of bare and T coatings. This confirms the protection of the metal surface from corrosion by the coated material.

The corrosion inhibition efficiency was calculated using the equation

$$IE \% = \frac{I_{Corr}^* - I_{Corr}}{I_{Corr}^*} \times 100 \quad (2)$$

where I_{Corr}^* and I_{Corr} represents the corrosion current density of the blank and coated mild steel.

From the data in Table 4 and Figure 13, it is clear that coated sample dried at 200°C shows better corrosion resistance than others. The I_{Corr} values obtained for T₂, TPVA₂ and TPNS₃ coated samples show declining trend from temperature 100°C to 200°C and thereafter increases towards 300°C.

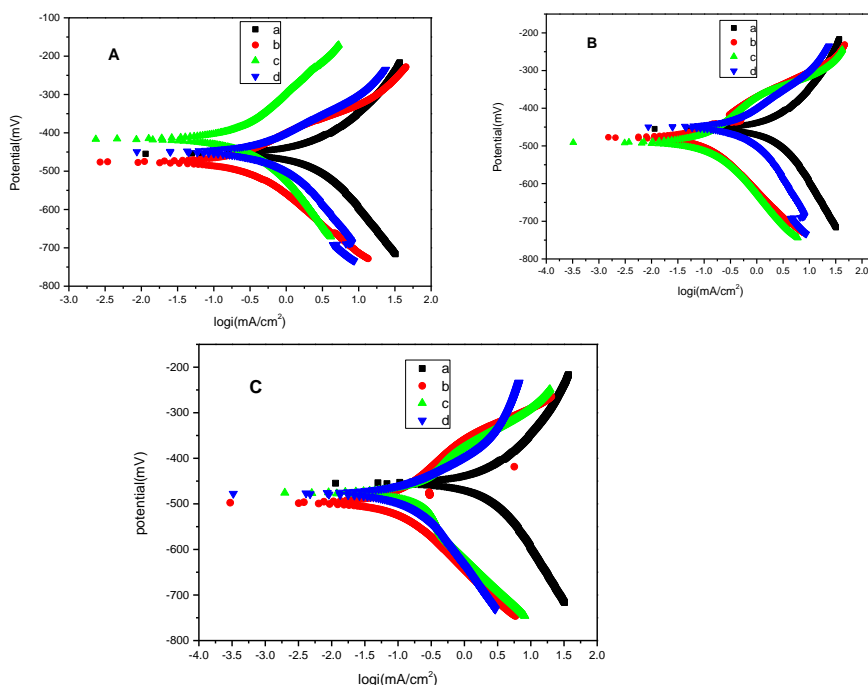


Figure 13. Tafel plots for a) bare mild steel b) 100 ° C c) 200 ° C d) 300 ° C A) T₂; B) TPVA₂ C) TPNS₃ coated on mild steel in 1M HCl

Table 4 Potentiodynamic polarization parameters for T, TPVA₂ and TPNS₃ coatings on mild steel for different drying temperature

Sample code	Calcination temperature (°C)	-ECorr(mV)	ICorr(mA/cm ²)	βa(mV/dec)	βc(mV/dec)	IE %
Bare mild steel		455.5	2.31	171.84	222.56	
T	100	474.17	0.280	95.32	150.61	87.8
	200	416	0.211	167.45	143.27	90.9
	300	450.78	0.323	101.56	100.36	86.0
TPVA ₂	100	460	0.148	96.25	142.8	93.5
	200	492	0.13	93.63	157.65	94.4
	300	448	0.212	100.2	110.8	90.8
TPNS ₃	100	473.2	0.138	87.34	167.16	94.0
	200	495.2	0.087	132.04	139.03	96.2
	300	410	0.154	107.92	84.86	93.3

Also, from the data in Table 4 and Figure 14, it is clear that coated samples show better corrosion resistance than others in 1M HCl solution. The I_{corr} values obtained for T₂, TPVA₂ and TPNS₃ coated samples decreases from 0.5M to 1M HCl thereafter increases towards 1.5M.

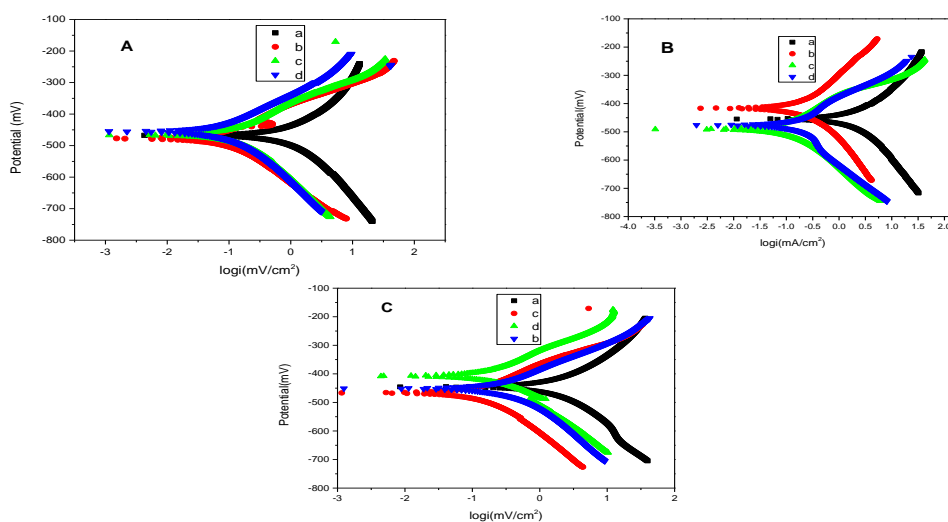

Figure.14. Tafel plots for a) bare mild steel b) T₂ c) TPVA₂ d) TPNS₃ in A) 0.5 M HCl B) 1M HCl and C) 1.5M HCl

Table 5 Potentiodynamic polarization parameters for T₂, TPVA₂ and TPNS₃ coatings on mild steel for different electrolyte concentration

Sample code	Concentration of acid(M)	-ECorr(mV)	ICorr(mA/cm ²)	βa(mV/dec)	βc(mV/dec)	IE %
Bare mild steel	0.5	469	1.25	186.9	210	
	1	455.5	2.31	171.84	222.56	
	1.5	443	2.52	162.5	183.8	
T ₂	0.5	474.1	0.280	95.32	150.61	87.8
	1	416	0.211	167.45	143.27	90.9
	1.5	450.7	0.323	101.56	100.36	86.0
TPVA ₂	0.5	468	0.1888	111.4	124.7	84.8
	1	492	0.13	93.63	157.65	94.4
	1.5	467	0.2664	118.5	191.4	89.4
TPNS ₃	0.5	473.2	0.138	87.34	167.16	94.0
	1	495.2	0.087	132.04	139.03	96.2
	1.5	410	0.154	107.92	84.86	93.3

The data in Table 6 and Figure 15 also showed that, protection efficiency was increased with increasing the PVA and thiourea loading. It can be inferred that there is an optimum percent of PVA and thiourea loading for beneficial effects on the corrosion resistance. As the amount of inhibitor in the nanocomposite increases, efficiency also increases as evident from I_{corr} values obtained. The data of polarization measurements were on line with the same acquired from EIS.

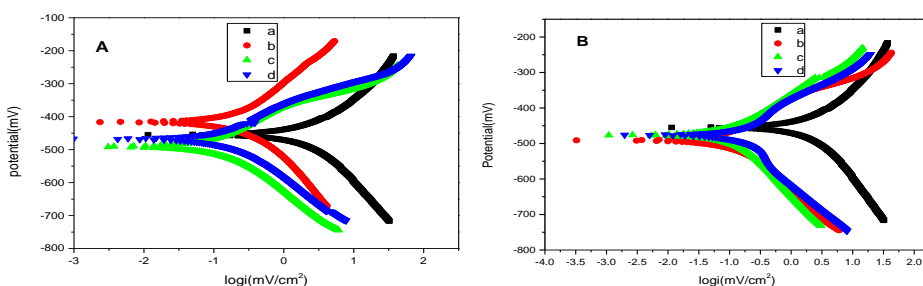


Figure 15. Tafel plots for A) a) bare mild steel b) TPVA₁ c) TPVA₂ d) TPVA₃ B) a) bare mild steel b) TPNS₁ c) TPNS₂ d) TPNS₃ coated on mild steel in 1M HCl

Table 6 Potentiodynamic polarization parameters for T₂, TPVA₂ and TPNS₃ coatings on mild steel for different PVA and thiourea loading.

Sample code	-ECorr(mV)	ICorr(mA/cm ²)	β _a (mV/dec)	β _c (mV/dec)	IE %
Bare mild steel	455.5	2.31	171.84	222.56	
T2	416	0.21	167.45	143.27	91.0
TPVA1	458	0.16	98.2	108.8	93.1
TPVA2	491	0.13	93.63	157.65	94.4
TPVA3	411	0.19	110	134.2	91.8
TPNS1	492	0.128	98.27	153.57	94.5
TPNS2	473.2	0.089	53.356	96.18	96.2
TPNS3	495.2	0.087	132.04	139.03	96.20

Thus from the EIS and PDP studies, it is confirmed that the thiourea-loaded titania-PVA nanocomposite coating enhances the protection ability of mild steel in 1M HCl compared to titania-PVA nanocomposite and bare titania.

3.4. Conclusions

- Novel, facile, low cost and environmentally benign anti-corrosion coatings titania,titania-PVA nanocomposite and titania-PVA nanocomposite with thiourea inhibitor were fabricated on mild steel, by dip-coating technique and compared.
- The structure and morphology of coatings confirmed by , Fourier Transform Infrared Spectroscopy (FTIR), Field Emission Scanning Electron Microscopy (FESEM), Energy

Dispersive X-ray Spectrometry (EDX) and Atomic Force Microscopy (AFM), DRS, XRD and Raman techniques.

- The corrosion protection behavior of these coating for mild steel in 1M HCl was evaluated by using weight loss study, EIS and polarization study.
- FESEM shows that thiourea and the modifier PVA results the cracked bare titania coating to a flower like hierarchical distribution all over the surface of mild steel. AFM analysis revealed that the surface was found to be spiky in nature with surface roughness root mean square (rms) value of 0.33 μm .
- From AFM, EDX FTIR, FESEM, XRD, UV absorbance spectra clearly indicated the presence of hybrid sol-gel coating on mild steel.
- Effect of drying temperature at 100°C, 200°C and 300°C on the corrosion protection nature of coated samples was analyzed. The coating dried at 200°C exhibit maximum corrosion protection ability.
- Corrosion studies of coatings conducted in different acid concentration 0.5 M, 1 M and 1.5 M and maximum corrosion inhibition efficiency is achieved in 1 M HCl.
- Effects of PVA loading in TiO_2 coating on corrosion efficiency have investigated. 0.3 g of PVA is found to offer better beneficial effects on corrosion resistance, while higher

loading percent of PVA in the sol–gel coating leads to the formation of a fragile film with poor barrier properties. It can be concluded that, the increasing of defects and cracks will be negatively affected on the formed sol– gel layer.

- The results of the study reveal that there is an optimum (1.8 w%) of thiourea loading for beneficial effects on the corrosion resistance and increase the efficiency significantly to 97%.
- Furthermore, TPNS coating offer excellent corrosion protection to mild steel coupons immersed in 1 M HCl solution for 70 days, which is far superior to the efficiency of conventional coatings. The T coating on mild steel surfaces on the other hand losses its efficiency day by day.
- Once localized corrosion occurs on the mild steel surface, simultaneous action of thiourea inhibitor from the composite results to form a compact molecular film with titania and PVA on the damaged surface and inhibiting corrosion spread and executing a self-healing function

Part B

3.5. Corrosion inhibition studies in 3.5 wt% NaCl solution

3.5.1. Electrochemical impedance spectroscopic studies

The EIS results obtained could be simulated by numerical fitting with Zsimp Win software using the best fit equivalent circuits as shown in Figure. 16 a and b. The experimental EIS data for bare samples are well fitted by the equivalent circuit pattern in Figure 16 a. In this R_s , Q_1 , and R_{ct} respectively denotes the electrolyte resistance, electric double layer capacitance, and charge transfer resistance. The equivalent circuit pattern for modified samples are well fitted in Figure 16 b. Among them, R_s , R_c , Q_2 , Q_{dl} , and R_{ct2} represents the electrolyte resistance, coating resistance, coating capacitance, double layer capacitance and charge transfer resistance at the substrate/coating interface in corrosion regions respectively. In these circuits, constant phase elements (CPE) have been used instead of pure double layer capacitance (Q_{dl}), because of the non-ideal character of the corresponding response[50].

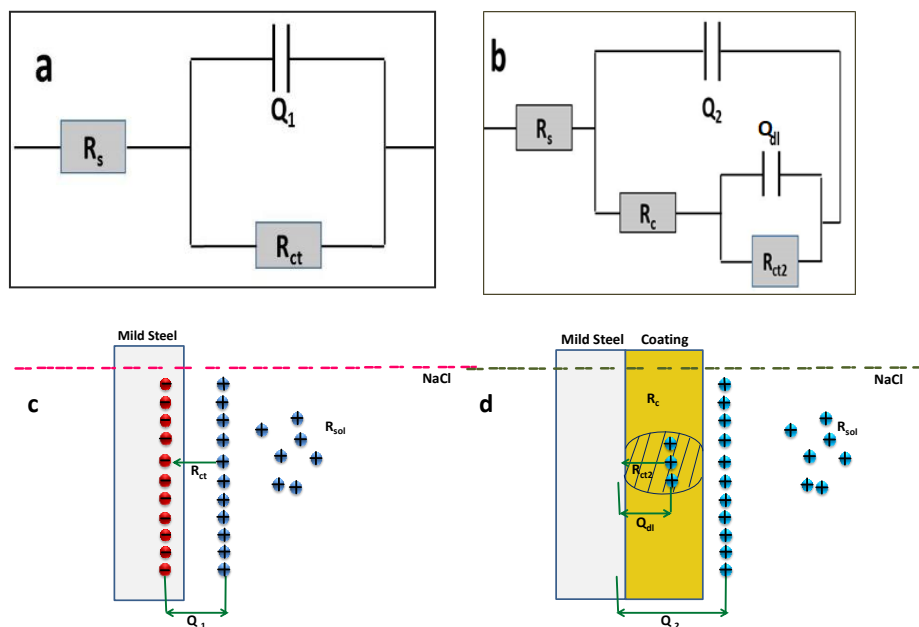


Figure 16 Proposed equivalent circuit model and corrosion mechanisms for a) & c) bare b) & d) modified samples

R_{ct} was inversely proportional to the pores and defects in the coating. The R_{ct} is used to indicate the ease of reaction with the metal when the corrosion medium reaches the metal surface. The larger the charge transfer impedance, the more difficult it is to react. Q_{dl} was formed by two layers of dissimilar charges on the surface[48]. The OCP plots are shown in the Figure 17. Nyquist plots are shown in Figures 18 A B C and D. It has been clearly found that the proposed circuit is well fitted with the EIS plot. A large R_{ct} value indicated a strong resistance against corrosion in the aggressive medium. The R_{ct} value of all coated samples are higher than bare metal which accounts for the barrier property of coating.

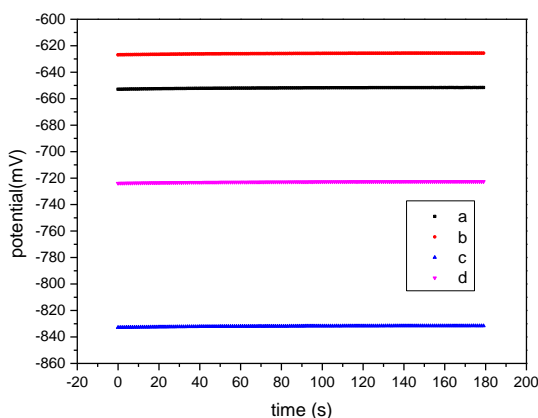


Figure 17 Open circuit potential (OCP) against time curves in 3.5 wt% NaCl solution for a) a) bare mild steel b) T₂ c) TPVA₂ d) TPNS₃ coating on mild steel at 35°C.

3.5.1.1. Effect of PVA loading on corrosion behavior

It can be seen from Figure 17 and Table 7 that the coating resistance and charge transfer resistance of coated mild steel substrates, gradually increased with increasing concentration of PVA. A high R_{ct} ($3.2 \times 10^4 \Omega \text{ cm}^2$) and low coating capacitance ($112 \mu\text{F}/\text{cm}^2$) value was obtained by TPVA₂ coating in comparison to other coated samples and the corresponding IE (%) was found to be 98.6. The result revealed that the increased loading of PVA from 10 to 20 w% in the TiO₂ matrix led to higher corrosion protection performance of the hybrid coatings with impedance modulus 2.15×10^4 to $3.26 \times 10^4 \Omega \text{ cm}^2$ but thereafter for 30 w% PVA ($1.45 \times 10^4 \Omega \text{ cm}^2$) decrease in IE (%) was observed. The order of the corrosion inhibition efficiency is as follows: TPVA₁ < TPVA₂ > TPVA₃. It can be inferred that there is an optimum amount for beneficial effects of PVA loading for corrosion resistance, while higher loading leads to the

formation of a breakable film with poor barrier properties. It can be concluded that the increasing of defects will be negatively affected on the sol– gel layer formed [11]. So, the optimum is fixed as 20 w% of PVA in TiO_2 which gives higher protection efficiency. Bode plots are shown in Figure 18 D. For coated samples unlike bare mild steel, one time constant was not observed.

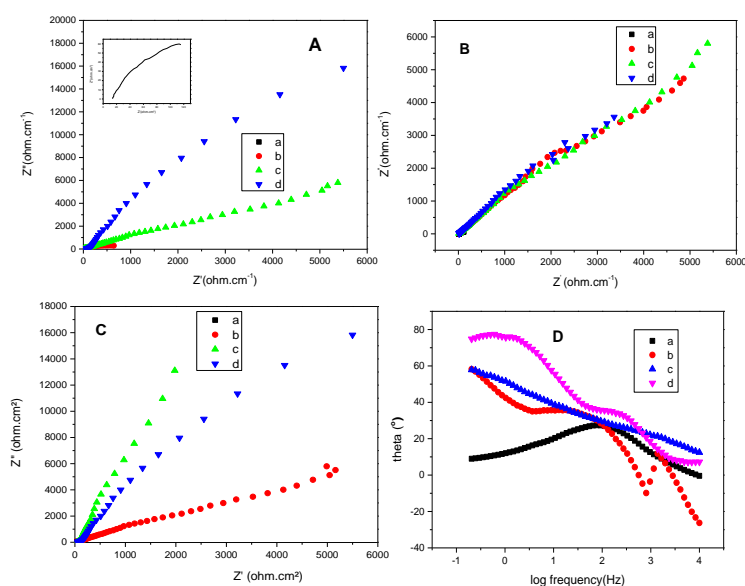


Figure 18. Nyquist plots for A) a) bare mild steel b) TiO_2 c) TPVA₂ d) TPNS₃ (inset bare mildsteel) B) a) bare mild steel b) TPVA₁ c) TPVA₂ d) TPVA₃ C) a) bare mild steel b) TPNS₁ c) TPNS₂ d) TPNS₃ D) Frequency Vs phase angle plots for a) bare mild steel b) TiO_2 c) TPVA₂ d) TPNS₃ coated on mild steel dried at 200 °C in 3.5 wt% NaCl medium at 35 °C

3.5.1.2. Effect of thiourea loading on corrosion behavior

The data in Table 6 and Figure 18 also showed that, protection efficiency was increased with increasing the thiourea loading whereas,

Q_{dl} values were decreased. From Figure 18 it is clear that the presence of thiourea in titania-PVA enhances the efficiency to a great extent. As the amount of thiourea in the nanocomposite increases, the efficiency also increases. At a concentration of 1 w% thiourea efficiency is 98.6 % and increases to 99.5% at 1.4 w% and further addition of thiourea (1.8 w%) the efficiency reaches to 99.8%. Corrosion inhibition efficiency for different coatings is in the order $TPNS_1 < TPNS_2 < TPNS_3$. Thus, the results of the study reveal that the addition of thiourea causes considerable increase in the corrosion inhibition potential of titania -PVA sol-gel coating by preventing the electrolytic diffusion.

Table 7 Electrochemical impedance parameters for blank mild steel substrate coated with T_2 , $TPVA_2$ and $TPNS_3$ composite in 3.5 wt% NaCl medium at room temperature

Sample code	$R_s(\Omega cm^2)$	$Q(\mu F/cm^2)$	$R_c(\Omega cm^2)$	$Q_{dl}(\mu F/cm^2)$	$R_{ct}(\Omega cm^2)$	IE %
Bare mild steel	1.25	458	-	-	447	
T_2	22.5	275	76	9.85	8642	94.8
$TPVA_1$	24.8	198	339.7	3.86	21548	97.9
$TPVA_2$	2.26	112	190.2	2.28	32600	98.6
$TPVA_3$	5.46	134	145.2	4.4 4	14587	96.9
$TPNS_1$	37.44	94.6	83.4	0.732	32620	98.6
$TPNS_2$	6.97	51.3	196.3	0.234	51568	99.5
$TPNS_3$	37.56	35.2	226.1	0.128	91390	99.8

3.5.1.3. Long term immersion study

Corrosion inhibition efficiency of $TPVA_2$ and $TPNS_3$ coating on mild steel in 3.5w% NaCl for 10, 20, 30 and 40 days were investigated and the obtained impedance parameters were displayed in Figure 17 and Table 6. As shown in Figure 19 and Table 7 during the 1

h – 15 days of immersion, the impedance modulus value was reduced significantly. During 15-40 days of immersion, very small amount of corrosion products occurred. As the immersion time went by, the electrolyte solution penetrated into the coating, making the anticorrosion effect of the coating reduce a little and the impedance modulus value come to be lower. Despite this, it has been found that after 40 days, the immersion efficiency was 92.8% and 96% for TPVA₂ and TPNS₃ samples suggesting better protection of coating. The corresponding FESEM and EDAX spectra were shown in Figure 4. Results of the study revealed that both coatings offer excellent long-term protection for mild steel in NaCl. But the decrease in efficiency of TPNS₃ coatings is much lower compared to TPVA₂, suggesting excellent durability of TPNS₃ coating in NaCl. The inhibitor thiourea enhances the corrosion resistance of TiO₂ –PVA composite.

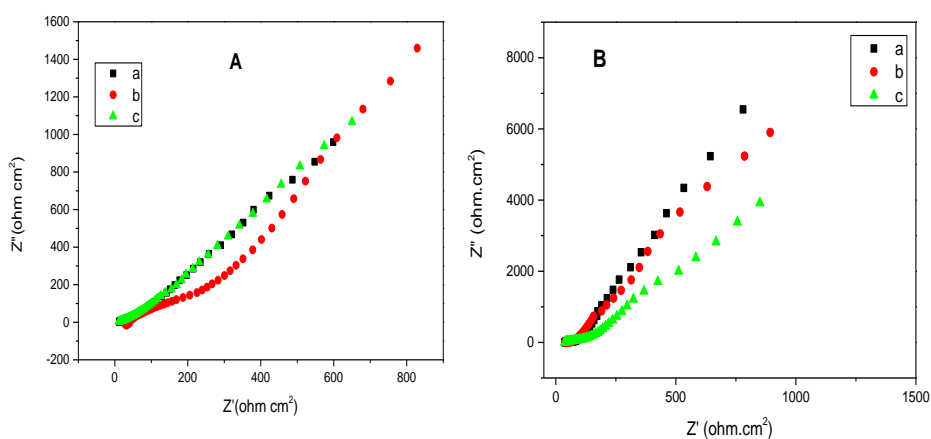


Figure 19 Nyquist plots of A) TPVA₂ B) TPNS₃ a) blank mild steel b) after 15 days c) 30 days d) 40 days immersed in 3.5 wt% NaCl medium at 35°C.

Table 8 Electrochemical impedance parameters for blank mild steel substrate coated with TPVA2 and TPNS3 in 3.5 wt% NaCl medium at room temperature during long term immersion study.

Sample code	$R_s(\Omega\text{cm}^2)$	$Q(\mu\text{F}/\text{cm}^2)$	$R_c(\Omega\text{cm}^2)$	$Q_{dl}(\mu\text{F}/\text{cm}^2)$	$R_{ct}(\Omega\text{cm}^2)$	IE %
Blank 15 days	3.89	576	-	-	259	
Blank 30 days	14.65	619	-	-	188	
Blank 40 days	8.95	654	-	-	102	
TPVA ₂ 15 days	33.68	188	616.4	2.87	6937	96.3
TPVA ₂ 30 days	6.96	221	196.3	3.92	3044	93.8
TPVA ₂ 40 days	10.94	275	244.9	4.88	1431	92.8
TPNS ₃ 15 days	34.5	146	986	1.45	16480	98.4
TPNS ₃ 30 days	42.8	174	695	2.22	9895	98
TPNS ₃ 40 days	32.9	193	398	2.95	4125	97.3

3.5.2. Potentiodynamic polarization study

Polarization curves have been widely used to predict the ability of the metallic substrates to withstand harsh corrosive environments [64]. Potentiodynamic polarization curves of coated and bare mild steel samples recorded after 60 minutes of immersion in 3.5w% NaCl are presented in Figure 20. Both cathodic and anodic polarization curves were significantly shifted to lower current densities for all coated samples as compared to the bare mild steel. The

electrochemical parameters such as corrosion potential (E_{corr}), corrosion current density (I_{corr}), corrosion rate (CR), protection efficiency (IE%), anodic and cathodic Tafel slopes (β_a , β_c) derived from the polarization curves by the extrapolation of the bare and coated mild steel substrates are summarized in Table 8.

Higher dissolution of metal ion results in increased corrosion current density (I_{corr}) which is directly proportional to the corrosion rate. The I_{corr} value is notified to be 0.2164 mA/cm^2 for mild steel substrate. As illustrated in Table 8, the I_{corr} value is decreased for all TPVA and TPNS coated mild steel compared to T_2 and bare mild steel. The decreased corrosion rate confirms that coating reduces the contact between metal and electrolyte and consequently reduces the corrosion rate. The I_{corr} value decreases, corrosion rate decreases for TPVA₂ and TPNS₃ coatings. This decrease in corrosion rate could be due to the strong bonding nature and chemical inertness of the protective coating. The I_{corr} value of TPVA₃ coating has increased when compared with TPVA₂ conforms that an optimum quantity of PVA loading is required for the beneficial effects on corrosion resistance. Among the three coatings, TPVA₂ coated mild steel shows lower I_{corr} value (0.0056 mA/cm^2) thus exhibiting a better corrosion resistance. The IE (%) obtained for TPVA₁, TPVA₂, and TPVA₃ are 95.1, 97.4, and 96.2% respectively.

The hybrid coating consists of PVA, TiO_2 and thiourea enclosed system with excellent barrier properties that obstruct the electrolyte penetration and thereby protect the metal from corrosion damage. At a concentration of 1 w% thiourea efficiency is 98.6 % and increases to 99.5% at 1.4 w % and on further addition of thiourea (1.8 w%) the efficiency reaches to 99.8%. The trends of the results of polarization studies were found to be similar to those of the EIS studies.

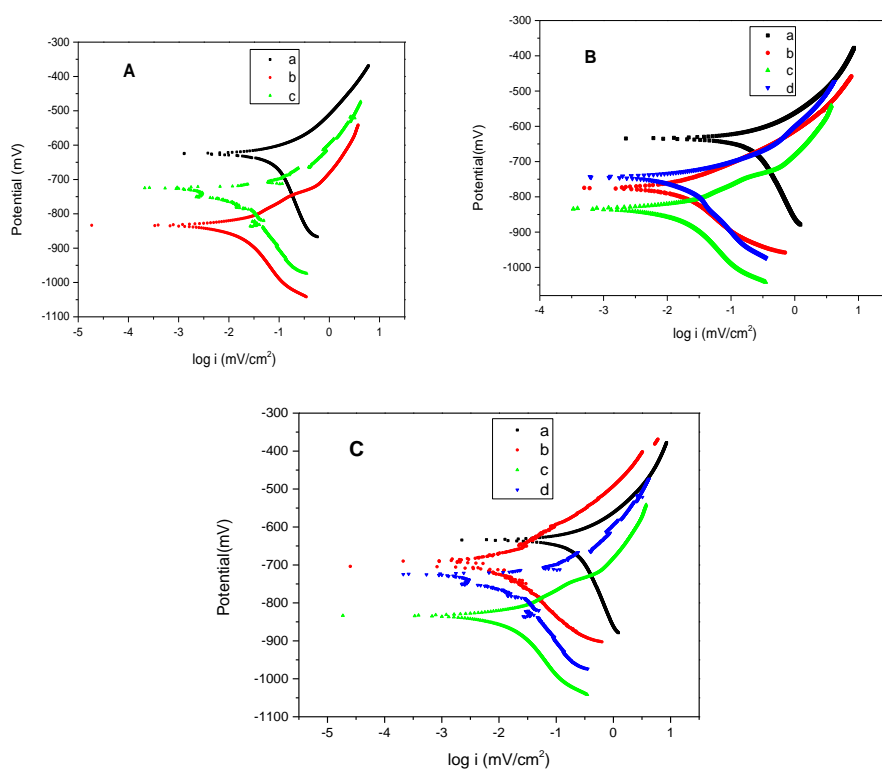


Figure 20 Tafel plots for A) a) bare mild steel b) T_2 c) TPVA_2 d) TPNS_3 B) a) bare mild steel b) TPVA_1 c) TPVA_2 d) TPVA_3 C) a) bare mild steel b) TPNS_1 c) TPNS_2 d) TPNS_3 coated on mild steel dried at 200°C in 3.5 wt% NaCl medium.

Table 9 Potentiodynamic polarization parameters for bare mild steel substrate coated with T₂, TPVA₂ and TPNS₃ composite in 3.5 wt% NaCl medium at room temperature.

Sample code	-E _{corr} (mV)	I _{corr} (mA/cm ²)	IE %	β _a (mV/dec)	β _c (mV/dec)
Bare mild steel	652	0.2164		65.3	119.9
T2	625	0.0128	93.8	128.8	72.9
TPVA1	727	0.0105	95.1	31.9	140.8
TPVA2	832	0.0056	97.4	56.7	101.6
TPVA3	774	0.0081	96.2	41.9	129.2
TPNS1	702	0.0041	98.1	81.6	98.6
TPNS2	818	0.0032	98.5	79.9	112.4
TPNS3	729	0.0024	99.2	132.2	85.2

3.5. 2. 2. Long term immersion study

Figure 20 B corresponds to the Tafel plots of TPVA₂ and TPNS₃ coated samples exposed in NaCl over time interval of 15, 30 and 40 days. For bare mild steel I_{corr} recorded at 0.3054 mA/cm² as seen from Table 9. When coated sample immersed in electrolyte for 40 days, the I_{corr} and corrosion rate decreases, and thereafter the I_{corr} value and corrosion rate increases. The coatings saved the metal from the corrosive medium by forming a barrier at the metal surface through which the movement of ions responsible for corrosion is restricted and hence the corrosion rate decreases.

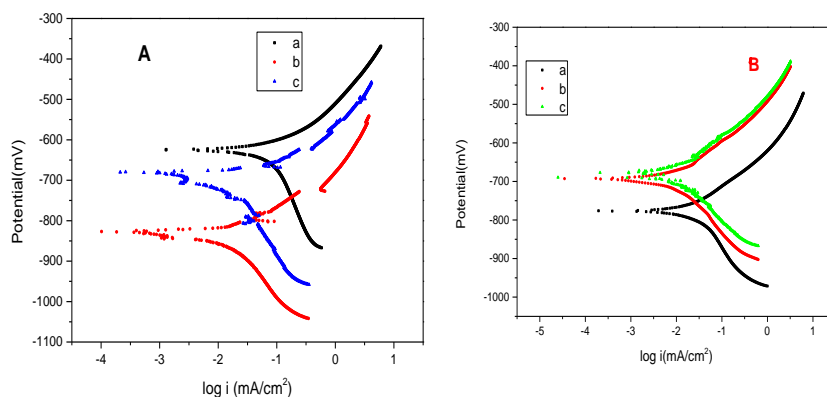


Figure 19 Tafel plots of A) TPVA₂ B) TPNS₃ a) blank mild steel b) after 15 days c) 30 days d) 40 days immersed in 3.5 wt% NaCl medium coated on mild steel at 35°C.

Table 10 Potentiodynamic polarization parameters for blank mild steel substrate coated with TPVA₂ and TPNS₃ in 3.5 wt% NaCl medium at room temperature during long term immersion study.

Sample code	-E _{corr} (mV)	I _{corr} (mA/cm ²)	IE %	β _a (mV/dec)	B _c (mV/dec)
Blank 15 days	648	0.3054		79.2	115.5
Blank 30 days	702	0.3998		95.9	100.8
Blank 40 days	664	0.4959		106.2	124
TPVA ₂ 15 days	624	0.0128	95.8	85.7	98.5
TPVA ₂ 30 days	828	0.0228	94.2	78.5	118.5
TPVA ₂ 40 days	678	0.0321	93.5	69.7	108.2
TPNS ₃ 15 days	779	0.0058	97.7	85.7	98.5
TPNS ₃ 30 days	696	0.0097	97.5	78.5	118.5
TPNS ₃ 40 days	691	0.0195	96	69.7	108.2

3.6. Corrosion protection mechanism

The probable mechanism of coating on mild steel surface is shown in Figure 16. Titanium ethoxide, after the completion of hydrolysis and condensation reactions a sol-gel network of Ti-O-Ti bonds are formed. Titania surface having large amount of OH groups on their surface thus enabling covalent bond among the components through condensation reaction. The obtained hybrid titania –PVA is capable of obtaining good adhesion to metallic surface via chemical bonding. To improve the protection ability of titania- PVA hybrid, thiourea was incorporated in to the hybrid which is electron donating in nature. The dopant added viz., thiourea gets impregnated, and on coating over metal it attaches itself to the metallic surfaces through the N atoms [50]. The enhanced protection efficiency attributed to well adhesion of sol-gel coatings on mild steel surface could be due to the formation of M-O-Ti and electronic interaction of N-M bonds. These results are consistent with the FTIR results.

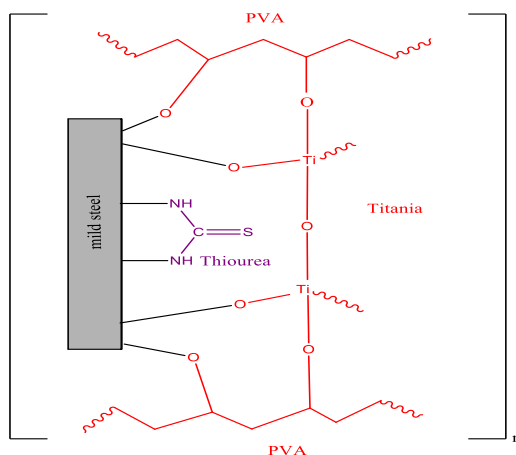


Figure 21. Pictorial representation of proposed coating mechanism on mild steel substrate

3.7. Conclusions

The corrosion protection behavior of the coatings on mild steel in 3.5 w% NaCl was evaluated by using EIS and polarization methods. Effects of PVA loading and thiourea loading on corrosion protection have also done. The results of the study reveal that PVA and thiourea loading increase the inhibition efficiency in NaCl. Among these TPVA₂ and TPNS₃ coatings shows maximum corrosion protection to mild steel coupons immersed in 3.5 w% NaCl solution. TPVA₂ and TPNS₃ coatings offered excellent protection efficiency up to 40 days, which is greater than the efficiency of conventional coatings. Without the incorporation of epoxy resins like adhesive materials TPVA₂ and TPNS₃ hybrid materials with excellent barrier performance could be coated on metal surface.

We must not wait for things to come, believing that they are decided by irrevocable destiny. If we want it, we must do something about it.

Erwin Schrodinger

References

- [1] K. Ramya, R. Mohan, K. Anupama, A. Joseph, Electrochemical and theoretical studies on the synergistic interaction and corrosion inhibition of alkyl benzimidazoles and thiosemicarbazide pair on mild steel in hydrochloric acid, *Materials Chemistry and Physics*, 149 (2015) 632-647.
- [2] K. Anupama, K. Ramya, K. Shainy, A. Joseph, Adsorption and electrochemical studies of Pimenta dioica leaf extracts as corrosion inhibitor for mild steel in hydrochloric acid, *Materials Chemistry and Physics*, 167 (2015) 28-41.
- [3] R. Mohan, K. Ramya, K. Anupama, A. Joseph, Density functional treatment and electro analytical measurements of liquid phase interaction of 2-ethylbenzimidazole (EBI) and ethyl (2-ethylbenzimidazolyl) acetate (EEBA) on mild steel in hydrochloric acid, *Journal of Molecular Liquids*, 220 (2016) 707-717.
- [4] A. Fihri, E. Bovero, A. Al-Shahrani, A. Al-Ghamdi, G. Alabedi, Recent progress in superhydrophobic coatings used for steel protection: A review, *Colloids and Surfaces A: Physicochemical and Engineering Aspects*, 520 (2017) 378-390.
- [5] M.J. Tsapakos, T. Hampton, P. Sinclair, J. Sinclair, W. Bement, K. Wetterhahn, The carcinogen chromate causes DNA damage and inhibits drug-mediated induction of porphyrin accumulation and glucuronidation in chick embryo hepatocytes, *Carcinogenesis*, 4 (1983) 959-966.
- [6] Y. Liu, D. Sun, H. You, J.S. Chung, Corrosion resistance properties of organic-inorganic hybrid coatings on 2024 aluminum alloy, *Applied Surface Science*, 246 (2005) 82-89.
- [7] T. Chou, C. Chandrasekaran, S. Limmer, S. Seraji, Y. Wu, M. Forbess, C. Nguyen, G. Cao, Organic-inorganic hybrid coatings for corrosion protection, *Journal of Non-Crystalline Solids*, 290 (2001) 153-162.
- [8] P. Zhang, T. Ge, H. Yang, S. Lin, Y. Cao, C.X. Zhao, H. Liu, A. Umar, Z. Guo, Antifouling of titania nanostructures in real maritime conditions, *Science of Advanced Materials*, 10 (2018) 1216-1223.

- [9] Y. Sheng, J. Yang, F. Wang, L. Liu, H. Liu, C. Yan, Z. Guo, Sol-gel synthesized hexagonal boron nitride/titania nanocomposites with enhanced photocatalytic activity, *Applied Surface Science*, 465 (2019) 154-163.
- [10] M. Zheludkevich, J. Tedim, M. Ferreira, “Smart” coatings for active corrosion protection based on multi-functional micro and nanocontainers, *Electrochimica Acta*, 82 (2012) 314-323.
- [11] H.M.A. El-Lateef, M.M. Khalaf, Corrosion resistance of ZrO₂-TiO₂ nanocomposite multilayer thin films coated on carbon steel in hydrochloric acid solution, *Materials Characterization*, 108 (2015) 29-41.
- [12] M. Qian, A.M. Soutar, X.H. Tan, X.T. Zeng, S.L. Wijesinghe, Two-part epoxy-siloxane hybrid corrosion protection coatings for carbon steel, *Thin Solid Films*, 517 (2009) 5237-5242.
- [13] M. Jasiorski, B. Borak, A. Baszczuk, J. Krzak-Ros, A. Łukowiak, Active oxide materials obtained by the sol-gel method: synthesis, identification, and application, *Ceramics*, 101 (2008) 175-182.
- [14] H. Cheraghi, M. Shahmiri, Z. Sadeghian, Corrosion behavior of TiO₂-NiO nanocomposite thin films on AISI 316L stainless steel prepared by sol-gel method, *Thin Solid Films*, 522 (2012) 289-296.
- [15] L. Ćurković, H.O. Ćurković, S. Salopek, M.M. Renjo, S. Šegota, Enhancement of corrosion protection of AISI 304 stainless steel by nanostructured sol-gel TiO₂ films, *Corrosion science*, 77 (2013) 176-184.
- [16] P. Jaseela, A. Joseph, Development of Flower Like Hierarchical Thiourea Loaded Titania-Poly Vinyl Alcohol Nano Composite Coatings for the Corrosion Protection of Mild Steel in Hydrochloric Acid, *Journal of Inorganic and Organometallic Polymers and Materials*, 28 (2018) 1468-1482.
- [17] M. Montemor, Functional and smart coatings for corrosion protection: a review of recent advances, *Surface and Coatings Technology*, 258 (2014) 17-37.
- [18] F. Luo, Q. Li, X. Zhong, H. Gao, Y. Dai, F. Chen, Corrosion electrochemical behaviors of silane coating coated magnesium alloy in NaCl solution containing cerium nitrate, *Materials and Corrosion*, 63 (2012) 148-154.

- [19] F. Sinapi, J. Delhalle, Z. Mekhalif, XPS and electrochemical evaluation of two-dimensional organic films obtained by chemical modification of self-assembled monolayers of (3-mercaptopropyl) trimethoxysilane on copper surfaces, *Materials Science and Engineering: C*, 22 (2002) 345-353.
- [20] H. Kang, Z. Cheng, H. Lai, H. Ma, Y. Liu, X. Mai, Y. Wang, Q. Shao, L. Xiang, X. Guo, Superlyophobic anti-corrosive and self-cleaning titania robust mesh membrane with enhanced oil/water separation, *Separation and Purification Technology*, 201 (2018) 193-204.
- [21] L.E. Palomino, I.V. Aoki, H.G. de Melo, Microstructural and electrochemical characterization of Ce conversion layers formed on Al alloy 2024-T3 covered with Cu-rich smut, *Electrochimica Acta*, 51 (2006) 5943-5953.
- [22] R. Lakshmi, G. Yoganandan, K. Kavya, B.J. Basu, Effective corrosion inhibition performance of Ce³⁺ doped sol-gel nanocomposite coating on aluminum alloy, *Progress in Organic Coatings*, 76 (2013) 367-374.
- [23] S. Cohen, Replacements for chromium pretreatments on aluminum, *Corrosion*, 51 (1995) 71-78.
- [24] W. Van Ooij, T. Child, Protecting metals with silane coupling agents, *Chemtech*, 28 (1998) 26-35.
- [25] D. Zhu, W.J. van Ooij, Corrosion protection of AA 2024-T3 by bis-[3-(triethoxysilyl) propyl] tetrasulfide in sodium chloride solution.: Part 2: mechanism for corrosion protection, *Corrosion Science*, 45 (2003) 2177-2197.
- [26] C. Ning, L. Mingyan, Z. Weidong, Fouling and corrosion properties of SiO₂ coatings on copper in geothermal water, *Industrial & engineering chemistry research*, 51 (2012) 6001-6017.
- [27] W. Van Ooij, D. Zhu, G. Prasad, S. Jayaseelan, Y. Fu, N. Teredesai, Silane based chromate replacements for corrosion control, paint adhesion, and rubber bonding, *Surface Engineering*, 16 (2000) 386-396.
- [28] M.S. Donley, R.A. Mantz, A. Khramov, V. Balbyshev, L.S. Kasten, D.J. Gaspar, The self-assembled nanophase particle (SNAP) process:

- a nanoscience approach to coatings, *Progress in organic coatings*, 47 (2003) 401-415.
- [29] M.L. Zheludkevich, D.G. Shchukin, K.A. Yasakau, H. Möhwald, M.G. Ferreira, Anticorrosion coatings with self-healing effect based on nanocontainers impregnated with corrosion inhibitor, *Chemistry of Materials*, 19 (2007) 402-411.
- [30] D. Wang, G.P. Bierwagen, Sol-gel coatings on metals for corrosion protection, *Progress in organic coatings*, 64 (2009) 327-338.
- [31] Y. Zhang, M. Zhao, J. Zhang, Q. Shao, J. Li, H. Li, B. Lin, M. Yu, S. Chen, Z. Guo, Excellent corrosion protection performance of epoxy composite coatings filled with silane functionalized silicon nitride, *Journal of Polymer Research*, 25 (2018) 130.
- [32] A. Javadi, Q. Zheng, F. Payen, A. Javadi, Y. Altin, Z. Cai, R. Sabo, S. Gong, Polyvinyl alcohol-cellulose nanofibrils-graphene oxide hybrid organic aerogels, *ACS applied materials & interfaces*, 5 (2013) 5969-5975.
- [33] R. Karthikaiselvi, S. Subhashini, Study of adsorption properties and inhibition of mild steel corrosion in hydrochloric acid media by water soluble composite poly (vinyl alcohol-omethoxy aniline), *Journal of the Association of Arab Universities for Basic and Applied Sciences*, 16 (2014) 74-82.
- [34] B. Ramezanzadeh, H. Vakili, R. Amini, The effects of addition of poly (vinyl) alcohol (PVA) as a green corrosion inhibitor to the phosphate conversion coating on the anticorrosion and adhesion properties of the epoxy coating on the steel substrate, *Applied Surface Science*, 327 (2015) 174-181.
- [35] K. Strawhecker, E. Manias, Structure and properties of poly (vinyl alcohol)/Na⁺ montmorillonite nanocomposites, *Chemistry of materials*, 12 (2000) 2943-2949.
- [36] Y. Liu, C. Hou, T. Jiao, J. Song, X. Zhang, R. Xing, J. Zhou, L. Zhang, Q. Peng, Self-assembled AgNP-containing nanocomposites constructed by electrospinning as efficient dye photocatalyst materials for wastewater treatment, *Nanomaterials*, 8 (2018) 35.
- [37] X. Luo, K. Ma, T. Jiao, R. Xing, L. Zhang, J. Zhou, B. Li, Graphene oxide-polymer composite Langmuir films constructed by interfacial

- thiol-ene photopolymerization, *Nanoscale research letters*, 12 (2017) 99.
- [38] X. Yue, L. Yingjie, L. Sha, Preparation and characterization of sol-gel coatings doping with cerium ingredients on aluminum alloy surface, *Journal of Rare Earths*, 25 (2007) 193-196.
- [39] V. Moutarlier, B. Neveu, M.P. Gigandet, Evolution of corrosion protection for sol-gel coatings doped with inorganic inhibitors, *Surface and Coatings Technology*, 202 (2008) 2052-2058.
- [40] F. Brusciotti, A. Batan, I. De Graeve, M. Wenkin, M. Biessemans, R. Willem, F. Reniers, J. Pireaux, M. Piens, J. Vereecken, Characterization of thin water-based silane pre-treatments on aluminium with the incorporation of nano-dispersed CeO₂ particles, *Surface and Coatings Technology*, 205 (2010) 603-613.
- [41] E. Matter, S. Kozhukharov, M. Machkova, V. Kozhukharov, Comparison between the inhibition efficiencies of Ce (III) and Ce (IV) ammonium nitrates against corrosion of AA2024 aluminum alloy in solutions of low chloride concentration, *Corrosion science*, 62 (2012) 22-33.
- [42] S. Peng, W. Zhao, Z. Zeng, H. Li, Q. Xue, X. Wu, Preparation of anticorrosion hybrid silica sol-gel coating using Ce (NO₃)₃ as catalyst, *Journal of sol-gel science and technology*, 66 (2013) 133-138.
- [43] N. Subramanyam, B. Sheshadri, S. Mayanna, Thiourea and substituted thioureas as corrosion inhibitors for aluminium in sodium nitrite solution, *Corrosion Science*, 34 (1993) 563-571.
- [44] S. Edrah, S. Hasan, Studies on thiourea derivatives as corrosion inhibitor for aluminum in sodium hydroxide Solution, *J Appl Sci Res*, 6 (2010) 1045-1049.
- [45] R.B. Vignesh, M.G. Sethuraman, Corrosion protection behaviour of sol-gel derived N, N-dimethylthiourea doped 3-glycidoxypropyltrimethoxysilane on aluminium, *Progress in Organic Coatings*, 77 (2014) 136-141.
- [46] J.-C. Lin, S.-L. Chang, S.-L. Lee, Corrosion inhibition of steel by thiourea and cations under incomplete cathodic protection in a 3.5% NaCl solution and seawater, *Journal of applied electrochemistry*, 29 (1999) 911-918.

- [47] N. Karthik, M.G. Sethuraman, Surface protection of copper by allyl thiourea and hybrid sol-gel coatings, *Progress in Organic Coatings*, 90 (2016) 380-389.
- [48] X. Cui, G. Zhu, Y. Pan, Q. Shao, M. Dong, Y. Zhang, Z. Guo, Polydimethylsiloxane-titania nanocomposite coating: fabrication and corrosion resistance, *Polymer*, 138 (2018) 203-210.
- [49] J. Balaji, M. Sethuraman, Chitosan-doped-hybrid/TiO₂ nanocomposite based sol-gel coating for the corrosion resistance of aluminum metal in 3.5% NaCl medium, *International journal of biological macromolecules*, 104 (2017) 1730-1739.
- [50] R.B. Vignesh, J. Balaji, M. Sethuraman, Surface modification, characterization and corrosion protection of 1, 3-diphenylthiourea doped sol-gel coating on aluminium, *Progress in Organic Coatings*, 111 (2017) 112-123.
- [51] M. Ye, Z. Lu, Y. Hu, Q. Zhang, Y. Yin, Mesoporous titanate-based cation exchanger for efficient removal of metal cations, *Journal of Materials Chemistry A*, 1 (2013) 5097-5104.
- [52] J. Cao, M. Shen, L. Zhou, Preparation and electrorheological properties of triethanolamine-modified TiO₂, *Journal of Solid State Chemistry*, 179 (2006) 1565-1568.
- [53] X. Yuan, M. Sun, Y. Yao, X. Lin, J. Shi, N/Ti 3+-codoped triphasic TiO₂/gC₃N₄ heterojunctions as visible-light photocatalysts for the degradation of organic contaminants, *New Journal of Chemistry*, 43 (2019) 2665-2675.
- [54] F. Zahedi, M. Behpour, S.M. Ghoreishi, H. Khalilian, Photocatalytic degradation of paraquat herbicide in the presence TiO₂ nanostructure thin films under visible and sun light irradiation using continuous flow photoreactor, *Solar Energy*, 120 (2015) 287-295.
- [55] M. Dong, Q. Li, H. Liu, C. Liu, E.K. Wujcik, Q. Shao, T. Ding, X. Mai, C. Shen, Z. Guo, Thermoplastic polyurethane-carbon black nanocomposite coating: fabrication and solid particle erosion resistance, *Polymer*, 158 (2018) 381-390.
- [56] P. Hegedús, E. Szabó-Bárdos, O. Horváth, P. Szabó, K. Horváth, Investigation of a TiO₂ photocatalyst immobilized with poly (vinyl alcohol), *Catalysis Today*, 284 (2017) 179-186.

- [57] N. Karthik, M.G. Sethuraman, Improved copper corrosion resistance of epoxy-functionalized hybrid sol–gel monolayers by thiosemicarbazide, *Ionics*, 21 (2015) 1477-1488.
- [58] P. Periyat, K. Baiju, P. Mukundan, P. Pillai, K. Warriar, High temperature stable mesoporous anatase TiO₂ photocatalyst achieved by silica addition, *Applied Catalysis A: General*, 349 (2008) 13-19.
- [59] S.Y. Choi, M. Mamak, N. Coombs, N. Chopra, G.A. Ozin, Thermally stable two- dimensional hexagonal mesoporous nanocrystalline anatase, meso- nc- TiO₂: Bulk and crack- free thin film morphologies, *Advanced Functional Materials*, 14 (2004) 335-344.
- [60] A.B. Radwan, R. Shakoor, A. Popelka, Improvement in properties of Ni-B coatings by the addition of mixed oxide nanoparticles, *Int. J. Electrochem. Sci*, 10 (2015) 7548-7562.
- [61] N.P. Tavandashti, S. Sanjabi, Corrosion study of hybrid sol–gel coatings containing boehmite nanoparticles loaded with cerium nitrate corrosion inhibitor, *Progress in Organic Coatings*, 69 (2010) 384-391.
- [62] M. Morad, An electrochemical study on the inhibiting action of some organic phosphonium compounds on the corrosion of mild steel in aerated acid solutions, *Corrosion Science*, 42 (2000) 1307-1326.
- [63] M. Kendig, S. Jeanjaquet, R. Addison, J. Waldrop, Role of hexavalent chromium in the inhibition of corrosion of aluminum alloys, *Surface and Coatings Technology*, 140 (2001) 58-66.
- [64] C. Kamal, M. Sethuraman, *Spirulina platensis*–A novel green inhibitor for acid corrosion of mild steel, *Arabian Journal of Chemistry*, 5 (2012) 155-161.



Development of Flower Like Hierarchical Thiourea Loaded Titania–Poly Vinyl Alcohol Nano Composite Coatings for the Corrosion Protection of Mild Steel in Hydrochloric Acid

P. K. Jaseela¹ · Abraham Joseph¹

Received: 5 December 2017 / Accepted: 1 March 2018
© Springer Science+Business Media, LLC, part of Springer Nature 2018

Abstract

A stable, thiourea doped titania–poly vinyl alcohol (PVA) hybrid nanocomposite anticorrosion coating on mild steel has been developed via sol–gel dip-coating method. For comparative studies, bare titania sol–gel is coated over mild steel and evaluated using electrochemical methods. To investigate structure and morphology of coating, fourier transform infrared spectroscopy (FTIR), field emission scanning electron microscopy (FESEM), energy dispersive X-ray spectrometry (EDX), X-ray diffraction (XRD), UV absorbance spectra, and atomic force microscopy (AFM) techniques were employed. Effect of drying temperature of coated samples at 100, 200 and 300 °C on the corrosion protection nature was analysed. The coating dried at 200 °C exhibit maximum corrosion protection ability. Thiourea at 1, 1.4, 1.8 wt% were incorporated into titania–PVA hybrid nanocomposite and the corrosion protection ability of these sol–gel coatings were evaluated by weight loss, impedance spectroscopic studies (EIS), and polarization measurement in 1 M HCl solution. FESEM shows that thiourea and the modifier PVA results the cracked bare titania coating to a flower like hierarchical distribution all over the surface of mild steel, AFM analysis revealed that the surface was found to be spiky in nature with surface roughness root mean square (rms) value of 0.33 μm and exhibit better corrosion resistance in 1 M HCl solution. The results of the study reveal that there is an optimum (1.8 wt%) of thiourea loading for beneficial effects on the corrosion resistance and increase the efficiency significantly (97%). This simple, facile and eco-friendly method has great potential to replace environmentally hazardous chromate conversion coatings. Moreover the modified coating on metal offers attractive protection efficiency on extending the exposure period in 1 M HCl to 70 days, which is far superior to the conventional sol–gel coating which losses efficiency day by day. The protective layer consists of a compact structure of hybrid PVA–titania and electron rich thiourea molecules on the surface of the metal offering significant physical barrier against the attack of corrosive ions from acid solution.

Electronic supplementary material The online version of this article (<https://doi.org/10.1007/s10904-018-0819-6>) contains supplementary material, which is available to authorized users.

✉ Abraham Joseph
drabrahamj@gmail.com

¹ Department of chemistry, University of Calicut,
Malappuram, Kerala, India

Published online: 08 March 2018

Springer



ORIGINAL ARTICLE

Excellent protection of mild steel in sodium chloride solution for a substantial period of time using a hybrid nanocoating of poly vinyl alcohol and Titania



P.K. Jaseela ^a, Mathew Kuruvilla ^b, Linda Williams ^a, Chinju Jacob ^b,
K.O. Shamsheera ^a, Abraham Joseph ^{a,*}

^a Department of Chemistry, University of Calicut, Calicut University P O, India

^b Department of Chemistry, St Thomas College, Ranni, Pathanathitta, India

Received 29 April 2020; accepted 2 July 2020

Available online 9 July 2020

KEYWORDS

Nanocomposite;
Hybrid material;
TiO₂;
PVA;
Corrosion inhibition

Abstract The production of eco-friendly hybrid sol–gel coatings for long term protection of metallic substrates from aggressive environments was one of the emerging areas, competing with conventional chromate and phosphate coatings. Herein, a nanocomposite has been synthesized from TiO₂ and PVA through a novel sol-gel route and the structure and morphology of the same was characterized using X-ray diffraction, FTIR, UV–Vis spectroscopy, FESEM with EDAX, and AFM studies. The flower-like structured composite offers excellent corrosion protection properties in NaCl solution of sea water salinity. Impedance and polarization studies were carried out to monitor the anticorrosion performance of the materials coating. This coating on mild steel offers 98% inhibition efficiency in NaCl. The influence of loading PVA on TiO₂ and its effect on corrosion efficiency have also been investigated. It is found that an optimum weight of 20 wt% PVA is required in the composite for beneficial corrosion resistance. 92% inhibition efficiency is registered by the coated MS in NaCl solution after 40 days of exposure and is quite encouraging compared to many of the recent reports. The Ti–O–Ti, and Fe–Ti–O linkage along with compactness and adherence of the material together contribute to better blocking of steel corrosion.

© 2020 The Author(s). Published by Elsevier B.V. on behalf of King Saud University. This is an open access article under the CC BY-NC-ND license (<http://creativecommons.org/licenses/by-nc-nd/4.0/>).

* Corresponding author.

E-mail address: abrahamjoseph@uoc.ac.in (A. Joseph).

Peer review under responsibility of King Saud University.



Production and hosting by Elsevier

<https://doi.org/10.1016/j.arabjc.2020.07.005>

1878-5352 © 2020 The Author(s). Published by Elsevier B.V. on behalf of King Saud University.

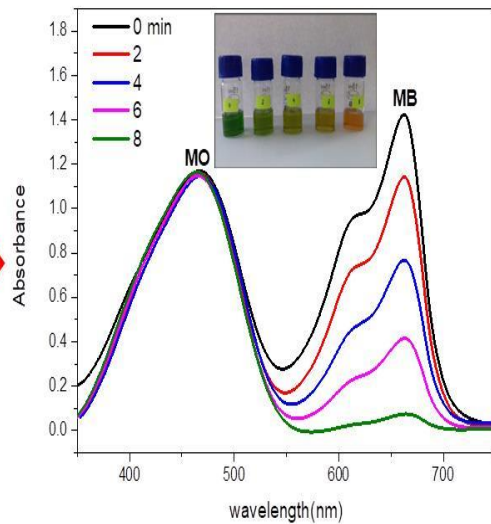
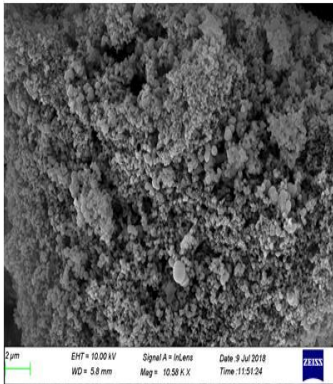
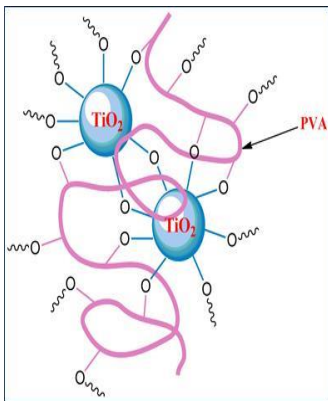
This is an open access article under the CC BY-NC-ND license (<http://creativecommons.org/licenses/by-nc-nd/4.0/>).

1. Introduction

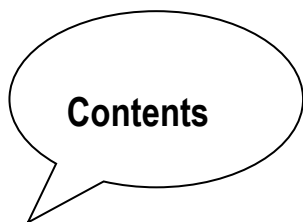
The design and fabrication of flexible nontoxic hybrid materials in simple and viable methods are needed to meet the demands of industry for various purposes including the protection of metals/materials from aggressive environments. Mild steel is a common material used in industries due to low cost,

Chapter 4

SYNTHESIS, CHARACTERIZATION AND DYE REMOVAL PROPERTIES OF TITANIA-PVA NANO HYBRID



Selective adsorption of MB



Contents

4.1	Introduction
4.2	Results and discussion
4.2.1	Characterization of Titania Hybrid
4.2.2	Adsorption study
4.2.3	Adsorption isotherm and kinetic studies
4.2.4	Selective adsorption
4.3	Conclusion

This chapter discusses the characterization and application of inorganic – organic hybrid nanocomposite containing TiO₂ and PVA. Through a simple and practical method, we could achieve a very high surface area and high pore volume hybrid. The composite shows remarkably enhanced adsorption capacity for cationic dye, methylene blue (MB) from a mixture of methylene blue and methyl orange (MO) mixture and thus utilised as a selective adsorbent for cationic dyes. The MB adsorption on hybrid was investigated under various experimental conditions.

4.1. Introduction

Water contamination due to dyes considered as one of the hot topics of research. Most of the industries such as textile, paper printing and pulp, rubber, plastics, leather, cosmetics, etc use dyes to colour the product synthesized in their domain[1]. The total dye consumption in the textile industry worldwide is more than 1000 tonnes/year and approximately 100 tonnes/year of dyes is discharged in to the water streams. These are being one among the important recalcitrant, allow for long distances in flowing water, inhibits photosynthetic activity, retard the expansion of aquatic biota by obstructing sunlight penetration and utilizing dissolve oxygen and decrease the recreation value of stream[2]. Conventional methods of water treatment such as coagulation [3], chemical precipitation [4], ozonisation [5], membrane filtration[6], and reverse osmosis are not effective in removing colour from waste effluent. Chemical and electrochemical oxidations and coagulation are generally not feasible in large scale industries due to their high cost and other issues. In contrast, an adsorption technique is by far the most versatile and widely used. It has been found to be superior to other techniques in terms of flexibility, simplicity of design, ease of operation, initial cost, insensitivity to toxic pollutants and does not produce harmful substances [7]. Activated carbon is an effective material for the dye removal from waste water but in industrial processes, it was restricted due to its high operational and investment costs[8]. The current research is focused on the need to develop a cost effective and potential alternative to commercial activated carbon. Factors that influence the adsorption efficiency

include adsorbate–adsorbent interaction, adsorbent surface area, adsorbent to adsorbate ratio, adsorbent particle size, temperature, pH[9, 10] etc.

In recent years, nano-porous particles [11] especially titanium oxide (TiO_2) [12-14], Fe_3O_4 [15], ZnO [16] and their composites have generated considerable interest due to their nontoxicity, physical and chemical stability, regular pore structure and uniquely large specific surface area and high catalytic efficiency [17-20]. TiO_2 is reported to possess a high adsorption capacity and the literature reports that modifications of TiO_2 enhances the surface area by controlling the growth of crystallites and gives higher porosity and adsorption efficiency [21-27] but its poor mechanical stability might limit their practical application in some fields. To further extend the application of the material, here, we introduce poly (vinyl alcohol) (PVA) into TiO_2 to enhance their mechanical strength. The resulting PVA modified hybrid was tough and flexible and exhibited good mechanical strength. The combination of PVA and TiO_2 results environmentally benign hybrid composite which can effectively separate MB dye from contaminated water. Methylene blue is a heterocyclic dye that has wide industrial applications, but cause serious environmental issues due to its high toxicity and accumulation in the environment[28]. There are limited number of works published based on PVA modified TiO_2 in the adsorption of dyes. Especially no outstanding research reported for the selective removal of cationic dyes from a combination. A few research works for the adsorption of MB dye using TiO_2 - polymer nanocomposite were displayed in Table 1 [29]. From the table it could

be seen that this material; TiO₂ – PVA, was proved to be more advantageous than other reported materials. The use of green PVA has been projected as a better alternative for most of the toxic polymers. The nanocomposite serves as an excellent adsorbent due to its fascinating properties and economically viable method of synthesis.

Table 1. Previous works-comparison.

Dye	Material	Results	Reference
MB	Sulfonated graphene/PVA	Adsorption, reaction conditions: 2 g of adsorbent/25 mL of the dye solution at 25°C	[29]
	Activated carbon/PVA	Adsorption, best reaction conditions: 24 h ,37°C, 100 rpm	[30]
	Chitosan/TiO ₂ composite	Initial concentration of MB 50 mg/L at 1 h	[31]
MO-MB mixture	Octa(maleimidophenyl)silsesquioxane–SiO ₂ /TiO ₂	80% Adsorption using 0.5 g, 2.5h	[32]
	TiO ₂ -poly(3-chloro-2-hydroxypropyl methacrylate) (TiO ₂ -PCHPMA)	99% MB Adsorption within 5 min at 28° C MB and MO (10 mg/L)	[33]

The present work explores i) a simple preparation of an inexpensive PVA modified titania nanocomposite with extremely high specific surface area, and large pore volume ii) characterization of the material by XRD, UV Vis spectra, PL spectra, FT Raman, FTIR, FESEM with EDAX, HRTEM, BET and DLS technology, iii) evaluation and investigation of removal efficiency of water soluble methylene blue dye iv) effect of adsorbent dosage, effect of initial dye concentration, pH, temperature, and v) selective removal of MB dye from MB- MO mixture and comparison with bare titania vi) removal of cationic Acridine orange dye (AO) from aqueous solution.

4.2. Results and discussion

4.2.1. Characterization of titania hybrid

The FTIR spectra of TPVA nanocomposite is shown in the Figure 1A. The bands between $500\text{--}900\text{cm}^{-1}$ are largely related to titanium oxide Ti-O, Ti-O-Ti stretching and bending modes was slightly shifted to $400\text{--}700\text{ cm}^{-1}$ in the composite is confirmed the cross-linked structure of the hybrid nanocomposite. A broad band observed between $3200\text{--}3600\text{ cm}^{-1}$ is shown in the sample corresponds to O-H stretching and deformation vibrations of weak-bound water molecules. Vibrations in the range of $1400\text{--}1700\text{ cm}^{-1}$ are indicative of CH_2 bond because of the introduction of PVA in the TiO_2 . The anti-symmetric and symmetric C-H stretching of methylene groups are observed respectively at 2931cm^{-1} and 2860 cm^{-1} [34].

Figure 1 B depicts the XRD patterns of TPVA nanocomposite. The peaks are shown to have resulted from the planes (101), (103), (200), (105), and (213) at theta 25.15°, 37.61°, 47.7°, 54.12°, 62.69° respectively. The reflection peaks can be indexed to anatase TiO₂ (JCPDS No 75-1537).

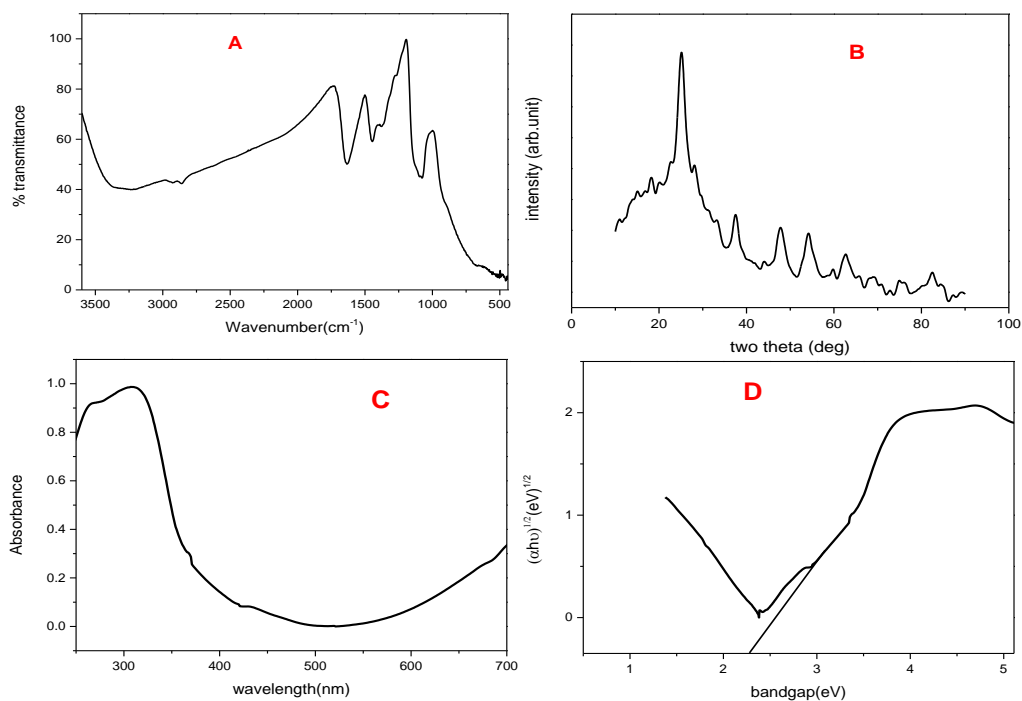


Figure 1. A) FTIR spectra B) XRD C) UV spectra D) Tauc plot of TPVA nanocomposite

The diffuse reflectance spectra and corresponding Tauc plot of the prepared sample are shown in Figure 1 C and D, the presence of TiO₂ in the sample was confirmed due to the characteristic broad

absorption peak in the 200-400 nm region. The band-gap energy (E_g) was calculated by the following relationship;

$$\alpha(h\nu) = \alpha_0 (h\nu - E_g)^n \quad (5)$$

where α is absorption coefficient, $h\nu$ is the photon energy, α_0 and n are the constants, E_g is the optical band gap of the material, and n depends on the type of electronic transition and can be any value between $\frac{1}{2}$ and 3 [35, 36]. The band gap energy of the material calculated from Tauc plot is 2.1 eV, which got lowered due to the introduction of PVA in to TiO_2 confirms the formation of the composite. The band gap further calculated by photoluminescence (PL) technique at excitation wavelength of 480 nm and was presented in Figure 2 A. The spectrum shows emission band at wavelength range 510-550 nm. The obtained band gap energy is 2.3 eV. The band gap value obtained from DRS technique and PL technique are very much comparable.

Raman spectroscopy was used to confirm the formation of TiO_2 and to its phase transformation of TiO_2 . The Raman spectra of the TPVA nanocomposite is shown in Figure 2 B. The anatase phase and the rutile phase of TiO_2 have different Raman active modes. The peaks were identified at values of 144, 395, 514 and 639 cm^{-1} [37]. The four peaks confirm the presence of anatase phase.

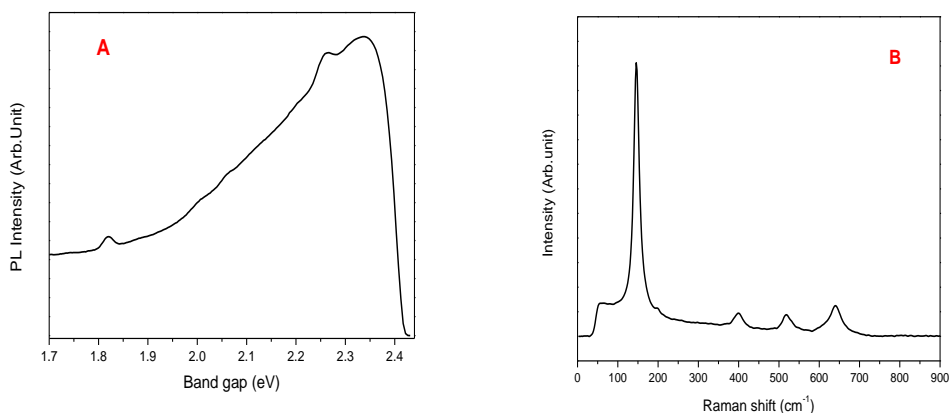


Figure 2 A) PL spectra for Band gap measurement B) Raman spectra of TPVA nanocomposite

Figure 3 depicts the surface morphologies of TiO₂- PVA composites obtained by FESEM. The spherical shaped nano-composite with extremely small particle size with an average size of 12 nm has been observed. The image indicated that the sample has a uniform morphology. Furthermore, the corresponding EDX spectra of the sample represented in the Fig. 3D clearly illustrates the distribution of C, N, O, and Ti throughout the sample.

Detailed information about the microstructure and morphology of nanocomposite has been provided by TEM of the sample. The image showed the formation of spherical shaped small nanoparticles throughout the sample. HRTEM image of the sample was considered to resolve more information of the structure. Figure 4 represents the high resolution TEM (HRTEM) image of the same sample. The observed lattice spacing of 0.33 nm corresponds to the (110) plane of anatase TiO₂ showing that the nanoparticles grows along (110) plane.

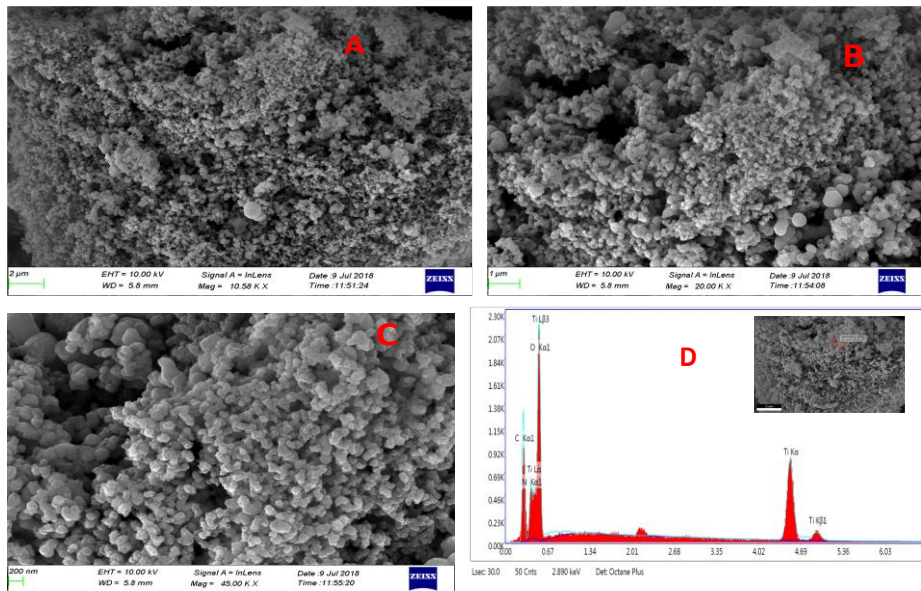


Figure 3. A) B) C) FESEM image of TPVA nanocomposite at different magnification D) EDAX spectra of the sample

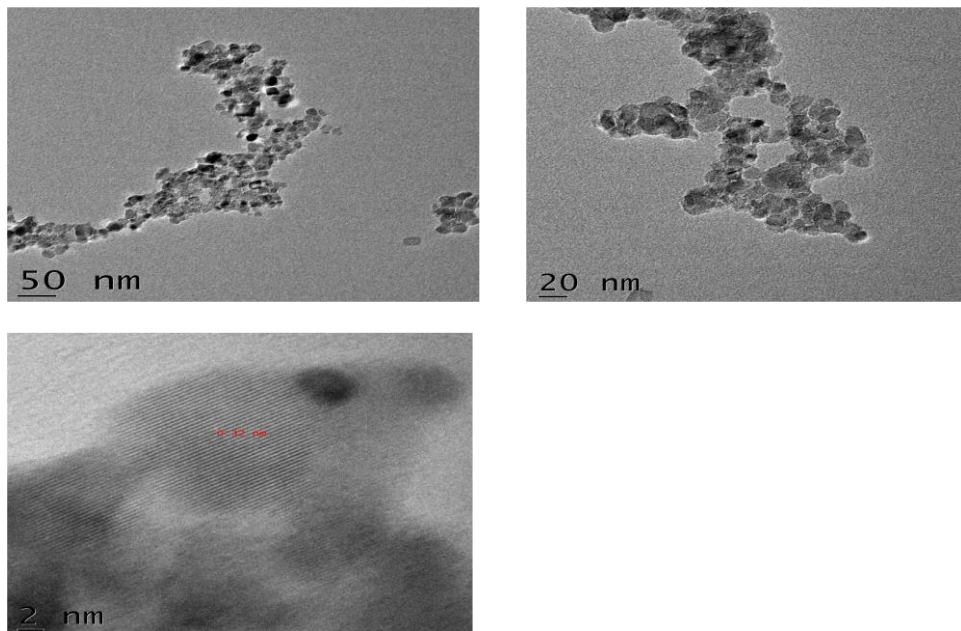


Figure 4. TEM and HRTEM image of TPVA nanocomposite

The textural properties of TiO₂-PVA were depicted from the Brunauer Emmette Teller (BET) nitrogen adsorption–desorption isotherm analysis and the average pore size was measured through the Barrer–Joyner–Halenda (BJH) technique at –195.80 °C as shown in Figure 5. This technique is used to understand the adsorption mechanism with respect to the surface area and porosity. The estimated surface area, pore diameter and pore volume of the sample is summarized in Table 4. The BET surface area was calculated to be 475 m²g⁻¹ and the pore diameter ranges from ~4 nm to 50 nm. Therefore, all pores in the composite are mesoporous and substantial contribution to adsorption surface is offered by mesopores [38]. The pores, in general, could perform as channels for the adsorption of MB impurities. The N₂ adsorption–desorption isotherm corresponds to the IUPAC type-IV pattern representing the existence of mesoporous structure in the prepared sample. The sorption isotherm exhibit typical H3 hysteresis indicates that network effects are important in the structure. The H3 type suggests slit like pores. The high surface area of 475 m²g⁻¹ along with mesoporous nature of composite leading to higher MB adsorption.

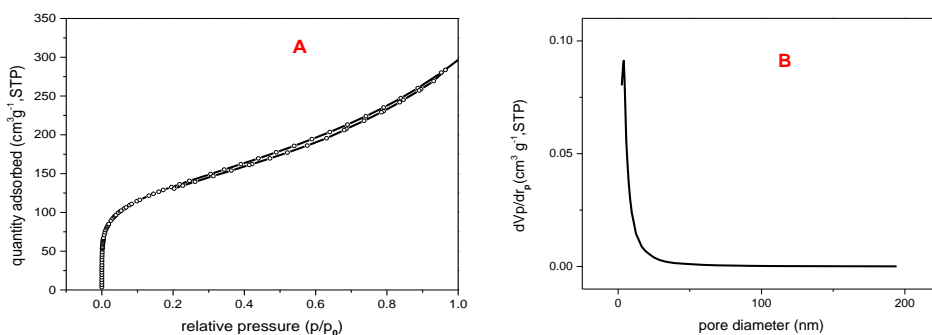


Figure.5. A) N₂ adsorption - desorption curve B) BJH pore size distribution curve of TPVA nanocomposite

4.2.2. Adsorption study

Figure 6 A and Table 2 shows adsorbent dosage on methylene blue dye removal. Adsorbent dosage is an important parameter to determine the capacity of an adsorbent. In general, with rising adsorbent dosage, the percentage of dye removal increases. Initially, a rapid increase of adsorption with the increase in adsorbent dosage was attributed to the availability of more adsorption sites [39]. The dye removal reached approximately 95.3% using 0.075g of the nanocomposite, which was attributed to the larger number of adsorption sites. A decrease in adsorption capacity of nanocomposite was observed on further addition of adsorbent. Therefore, the optimal dosage for dye removal was 0.075g of the nanocomposite. The decrease of adsorption was due to the concentration gradient between the adsorbent and adsorbate [40].

For comparison adsorption study was conducted with bare titania as shown in Figure 6. It was found that MB adsorption rate was lower for bare titania compared to titania PVA hybrid

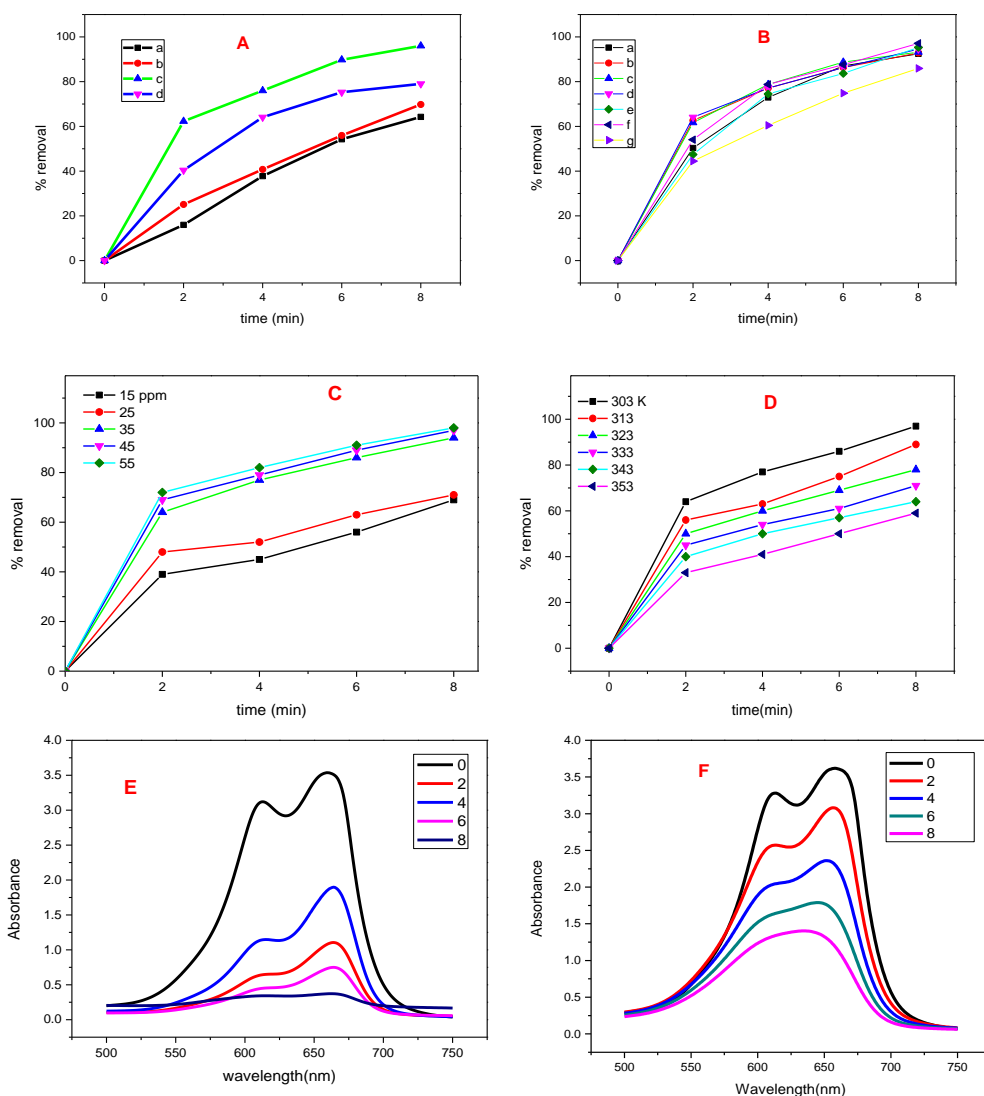


Figure 6. Adsorption plots A) % removal Vs time at different adsorbent dosage a) 0.025g b) 0.05g c) 0.075g d) 0.1g B) % removal Vs time at different pH a) 3 b) 4 c) 5 d) 6 e) 7 f) 8 g) 9 C) % removal Vs time at different adsorbate dosage D) % removal Vs time at different temperature E) and F) Absorbance spectra of MB adsorption at pH 8 and 303 K of titania PVA hybrid and titania respectively.

Table 2 % removal efficiency of MB uptake on TPVA nanocomposite at different catalyst dosage, pH.

pH	% removal efficiency	SD	Adsorbent dosage(g)	% removal efficiency	SD
3	92.4	0.07	0.025	70.2	0.42
4	92.8	0.04	0.05	79.5	0.17
5	93.2	0.05	0.075	95.3	0.38
6	94.5	0.21	0.1	75.7	0.14
7	95.3	0.42			
8	97.1	0.07			
9	85.9	0.49			

Table 3 % removal efficiency of MB uptake on TPVA nanocomposite at different adsorbate concentration and temperature.

Adsorbate Concentration (ppm)	% removal efficiency	SD	Temperature (K)	% removal efficiency	SD
15	69	0.15	303	97	0.56
25	71	0.56	313	89	0.28
35	94	0.28	323	78	1.4
45	97	0.21	333	71	0.49
55	98	0.11	343	64	0.28
			353	59	0.21

Table 4 Textural properties of TPVA nanocomposite

Sample	S _{BET} (m ² g ⁻¹)	Pore volume (cm ³ g ⁻¹)	Pore diameter (nm)
TPVA	475	0.4535	3.8138

The pH of the solution is another important parameter that affects the adsorption of the dye molecules. The efficiency of

adsorption is dependent on the solution pH, since variation in pH leads to the variation in the degree of ionisation of the adsorbate molecule and the surface properties of the adsorbent[40]. The variation of pH can affect the surface charge of the nanocomposite. The effect of the solution pH on the dye adsorption was monitored by keeping the dye concentration (35ppm) and adsorbent dosage (0.075g) constant at 303K. The experiments were performed at different pH ranging from 3 to 9. As shown in Figure 6 B and Table 2, the percentage of dye removal increased gradually from 92.4 to 97.1 as the pH increased from 3 to 8 because the electrostatic interactions between the positively charged dye molecules and the negatively charged nanocomposite could be the main adsorption mechanism. On the other hand, a decreasing trend in the dye removal efficiency from 97.1 to 85.9% was observed with a further increase in pH to 9. The optimal pH was found to be 8. Initial dye concentration depends on the adsorption capacity of adsorbent. The effect of initial dye concentration depends on the immediate relation between the concentration of the dye and the available sites on an adsorbent surface and was shown in Figure 6 C and Table 3. The increase in initial dye concentration will cause an increase in the capacity of the adsorbent and this may be due to the high driving force for mass transfer at a high initial dye concentration [41].

Temperature will change the adsorption capacity of the adsorbent so and it is a very important parameter for optimizing the adsorption process. Decrease in adsorption trend has been observed and the results are given in Figure 6 D and Table 3. The decrease of

adsorption capacity with increase in temperature indicates that the adsorption is an exothermic process. This may be due to the decrease in the adsorptive forces between the dye molecules and the active sites on the adsorbent surface with rise in temperature [18].

4.2.3. Adsorption isotherm and kinetic studies

An adsorption isotherm describes how adsorbate interacts with the adsorbent. Thus, the correlation of equilibrium data by either a theoretical or an empirical equation is essential for the practical design and operation of an adsorption system. Langmuir and Freundlich isotherm models have been used to evaluate the adsorption data for Methylene blue. Linearized forms of Langmuir and Freundlich adsorption isotherms can be expressed as follows

$$\frac{C_e}{q_e} = \frac{1}{K_L q_{max}} + \frac{1}{q_{max}} C_e \quad (6)$$

$$\log q_e = \log K_F + \frac{1}{n} \log C_e \quad (7)$$

where C_e , q_{max} , and q_e represents the equilibrium dye concentration (mg L^{-1}), maximum adsorption capacity (mg L^{-1}) and amount of dye adsorbed per gram of adsorbent (mg g^{-1}) respectively. K_L and K_F are the constants in the equation and n is a dimensionless heterogeneity factor [42].

Langmuir isotherm is based on the assumption of uniform adsorption energy throughout the surface of the adsorbent. Equation (6) was applied to the experimental adsorption results through a linear regression plot of $\frac{C_e}{q_e}$ Vs. C_e to obtain q_{max} and K_L values. The

Freundlich model is an empirical equation for a highly heterogeneous surface having an exponential distribution of adsorption sites and energies. The values of the Freundlich's constant k_F and n can be calculated by a linear plot of $\log q_e$ Vs $\log C_e$ and applied to the adsorption study [43] shown in Figure 7 A and B, Langmuir and Freundlich constant are given in Table 5. The experimental data on the uptake of methylene blue at 8 min have been fitted in the Langmuir equation and the plot obtained is shown in Figure 7 A which suggests the Langmuir adsorption model was more suitable for MB adsorption using the nanocomposite with a regression coefficient value of around 0.9914. The experimental data give good fit for both Langmuir and Freundlich models, but the Langmuir isotherm was found to fit the experimental data better than the Freundlich isotherm. The best fit of equilibrium data in the Langmuir isotherm expression predicted the monolayer coverage of methylene blue onto the adsorbent surface.

Pseudo first-order and pseudo second-order kinetic models are most widely used and were applied here to determine the rate of adsorption at different time intervals and were presented in Figure 7 C and D. The first-order kinetics proposed by Lagergren and improved by Krishnan was given by,

$$\log(q_e - q_t) = \frac{-k_1}{2.303} t + \log q_e \quad (8)$$

where k_1 is the rate constant for the first-order adsorption reaction, and q_e and q_t are the amount of dye adsorbed at equilibrium and time t

respectively. The pseudo second-order rate equation by Ho and Mckay can be expressed as follows,

$$\frac{t}{q_t} = \frac{1}{k_2 q_e^2} + \frac{t}{q_e} \quad (9)$$

The appropriate model was found using a straight line, which suggests that the pseudo-second-order kinetic model was more suitable for MB adsorption using the nanocomposite with a regression coefficient value of around 0.9974 [43].

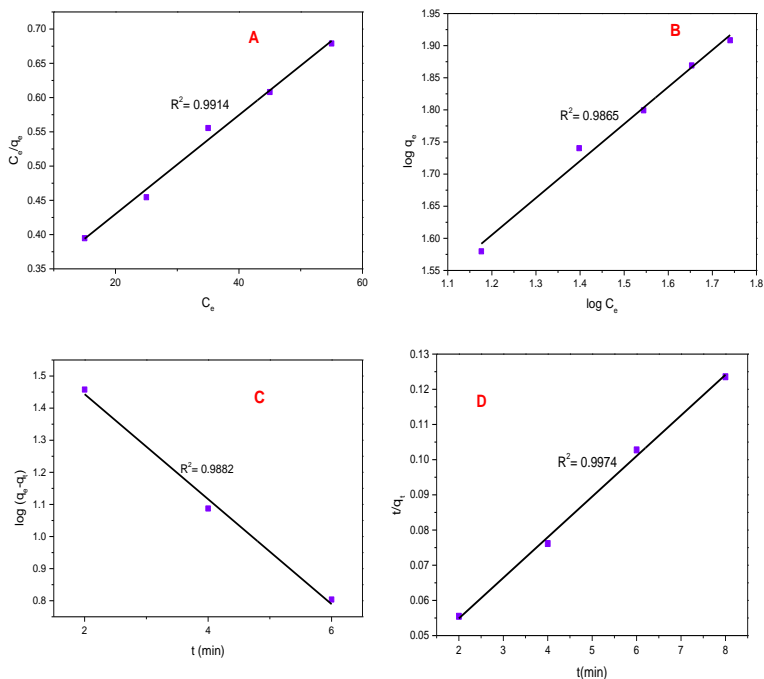


Figure . 7. A) Langmuir and B) Freundlich Adsorption isotherms C) Pseudo 1st order and D) Pseudo 2nd order Kinetic plots

Table 5 Langmuir and Freundlich adsorption isotherm parameters at 303 K

Equation	Langmuir parameters			Equation	Freundlich parameters		
	K_L	q_{max}	R^2		K_F	n	R^2
$y = 0.007x + 0.285$	0.0	138.8	0.9	$y = 0.575x + 0.914$	8.2	1.7	0.9
	25	88	91		11	36	89

4.2.4. Selective adsorption

In addition, a nice adsorbent should be able to separate a certain dye from a dye mixture. An equimolar solution of MB and MO were subjected to adsorption studies. The selective adsorption of MB from the mixture of MO and MB was studied, as depicted in Figure 8 A. After the addition of TiO_2 -PVA nanocomposite, the colour of the mixture gradually turned from dark green to light yellow (Fig. 8 inset). After adsorption for 8 min, the intensity of peak at 662 nm associated with MB decreased remarkably whereas no obvious decrease at 463 nm corresponding to MO was observed, demonstrating the high selectivity of titania PVA composite for the adsorption of MB dye. The high selectivity is possibly due to the fact that the electrostatic attraction between nanocomposite and MB for the adsorption process. Thus, the cationic dye well adsorbed on the surface of nanocomposite while MO being an anionic dye remained as un-adsorbed. The adsorption of MB on the nanocomposite found to be selective in the presence of MO.

The selective adsorption study of bare titania was also carried out and results shown in Figure 8 E. The selectivity of bare titania towards MB is less compared to the hybrid material. The MO dye can undergo adsorption in slower rate with bare titania. The selectivity of titania catalyst was more pronounced with the presence PVA. Also, adsorption experiment of titania PVA hybrid was conducted with another cationic dye acridine orange (AO) and the results depicted in Figure 8 F. The catalyst can adsorb AO dye from water (10⁻⁴ M) confirming the selective nature of adsorbent towards cationic dye.

Measurement of the zeta (ζ)-potential of TiO₂ particles was also carried out to further confirm minute details regarding the adsorption of MB on the TiO₂ particle surface. Figure 8 B summarizes the results of zeta potential measurement. From the data it is clear that the zeta potential value of titania and hybrid is 14.2 mV and -29.5mV respectively which explains that the cationic MB dye is well adsorbed on the negatively charged hybrid surface. The anionic dye methyl orange will not undergo adsorption on hybrid composite also supports this observation.

Herein, the regeneration experiments were carried out by immersing dye-adsorbed TiO₂ -PVA in HCl solution (0.1 M) and then centrifuged for 1 h. After desorption, the regenerated nanocomposite was reused for the next cycle of adsorption, as presented in Figure 8 C. Results indicated that the removal efficiency reduced not more than 13%, even after ten successive cycles of desorption– adsorption, as compared with the original adsorption capacity. It was found that 90% of MB recovered from the adsorbent.

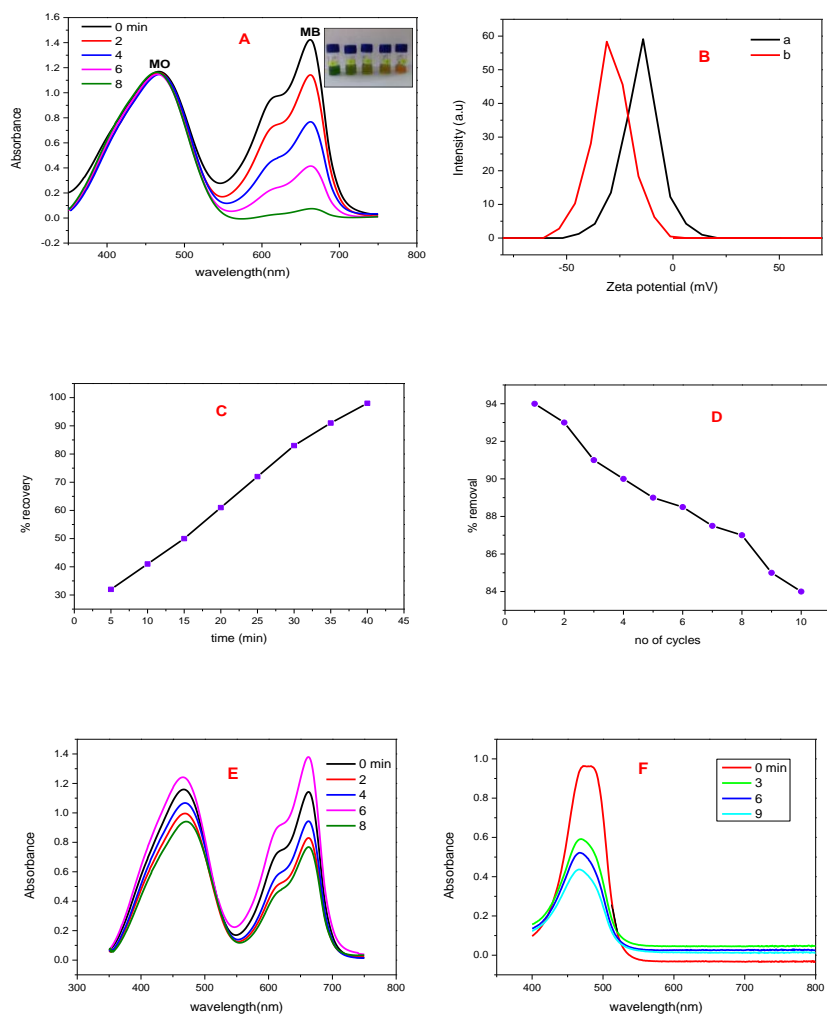


Figure 8. A) Selective adsorption of MB in equimolar mixture of MB and MO (inset: photograph showing selective adsorption) B) zeta potential (ζ) measurement plot for a) titania and b) hybrid nanocomposite at pH 8 C) % recovery Vs time of hybrid nanocomposite using 0.1M HCl D) Reusability of hybrid nanocomposite, % removal Vs number of cycles of hybrid nanocomposite E) Selective adsorption of MB in equimolar mixture of MB and MO of titania. F) Adsorption of acridine orange dye by titania PVA hybrid.

Reusability is another important characteristic of an adsorbent in industrial processes because use for longer periods of time leads to a substantial decrease in the cost of the process. The removal efficiency of MB recovery using a dye concentration of 35 ppm with an adsorbent dosage of 0.075 g was repeated 10 times, and the results (Figure 8 D) indicated that the adsorbent showed good activity, even after 10 repeated recycles.

4.3. Conclusions

- The synthesis of inorganic – organic hybrid nanocomposite containing TiO₂ and PVA has been done by sol-gel technique.
- The hybrid nanocomposite was characterized using X-ray diffraction (XRD), Fourier Transform Infrared Spectroscopy (FTIR), UV-Vis spectroscopy, Photoluminescence Spectroscopy (PL), Fourier Transform Raman Spectroscopy (FT Raman), Field Emission Scanning Electron Microscopy (FESEM) with (EDAX), and High-Resolution Transmission Electron Microscopy (HRTEM). The Surface charge of the nanocomposite was probed with Zeta potential (ζ) measurement by Dynamic Light Scattering (DLS) technique.
- The composite shows remarkable adsorption capacity for cationic methylene blue (MB) dye from methylene blue and methyl orange (MO) mixture utilised as a selective adsorbent for cationic dyes. The experiment was conducted with bare

titania also. The selectivity of catalyst was confirmed with another cationic dye acridine orange (AO).

- The surface area and pore volume of the composite were determined using BET method and achieved very high surface area of $475 \text{ m}^2\text{g}^{-1}$ and high pore volume $0.4535 \text{ cm}^3 \text{ g}^{-1}$.
- The MB adsorption on nanocomposite was investigated under various experimental conditions. Uptake of MB dependent on temperature, pH, initial dye concentration, and catalyst dosage.
- The nanocomposite showed 97.1% of MB removal within 8 minutes.
- The experimental data give good fit for both Langmuir and Freundlich models and detailed adsorption studies reveal that the adsorption kinetics and isotherms can be well-described by pseudo-second-order model and Langmuir isotherm model.
- More over the adsorbent could be well regenerated in acid solution with good activity, even after 10 repeated cycles.
- The negative surface charge, very high surface area, high pore volume, and mesoporous structure of nanocomposite contributed to the selective adsorption of MB dye from MB-MO mixture.

Discovery consists of looking at the same thing as everyone else and thinking something different.

Albert Szent-Gyorgyi

References

- [1] R. Monsef, M. Ghiyasiyan-Arani, M. Salavati-Niasari, Utilizing of neodymium vanadate nanoparticles as an efficient catalyst to boost the photocatalytic water purification, *Journal of environmental management*, 230 (2019) 266-281.
- [2] S. Mahdavi, M. Jalali, A. Afkhami, Removal of heavy metals from aqueous solutions using Fe₃O₄, ZnO, and CuO nanoparticles, *Nanotechnology for Sustainable Development*, Springer2012, pp. 171-188.
- [3] N. Dizge, C. Aydiner, E. Demirbas, M. Kobya, S. Kara, Adsorption of reactive dyes from aqueous solutions by fly ash: Kinetic and equilibrium studies, *Journal of Hazardous Materials*, 150 (2008) 737-746.
- [4] K. Ravikumar, S. Krishnan, S. Ramalingam, K. Balu, Optimization of process variables by the application of response surface methodology for dye removal using a novel adsorbent, *Dyes and Pigments*, 72 (2007) 66-74.
- [5] M. Muthukumar, D. Sargunamani, N. Selvakumar, Statistical analysis of the effect of aromatic, azo and sulphonic acid groups on decolouration of acid dye effluents using advanced oxidation processes, *Dyes and pigments*, 65 (2005) 151-158.
- [6] M.F.R. Pereira, S.F. Soares, J.J. Órfão, J.L. Figueiredo, Adsorption of dyes on activated carbons: influence of surface chemical groups, *Carbon*, 41 (2003) 811-821.
- [7] B. Dash, Competitive Adsorption of dyes (congo red, methylene blue, malachite green) on Activated Carbon, 2010.
- [8] H. Wang, H. Gao, M. Chen, X. Xu, X. Wang, C. Pan, J. Gao, Microwave-assisted synthesis of reduced graphene oxide/titania nanocomposites as an adsorbent for methylene blue adsorption, *Applied Surface Science*, 360 (2016) 840-848.
- [9] G. Crini, Non-conventional low-cost adsorbents for dye removal: a review, *Bioresource technology*, 97 (2006) 1061-1085.

- [10] S. Allen, B. Koumanova, Decolourisation of water/wastewater using adsorption, *Journal of the University of Chemical Technology and Metallurgy*, 40 (2005) 175-192.
- [11] K. Anitha, S. Namsani, J.K. Singh, Removal of heavy metal ions using a functionalized single-walled carbon nanotube: a molecular dynamics study, *The Journal of Physical Chemistry A*, 119 (2015) 8349-8358.
- [12] S. Mahdavi, M. Jalali, A. Afkhami, Heavy metals removal from aqueous solutions using TiO₂, MgO, and Al₂O₃ nanoparticles, *Chemical Engineering Communications*, 200 (2013) 448-470.
- [13] X. Zhao, Q. Jia, N. Song, W. Zhou, Y. Li, Adsorption of Pb (II) from an aqueous solution by titanium dioxide/carbon nanotube nanocomposites: kinetics, thermodynamics, and isotherms, *Journal of Chemical & Engineering Data*, 55 (2010) 4428-4433.
- [14] K.J. Chen, F. Boucher, D. Jacquemin, How Adsorption Onto TiO₂ Modifies the Properties of Multiswitchable DTE Systems: Theoretical Insights, *The Journal of Physical Chemistry C*, 119 (2015) 16860-16869.
- [15] C.-Y. Cao, J. Qu, W.-S. Yan, J.-F. Zhu, Z.-Y. Wu, W.-G. Song, Low-cost synthesis of flowerlike α -Fe₂O₃ nanostructures for heavy metal ion removal: adsorption property and mechanism, *Langmuir*, 28 (2012) 4573-4579.
- [16] N.A. Fromer, M.S. Diallo, Nanotechnology and clean energy: sustainable utilization and supply of critical materials, *Nanotechnology for Sustainable Development*, Springer 2013, pp. 289-303.
- [17] S. Abbasizadeh, A.R. Keshtkar, M.A. Mousavian, Preparation of a novel electrospun polyvinyl alcohol/titanium oxide nanofiber adsorbent modified with mercapto groups for uranium (VI) and thorium (IV) removal from aqueous solution, *Chemical engineering journal*, 220 (2013) 161-171.
- [18] H. Khojasteh, M. Salavati-Niasari, A. Abbasi, F. Azizi, M. Enhessari, Synthesis, characterization and photocatalytic activity of PdO/TiO₂ and Pd/TiO₂ nanocomposites, *Journal of Materials Science: Materials in Electronics*, 27 (2016) 1261-1269.

- [19] H. Khojasteh, M. Salavati-Niasari, M.-P. Mazhari, M. Hamadianian, Correction: Preparation and characterization of Fe₃O₄@ SiO₂@ TiO₂@ Pd and Fe₃O₄@ SiO₂@ TiO₂@ Pd–Ag nanocomposites and their utilization in enhanced degradation systems and rapid magnetic separation, *RSC Advances*, 6 (2016) 86385-86385.
- [20] S. Mortazavi-Derazkola, M. Salavati-Niasari, O. Amiri, A. Abbasi, Fabrication and characterization of Fe₃O₄@ SiO₂@ TiO₂@ Ho nanostructures as a novel and highly efficient photocatalyst for degradation of organic pollution, *Journal of energy chemistry*, 26 (2017) 17-23.
- [21] Z.-l. Shi, H. Lai, S.-h. Yao, S.-f. Wang, Preparation, characterization and photocatalytic activity of lanthanum doped mesoporous titanium dioxide, *Chinese Journal of Chemical Physics*, 25 (2012) 96.
- [22] R. Shwetharani, M. Jyothi, P. Laveena, R. Geetha Balakrishna, Photoactive titania float for disinfection of water; evaluation of cell damage by bioanalytical techniques, *Photochemistry and photobiology*, 90 (2014) 1099-1107.
- [23] R. Shwetharani, C. Fernando, G.R. Balakrishna, Excellent hydrogen evolution by a multi approach via structure–property tailoring of titania, *RSC Advances*, 5 (2015) 39122-39130.
- [24] R. Shwetharani, R.G. Balakrishna, Photo-active float for field water disinfection, *Photochemical & Photobiological Sciences*, 15 (2016) 447-455.
- [25] L.P. D'Souza, R. Shwetharani, V. Amoli, C. Fernando, A.K. Sinha, R.G. Balakrishna, Photoexcitation of neodymium doped TiO₂ for improved performance in dye-sensitized solar cells, *Materials & Design*, 104 (2016) 346-354.
- [26] M. Masjedi, N. Mir, E. Noori, T. Gholami, M. Salavati-Niasari, Effect of Schiff base ligand on the size and the optical properties of TiO₂ nanoparticles, *Superlattices and Microstructures*, 62 (2013) 30-38.
- [27] H. Khojasteh, M. Salavati-Niasari, F.S. Sangsefidi, Photocatalytic evaluation of RGO/TiO₂NWs/Pd-Ag nanocomposite as an improved catalyst for efficient dye degradation, *Journal of Alloys and Compounds*, 746 (2018) 611-618.

- [28] H. Safardoust-Hojaghan, M. Salavati-Niasari, Degradation of methylene blue as a pollutant with N-doped graphene quantum dot/titanium dioxide nanocomposite, *Journal of cleaner production*, 148 (2017) 31-36.
- [29] H. Li, J. Fan, Z. Shi, M. Lian, M. Tian, J. Yin, Preparation and characterization of sulfonated graphene-enhanced poly (vinyl alcohol) composite hydrogel and its application as dye absorbent, *Polymer*, 60 (2015) 96-106.
- [30] S.R. Sandeman, V.M. Gun'ko, O.M. Bakalinska, C.A. Howell, Y. Zheng, M.T. Kartel, G.J. Phillips, S.V. Mikhalovsky, Adsorption of anionic and cationic dyes by activated carbons, PVA hydrogels, and PVA/AC composite, *Journal of colloid and interface science*, 358 (2011) 582-592.
- [31] M.H. Farzana, S. Meenakshi, Synergistic effect of chitosan and titanium dioxide on the removal of toxic dyes by the photodegradation technique, *Industrial & Engineering Chemistry Research*, 53 (2013) 55-63.
- [32] M. Hossan, B. Ochiai, Preparation of TiO₂-Poly (3-Chloro-2-Hydroxypropyl Methacrylate) Nanocomposite for Selective Adsorption and Degradation of Dyes, *Technologies*, 6 (2018) 92.
- [33] S. Ramesh, H.S. Kim, A. Sivasamy, J.-H. Kim, Synthesis of Octa (maleimidophenyl) silsesquioxane-SiO₂/TiO₂ Hybrid Nanocomposites: Adsorption Behavior for the Removal of an Organic Methylene Blue Dye and Antimicrobial Activity against Pathogens, *Polymer-Plastics Technology and Engineering*, 57 (2018) 185-195.
- [34] K. Das, S.K. Panda, S. Chaudhuri, Solvent-controlled synthesis of TiO₂ 1D nanostructures: growth mechanism and characterization, *Journal of Crystal Growth*, 310 (2008) 3792-3799.
- [35] F. Mazloom, M. Ghiyasiyan-Arani, R. Monsef, M. Salavati-Niasari, Photocatalytic degradation of diverse organic dyes by sol-gel synthesized Cd₂V₂O₇ nanostructures, *Journal of Materials Science: Materials in Electronics*, 29 (2018) 18120-18127.
- [36] R. Monsef, M. Ghiyasiyan-Arani, M. Salavati-Niasari, Application of ultrasound-aided method for the synthesis of NdVO₄ nano-

- photocatalyst and investigation of eliminate dye in contaminant water, *Ultrasonics sonochemistry*, 42 (2018) 201-211.
- [37] S.Y. Choi, M. Mamak, N. Coombs, N. Chopra, G.A. Ozin, Thermally stable two-dimensional hexagonal mesoporous nanocrystalline anatase, meso-nc-TiO₂: Bulk and crack-free thin film morphologies, *Advanced Functional Materials*, 14 (2004) 335-344.
- [38] B. Thomas, L. Alexander, Enhanced synergetic effect of Cr (VI) ion removal and anionic dye degradation with superparamagnetic cobalt ferrite meso–macroporous nanospheres, *Applied Nanoscience*, 8 (2018) 125-135.
- [39] C. Almeida, N. Debacher, A. Downs, L. Cottet, C. Mello, Removal of methylene blue from colored effluents by adsorption on montmorillonite clay, *Journal of colloid and interface science*, 332 (2009) 46-53.
- [40] B. Nandi, A. Goswami, M. Purkait, Removal of cationic dyes from aqueous solutions by kaolin: kinetic and equilibrium studies, *Applied Clay Science*, 42 (2009) 583-590.
- [41] Y. Bulut, H. Aydın, A kinetics and thermodynamics study of methylene blue adsorption on wheat shells, *Desalination*, 194 (2006) 259-267.
- [42] A.R. Prasad, A. Joseph, Synthesis, characterization and investigation of methyl orange dye removal from aqueous solutions using waterborne poly vinyl pyrrolidone (PVP) stabilized poly aniline (PANI) core–shell nanoparticles, *RSC Advances*, 7 (2017) 20960-20968.
- [43] R. Shwetharani, A. Poojashree, G.R. Balakrishna, M. Jyothi, La activated high surface area titania float for the adsorption of Pb (ii) from aqueous media, *New Journal of Chemistry*, DOI (2018).



Selective adsorption of methylene blue (MB) dye from aqueous mixture of MB and methyl orange (MO) using mesoporous titania (TiO₂) – poly vinyl alcohol (PVA) nanocomposite

Jaseela P.K., Julia Garvasi, Abraham Joseph *

Department of Chemistry, University of Calicut, Calicut University P O, Kerala, India

ARTICLE INFO

Article history:

Received 25 January 2019

Received in revised form 28 April 2019

Accepted 2 May 2019

Available online 04 May 2019

Keywords:

Nanocomposite

Mesoporous

MB

PVA

Selective adsorption

ABSTRACT

A very simple, rapid and practical method was proposed for the synthesis of an inorganic – organic hybrid nanocomposite containing TiO₂ and PVA, which possess remarkable selectivity for the adsorption of methylene blue (MB), from the mixture of methylene blue and methyl orange (MO) in aqueous environment. The nanocomposite was characterized by using X-ray diffraction (XRD), Fourier transform infrared spectroscopy (FTIR), UV-Vis spectroscopy, Photoluminescence spectroscopy (PL), Fourier transform Raman spectroscopy (FT Raman), Field emission scanning electron microscopy (FESEM) with (EDAX), and High-resolution transmission electron microscopy (HRTEM). The surface charge of the nanocomposite was probed with Zeta potential (ζ) measurement by Dynamic Light Scattering (DLS) technique. The surface area and pore volume of the material were determined using BET method and achieved very high surface area of 475 m²g⁻¹ and high pore volume of 0.4535 cm³g⁻¹. The MB adsorption was investigated under various experimental conditions and results strongly dependent on temperature, pH, initial dye concentration, and catalyst dosage. The nanocomposite showed 97.1% of MB removal within 8 min. The experimental data give good fit for both Langmuir and Freundlich models and the adsorption kinetics can be well-described by pseudo-second-order pathway. The adsorption process was exothermic and the adsorbent could be regenerated in acid solution with good activity, even after 10 repeated cycles.

© 2019 Elsevier B.V. All rights reserved.

1. Introduction

Water contamination due to dyes considered as one of the hot topics of research in contemporary world. Most of the industries such as textile, paper printing and pulp, rubber, plastics, leather, cosmetics, etc. use different dyes to colour their products synthesized [1]. The total dye consumption in the textile industry worldwide is more than 1000 t/year and approximately 100 tonnes/year of dyes is discharged directly in to the water streams. These are being one among the important recalcitrant, allow for long distances in flowing water, inhibits photosynthetic activity, retard the expansion of aquatic biota by obstructing sunlight penetration and utilizing dissolve oxygen and decrease the recreation value of stream [2]. Conventional methods of water treatment such as coagulation [3], chemical precipitation [4], ozonisation [5], membrane filtration [6], and reverse osmosis are not effective in removing colour from waste effluent. Chemical and electrochemical oxidation sand coagulation are generally not feasible in large scale industries due to their high cost and economic disadvantages and this gap is filled by the most versatile adsorption techniques. Adsorption technique has been found to be superior to other methods in terms of flexibility,

simplicity of design, ease of operation, initial cost, insensitivity to toxic pollutants and does not produce harmful substances [7]. Activated carbon is an effective material for the dye removal from wastewater, but in industrial processes it was restricted due to high operational and investment costs [8]. The current research is therefore focused on the need to develop alternative to commercial activated carbon with a cost effective, but potential adsorbent possessing optimum adsorbate-adsorbent interaction, adsorbent surface area, adsorbent to adsorbate ratio, adsorbent particle size, temperature, and pH [9,10].

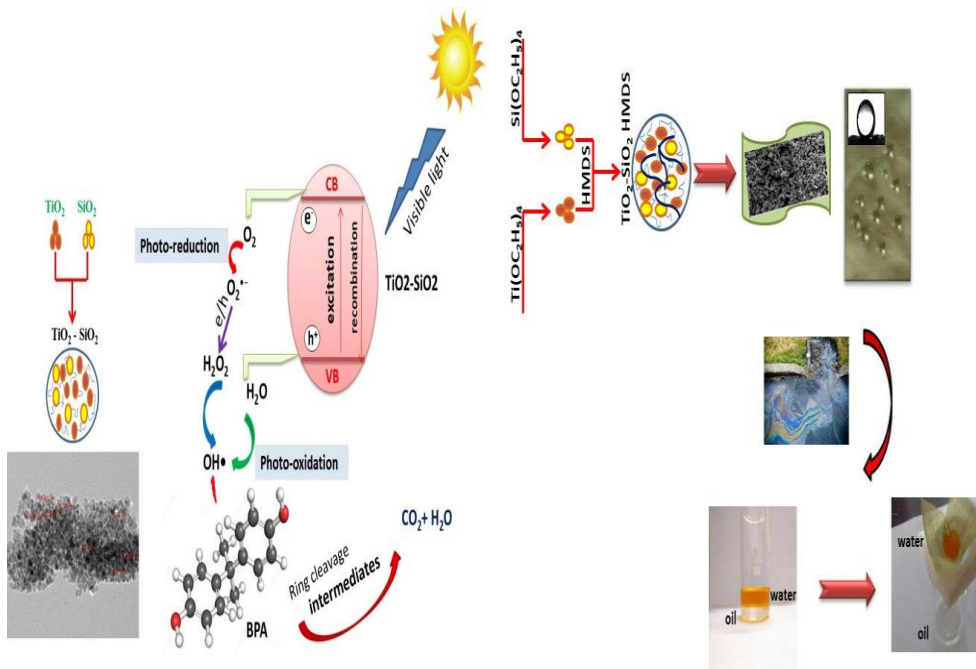
In recent years, nano-porous particles [11] especially titanium oxide (TiO₂) [12–14], Fe₃O₄ [15], ZnO [16] and their composites have generated considerable interest due to their nontoxicity, physical and chemical stability, regular pore structure, uniquely large specific surface area and exhibiting high catalytic efficiency [17–20]. TiO₂ possess high adsorption capacity and its modifications further enhances the surface area by controlling the growth of crystallites and gives higher porosity leading to high adsorption efficiency [21–27]. But its poor mechanical stability perhaps limits their practical application in some fields. To further extend the application of this material, we introduce poly(vinyl alcohol) (PVA) into TiO₂ and the results discussed in this paper. The resulting PVA modified hybrid was tough and flexible and exhibited good mechanical strength. The combination of PVA and TiO₂ results environmentally benign hybrid composite which can effectively separate

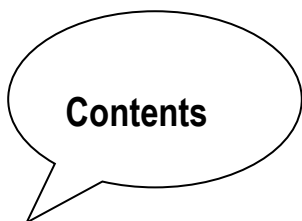
* Corresponding author.

E-mail address: abrahamjoseph@uoc.ac.in (A. Joseph).

Chapter 5

SYNTHESIS, CHARACTERIZATION AND APPLICATIONS OF TITANIA NANO HYBRIDS IN PHOTOCATALYSIS AND WATER PURIFICATION





Contents

5.1	Introduction
Part A	
5.2	Photocatalytic degradation of BPA with TiO ₂ - SiO ₂
5.2.1.	Results and discussion
5.3.	Photocatalytic activity analysis by HPLC
5.3.1.	Measurement of hydroxyl radical content through fluorescence spectra
5.3.2.	Photodegradation intermediates and pathways
5.3.3.	TOC measurement
5.3.4.	Kinetic study
5.4	Conclusions
Part B	
5.5	Superhydrophobic cotton fabric coated with GPTMS -HMDS modified Titania Silica nanocomposite for oil water separation
5.5.1	Results and discussion
5.5.2	Durability of the super-hydrophobic fabric
5.5.3	Separation of oil–water mixtures
5.6	Conclusions

This chapter is divided into two parts; Part A explains the characterization and application of titania and titania silica nanocomposite as photocatalyst for the degradation of BPA. The radical intermediates formed during the degradation of BPA, mineralization rate and degradation products exist in the solution were identified. Part B focuses the modification of titania silica nanocomposite with GPTMS and HMDS for the fabrication of super-hydrophobic coating on cotton fabric for the separation of oil from water. The durability of the coating was evaluated by exposing the specimen at harsh environments. The coated fabric free of fluorine and chlorine can be effectively utilized in various fields.

5.1. Introduction

The inflow of contaminants like organic dyes, heavy metals, organic compounds and oils etc., into water resources present a rising global issue. Choosing the most suitable method of wastewater treatment studies requires operating and investment costs. In this way advanced oxidation processes (AOPs) may become the foremost widely used water treatment technologies for organic pollutants. They are not treatable by conventional techniques due to their high chemical stability and/or low biodegradability [1]. AOPs are often used efficiently in wastewater treatment to remove persistent organic contaminants. The mechanism of oxidation process is determined by the very high oxidative potential of HO radical. Radicals produced by different mechanisms into the reaction medium [2].

Photocatalysis, also called the "green" technology, represents one of the main challenges in the field of treatment and decontamination systems, especially for water [3]. The degradation of pollutants under visible light using the photocatalytic properties of semiconductor materials synthesised by easy routes have been a hot area of research. Most of the semiconductor materials like TiO_2 , CdSe , WO_3 , Bi_2WO_6 , Bi_2O_3 , NiTiO_3 , ZnO and carbon dots, etc. are reported to have photocatalytic activity for the degradation of dyes and other organic pollutants, water splitting, solar cells etc[1]. Among these systems TiO_2 has a unique position in the field of photo-catalysis mainly due to its high photo-activity, good photothermal stability, low cost, and its eco-benign nature. The spectrum of activity of TiO_2

includes degradation of organic pollutants [2] treatment of endocrine disrupting compounds (EDCs) and emerging contaminants [3]. Bisphenol A (2, 2-bis (4-hydroxyphenyl) propane, BPA) is a representative xenoestrogens typically used in the manufacturing of numerous chemical products [4] and is suspected to several adverse effects including endocrine disruption [5]. Huge quantities of BPA are directly discharged into aquatic systems from a vast array of industrial sectors. In 2010, the United States Environmental Protection Agency (EPA) reported that over one million pounds of BPA were released into the environment annually, of which the possible hazards to fetuses, infants and young children were identified by the United States Food and Drug Administration (FDA) [2]. Possible sources of BPA in the environment include (i) discharges from wastewater treatment plants, (ii) landfills where BPA-containing products have been disposed of, (iii) sewage sludge used in agriculture, and (iv) leakages during its production and transportation [6]. It shows the extreme focus warranted in the treatment of water polluted by organic molecules including BPA [7, 8]. The conventional strategies used for the removal BPA from water include microbial degradation [2], adsorption [9], photo-catalytic degradation [2, 10, 11], etc. are not free from disadvantages like time-consumption and low efficiency.

Photo-illumination of TiO_2 cause electronic excitations and consequent generation of electron-hole (e-h) pairs. These e-h pairs later diffuse to the surface of TiO_2 and combine with molecular oxygen and hydroxide ions forming reactive radicals essential for the oxidation of pollutants. However, some inherent defects like relatively wide

band gap (about 3.2 eV) and low surface area have limited the practical applications of bare TiO₂. The efficiency of the degradation process depends on the production and subsequent reactions of •OH at or very near the surface of TiO₂[12-14]. As a consequence, modifications demand to improve the light absorption, charge separation, surface area, and surface reactivity of TiO₂[15-17].

Different strategies have been used for the addressing the limitations of TiO₂. Fabrication of mesoporous nanocomposite has been considered as one of the most promising ways to improve the photocatalytic activities of TiO₂. Mesoporous nanocrystalline TiO₂ and their composites has been demonstrated to be a more effective photocatalyst, because of its environmental friendliness, large surface area, ordered porous structure and large pore volume, which results in increasing surface reactive sites and improving mass transport. Weiyao Hu reported an easy strategy for the controllable synthesis of stable mesoporous black TiO₂ hollow spheres with a narrow band gap inhibits grain growth and anatase-to-rutile phase transformation, as well as maintaining high structural integrity, resulting in an increased photo-response from UV to visible light region and a significant improvement in the solar-driven photocatalytic hydrogen evolution rate[18]. Wei Zhou et al report the easy synthesis of ordered mesoporous black TiO₂ (OMBT) materials, which exhibit excellent photocatalytic hydrogen evolution efficiency, maintain ordered mesoporous structures as well as inhibit phase transformation (from anatase to rutile) and crystal growth during hydrogenation at 500 ° C and exhibit a high solar-driven hydrogen production rate[19]. Wei

Zhou et al prepared thermally stable ordered mesoporous anatase TiO_2 with high crystallinity and large pore size (10 nm) through an EISA approach combining with encircling EN protectors to maintain the liquid crystal mesophase structure of mesoporous TiO_2 primary particles, followed by calcination at higher temperature. The same group also synthesized ordered mesoporous TiO_2 with a large pore size ranging from 8 to 14 nm through evaporation-induced self-assembly (EISA) approach and butanol released in situ as swelling agent [20]. Several investigations have focused on anchoring the TiO_2 on supports with high surface area and porosity [21]. The approach of fabrication of ordered mesoporous TiO_2 -based photocatalysts with uniform pore channels, high BET surface area, and large pore size improves the photocatalytic activity of the resulting material [22, 23]. It is reported that SiO_2 improves the surface area of TiO_2 which is essential for the enhanced photocatalytic activity of TiO_2 . Linlin Zhang et al fabricated novel ordered mesoporous SiO_2 - TiO_2 coated circulating-bed biofilm reactor is promising in the environmental field [24]. It was reported by Chao Xie [25] and co-workers that the surface adsorbed water and hydroxyl groups are crucial for photo-catalytic activity and anatase phase is more active than rutile in adsorbing water and hydroxyl groups. Thus, SiO_2 was introduced into TiO_2 framework to create composites with well-defined mesoporous structure and enhanced thermal stability of the anatase phase [26]. Cheng et al. reported that SiO_2 -doped TiO_2 have high photocatalytic activity due to the suppression of the anatase to rutile phase transition and the formation of oxygen vacancies [27]. The high crystallinity and anatase phase of

TiO₂ will favour Photocatalysis. The introduction of SiO₂ could inhibit crystal phase transform of TiO₂ from anatase to rutile. Mesoporous SiO₂ -TiO₂ would improve photon utilization, organic molecule adsorption, and microorganism loading, and increase the surface reactive sites, due to its large surface area, ordered pore structure and large pore volume[24]. Consequently, the incorporation of SiO₂ into a TiO₂ matrix have high surface area, enhanced thermal stability of the anatase phase, efficient electron–hole separation and absorption of light from the visible range. Several reports are available on the photo-catalytic degradation of BPA using visible light sensitive photo-catalysts including TiO₂ based composites [20,26-29]. However, limited information is available with TiO₂ - SiO₂ composite as photocatalyst for the degradation of BPA under visible light. Yuxin et.al [28]reported metallic platinum doped ordered mesoporous TiO₂ - SiO₂ material for the degradation of BPA under light irradiation.

In this work we also focussed on a serious environmental issues that cause threat to living system due to water contamination by oil which resulted from oil production, oil delivery, oil refining industries and petrochemical operations. Millions of tons of refined oil and crude oil leak into the sea every year, which is responsible for pollution of natural aquatic environment and ecological, damage [29-34]. A typical mining operation produces 1,40,000 L of oil-contaminated water per day[35]. Many industries, such as mining, textiles, foods, petrochemicals, and metal/steel industries, produce massive volumes of oily wastewater, which has become an extremely common pollutant all over the world, and is now a serious global environmental

concern[36, 37]. For example, several types of mechanical devices, including oil skimmers or booms, have been used to purify these oil/water mixtures, but they require an input of energy or high pressure to operate. Therefore, it is of great significance to explore a simple, economical and effective method for the separation and collection of oil from oil–water mixtures. Studies related to this field are mainly focused on surface super wettability, such as superhydrophobicity, superhydrophilicity, superoleophobicity, and superoleophilicity [38].

Super hydrophobic cotton as filter material has been used recently[39]. Mimicking the hierarchical micro/nanoscale morphologies of lotus leaves and butterfly wings that possess superhydrophobic property (surfaces with a water contact angle greater than 150°) has led to the fabrication of numerous artificial superhydrophobic surfaces. Various strategies have been proposed for imparting hierarchical surface to substrates, such as template methods, colloidal self-assembly, sol–gel processing, electro-spinning, layer-by-layer deposition, lithography and others [40-42]. The dip coating method is considered to be a superior method compared to others because it is inexpensive, simple and provides an easy adjustment of the chemical composition needed for super-hydrophobic behavior. Super-hydrophobic materials have a wide range of applications [43-47]. Many findings have also been reported on the preparation of super-hydrophobic surfaces and its applications in oil–water separation [48-52]. Although these coatings on cotton fabrics offer high oil–water separation efficiency, the use of fluorinated and chlorinated compounds during its preparation limits its direct use. Halogenated compounds are more expensive, toxic, non- biodegradable and easily reactive with other materials and sometimes produces halo acids [53].

Therefore, it is necessary to obtain fluorine and chlorine free coated fabrics with super-hydrophobic and super-oleophilic properties.

In recent years widespread applications have been emerged for titania as well as silica-based hybrids. Silica or titania are best choices to fabricate super-hydrophobic surfaces due to their low toxicity, controllable structure and promising thermal stability, strength and durability under drastic environmental conditions [54, 55]. Some of the materials with poor hydrophobicity allow both water and oil to pass and hence non-effective for oil- water separation. Considering these issues, it is highly desirable to develop some durable, super-hydrophobic materials under acidic, alkaline, salty UV light conditions using inexpensive and simple chemical routes. Some of the earlier works conducted for the oil water separation using different materials are summarised in Table 1.

In the first part of this chapter, we focus on the photodegradation efficiency of TiO_2 and TiO_2 - SiO_2 mesoporous composites for the removal of BPA under visible light irradiation. Major degradation products were identified and possible reaction pathways were proposed. In the second part, we demonstrated a simple, effective and viable approach to prepare super-hydrophobic cotton material. The resultant fabric has been effective for the separation oil from oil- water mixtures. Moreover, the durability of the coating was evaluated under harsh environmental conditions like exposure to acidic, alkaline, salty solutions, ultraviolet irradiation, and stability by using the adhesive tape test, abrasion test, and under washing.

Part A

5.2. Photocatalytic degradation of BPA with TiO₂ - SiO₂

5.2.1. Results and discussions

5.2.1.1. XRD

The XRD patterns are displayed in the Figure 1 A and B. Generally, TiO₂ undergoes anatase to rutile transformation from 600°C. It is clear from Figure 1 that bare TiO₂ (TS) as well as TiO₂ - SiO₂ (TS) nanocomposite calcined at 500°C and 600°C (T₅, T₆ and TS₅, TS₆) has achieved pure anatase phase (JCPDS 75-1537). The peaks for bare TiO₂ at 700°C (T₇) are shown to have resulted from both anatase (A) and rutile (R) at theta 27.46° (R), 37.61° (A), 39.21° (R), 41.34° (R), 44.14° (R), 47.7° (A), 54.12° (A), 64.2° (R). The peaks for TiO₂ - SiO₂ nanocomposite at 700°C (TS₇) register at theta 25.46° (A), 37.86° (A), 48.28° (A), 54.02° (A), 55.22° (A), 62.82° (A) respectively. It was observed from the Figure 1(A) that for bare TiO₂ the transformation from anatase to rutile was occurred at 700°C while for the TiO₂ - SiO₂ nanocomposite at 700°C, the anatase phase was observed (Figure 1B). The phase transition from anatase to rutile is inhibited at this temperature confirms the high temperature anatase phase stability of TiO₂ - SiO₂ composite. The crystallite size of T₅, T₆, T₇ and TS₅, TS₆, TS₇ samples was calculated using the Scherrer equation (1) and the results were tabulated in Table 1. It has been found that the TiO₂ - SiO₂ crystallite size of samples are lower than bare TiO₂. It has been reported that, at the interface, the SiO₂ lattice locks the Ti-O species at the interface of the TiO₂ domains, preventing

the nucleation which is necessary for the phase transformation from anatase to rutile. Hence, greater heat is required to drive the crystallization [56]. Therefore, even though silica is a subsidiary component in the present study, it plays a critical role in effectively preventing the complete transformation of anatase to rutile phase even at high calcination temperature [57].

Table 1. Crystallite size calculated from XRD data

Sample	Crystallite size (nm)
T ₅	12.5
T ₆	13.2
T ₇	21.8
TS ₅	8.3
TS ₆	8.8
TS ₇	15.8

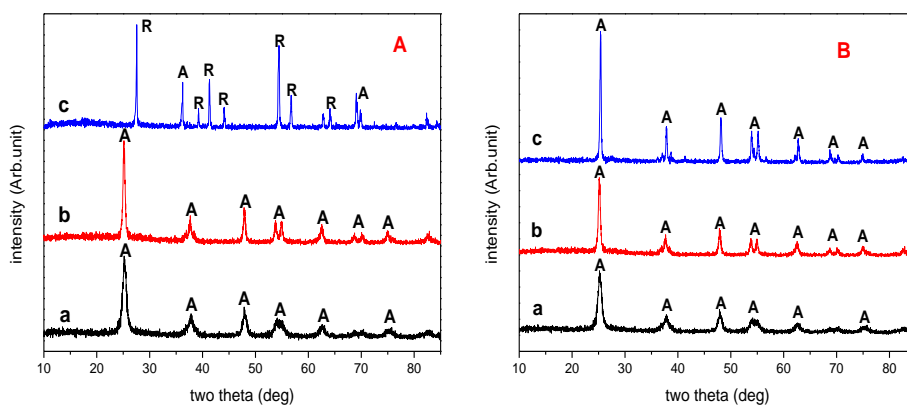


Figure 1 XRD spectra of A) a) T₅ b) T₆ and c) T₇ sample and B) a) TS₅ b) TS₆ and TS₇ sample

5.2.1.2. FTIR Spectra

The FTIR spectra for T₅, T₆, T₇ and TS₅, TS₆, TS₇ samples are shown in Figure 2 A and B. The characteristic absorption band of Ti-O-Ti stretching (bridging) mode lies at around 500 cm⁻¹. Specifically, the bands located at 800 cm⁻¹ and 1080 cm⁻¹ are attributed to Si-O-Si bending; the band at 960 cm⁻¹ is attributed to Si-OH stretching; and the broad band in the 3400 cm⁻¹ is attributed to the stretching of OH groups of absorbed water molecules. This band may also contain the contribution of absorbed molecular water on Ti-OH from the surface of TiO₂ particles[58]. Regarding the peaks associated with TiO₂, it is often reported[59] that bands observed in the range 900-1000 cm⁻¹ may be associated with Ti-OH and Si-O-Ti species.

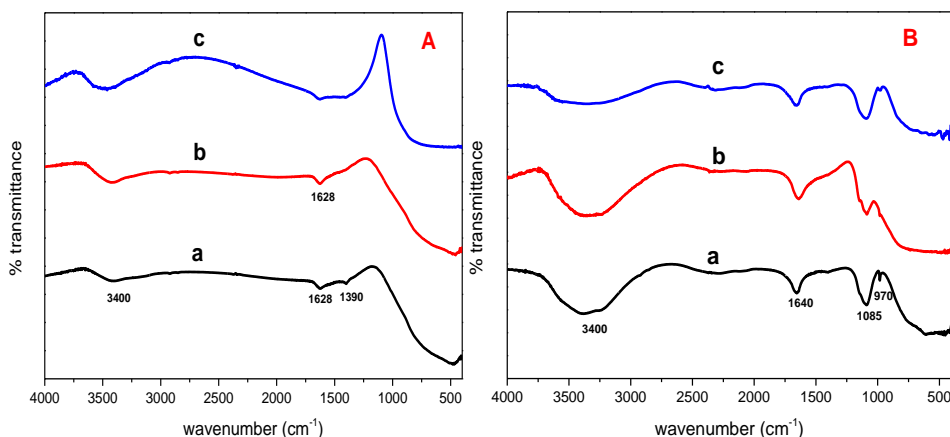


Figure 2. FTIR spectra of A) a) T₅ b) T₆ and c) T₇ sample and B) a) TS₅ b) TS₆ and TS₇ sample

5.2.1.3. FESEM with EDX Analysis

For studying the morphology of products formed during the reaction, SEM analysis was carried out. FESEM images of T₇ and TS₇

is displayed in the Figure 3 A and B. FESEM images of T_7 and TS_7 shows nanoscale textures. TiO_2 as well as composite exhibit spherical shape with particle size in the range of 25 nm, and 10 nm respectively. The hydrothermal treatment allows the nanocomposite to have smooth and uniform texture without agglomeration.

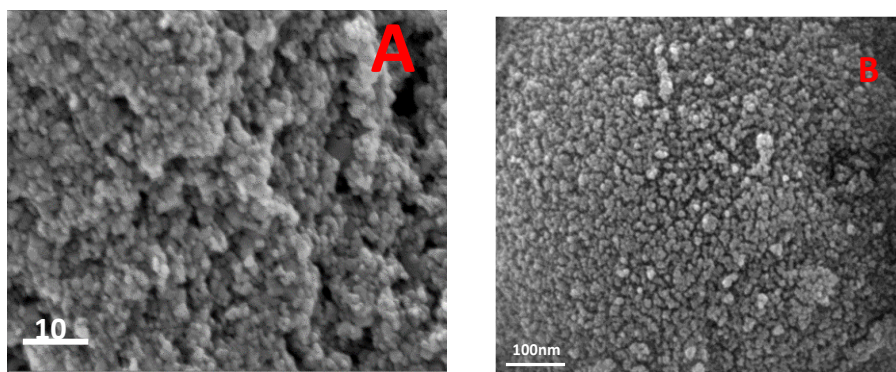


Figure 3. FESEM images of (A) T_7 , (B) TS_7 sample.

5.2.1.4. HRTEM Studies

The morphological analysis of T_7 and TS_7 was done through HRTEM and the image is provided in Figure 4 A and B. For the T_7 sample, the TiO_2 particle has a size of 20 nm and the lattice fringes corresponding to the (101) plane of rutile having inter-planar spacing of 0.31 nm. For the TS_7 sample the particle size of 11 nm was observed. The TiO_2 - SiO_2 composite having sizes of 11 nm was observed in the TEM image. The high-resolution image Figure 4 C and D shows the lattice fringes corresponding to the (101) plane of anatase TiO_2 with an inter-planar spacing of 0.33 nm

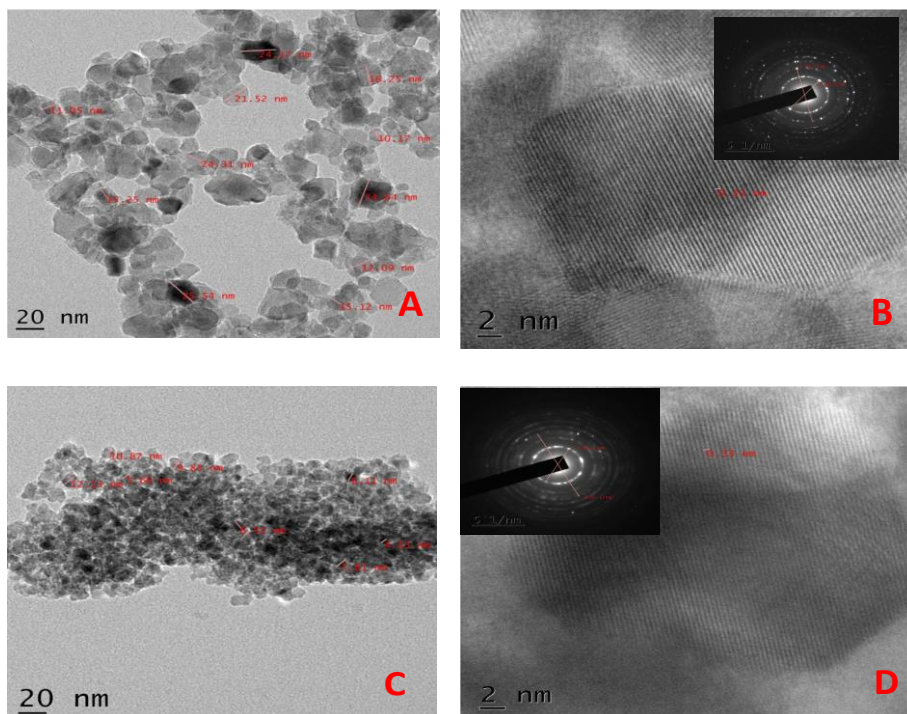


Figure 4. TEM images of (A) T₇, (B) TS₇ and HRTEM images of (C) T₇ and (D) TS₇

5.2.1.5. XPS Analysis

XPS study was performed to gather more evidence to substantiate the purity and the existence of Ti–O–Si bonds in TS₇ composite as shown in Figure 5A-D. The binding energy of Ti_{2p}_{3/2} appeared at 459.5 eV; and Ti_{2p}_{1/2} appeared at 465.3 eV for TS₇ sample (Figure 5A&B). The difference between the two peaks was found to be 5.7 eV which is the characteristics of the abundance of Ti⁴⁺ on the surface of the catalyst [60]. The results significantly reveal the strong interaction exist between SiO₂ and TiO₂. The binding energy of Ti_{2p}_{3/2}

appeared at 458.8 eV; while that of O1s appeared at 530.7 eV (Si–O–Ti) and 532.4 eV (Si–O–Si) respectively (Figure 5C&D).

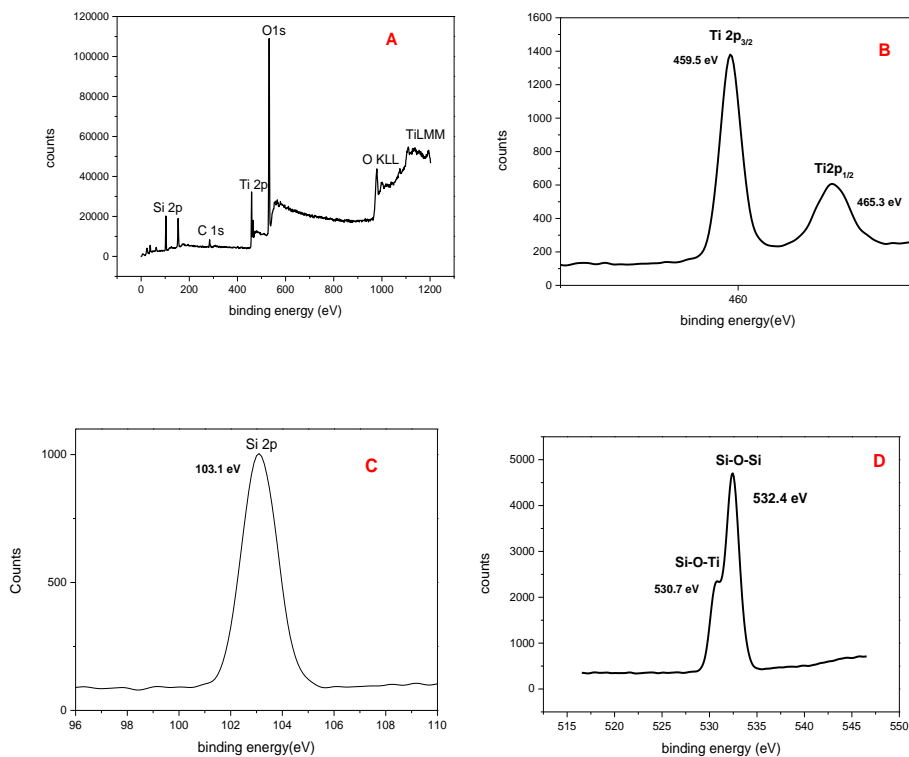


Figure 5. XPS survey spectra of A) TS₇, High resolution XPS spectra of (B) Ti2p (C) Si2p (D) O1s of TS₇ sample.

The peak of higher energy was attributed to the oxygen bonded to the silicon atom and of lesser energy to the oxygen bonded to the titanium atom [61]. The binding energy of Si2p appeared at 103.1 eV. The charge of the Ti atom of TS₇ changes due to the interface formation of TiO₂-SiO₂. The formation of interface Ti-O-Si linkages decreases the positive charge on the Ti atoms at the interface, resulting

in a lower binding energy of the 2p electron of Ti in TiO₂-SiO₂. Generally, for pure TiO₂ the binding energy of Ti2p_{3/2} appeared at higher energy ranges.

5. 2.1.6. DRS Studies

The absorbance spectra and Tauc plot of T₇ and TS₇ samples were displayed in Figure 6 A and B respectively, Band gap calculated from Tauc plot for T₅, T₆, T₇ and TS₅, TS₆, TS₇ samples calcined at various temperatures were shown in Table 2.

The band-gap energy (E_g) was calculated by the following relationship;

$$\alpha(h\nu) = \alpha_0 (h\nu - E_g)^n \quad (3)$$

where α is absorption coefficient, $h\nu$ is the photon energy, α_0 and n are the constants, E_g is the optical band gap of the material, and n depends on the type of electronic transition and can have values between 1/2 and 3 [62, 63]. The band gap energy of the TS₅, TS₆, and TS₇ calculated from Tauc plot is lower than T₅, T₆, and T₇ samples. This is due to the introduction of SiO₂ in to TiO₂ and confirms the formation of composite. The absorption edge is significantly extended towards the visible light range for TiO₂ - SiO₂ samples. The red shift in the absorption spectra of TS₇ sample from UV to visible region can be seen in the Figure 6 A, which results an enhancement in the photocatalytic activity.

Table 2. Band gap calculated from DRS spectra

Sample	Band gap (eV)
T ₅	2.80
T ₆	2.64
T ₇	2.70
TS ₅	2.65
TS ₆	2.58
TS ₇	2.45

5.2.1.7. BET analysis

The surface area and pore volume were depicted from the Brunauer Emmette Teller (BET) nitrogen adsorption–desorption isotherm analysis and the average pore size was measured through the Barrer–Joyner–Halenda (BJH) technique at $-195.80\text{ }^{\circ}\text{C}$ of T₇ and TS₇ shown in Figure 6 C and D.

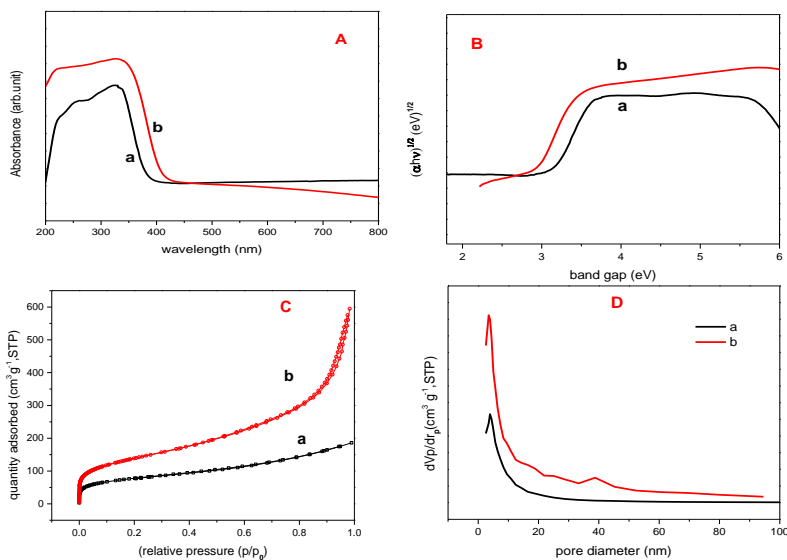


Figure 6 A) UV spectra and B) Tauc plot C) N₂ adsorption - desorption curve D) BJH pore size distribution curve of a) T₇ and b) TS₇ sample.

The adsorption and desorption isotherm of samples exhibit Type IV behaviour with a typical H3 hysteresis loop and which represents the mesoporous nature of the material[60]. The estimated surface area, pore volume and desorption pore size of the synthesised samples were shown in Table 3. The BET surface area of T₇ and TS₇ was calculated to be 278 m²g⁻¹ and 495 m²g⁻¹ respectively. The specific surface area of TS increasing after the incorporation of SiO₂. The TS₇ sample has higher surface area when compared with other samples and it is due to the presence of SiO₂ on the surface of TiO₂. The pore diameter varied from ~ 4 nm to 50 nm. For T₇ pore diameter found to be 3.5nm and for TS₇ is 7.9 nm indicating its mesoporous structure.

Table 3. Textural properties of synthesized catalysts.

Sample	S _{BET} (m ² g ⁻¹)	Pore volume (cm ³ g ⁻¹)	Pore diameter (nm)
T5	267.2	0.159	2.38
T6	223.3	0.189	3.39
T7	278.9	0.288	4.13
TS5	415.5	0.947	9.12
TS6	472.3	0.904	7.66
TS7	497.7	0.919	7.39

5.3. Photocatalytic activity analysis by HPLC

Figure 7 A and B shows degradation curve of T₅, T₇; T₆, TS₅ and TS₆, & TS₇ samples. Prior to visible light irradiation, the reaction mixture was magnetically stirred for 15 min in dark in order to obtain a homogeneous suspension having adsorption– desorption equilibrium and the adsorption of photocatalysts for the BPA was found to be negligible. From Figure 7, it is observed that 99% BPA degradation occurred within 32 min of reaction time using TS₇. Among the T₅, T₆,

& T₇ samples photocatalytic activity is superior for T₆ sample. Similarly, by comparing TS₅, TS₆, & TS₇ samples better photocatalytic activity is exhibited by TS₇. For T₆ around 50% degradation occurred in 32 min of reaction time and the same for T₇ sample is only 37%.

It was reported that the active species could be different for different catalysts or for photo-degradation of different contaminants. In the process of photocatalytic degradation of organic dyes, semiconductor photocatalyst produces various active intermediates under irradiation. The effects of various kinds of trapping agents were investigated to identify the function of each active species in the photocatalytic cycle of BPA. We have studied different interfering ions involved in the reaction using different radical scavengers on photo-degradation processes. The radical trapping agents potassium iodide (KI) was added to determine the participation of holes (h^+), tert.butanol (tBuOH) was added to recognize $\bullet OH$, sodium azide (NaN_3) and benzoquinone (BQ) as O_2 and $O_2^{\bullet -}$ radical scavengers to investigate specific reactive species [64]. Photocatalytic efficiency of TS₇ catalyst in the presence of these scavengers was noted as it possesses high efficiency. After the addition of scavengers, degradation rate was noted and the results were displayed in the Figure 7 C. From the Figure it can be concluded that the addition of NaN_3 and BQ will not alter the degradation rate of BPA. However, the degradation rate of BPA was decreased in the presence of tert.butanol (tBuOH), and KI. The quenching of reaction clearly confirms that $\bullet OH$ and h^+ are the main active species responsible for the degradation process. It can be concluded that due to the combined effects of high surface area, heteronano structure, thermo stable anatase phase and low

crystallite size contributed to the higher photo-degradation efficiency of TiO_2 - SiO_2 composites.

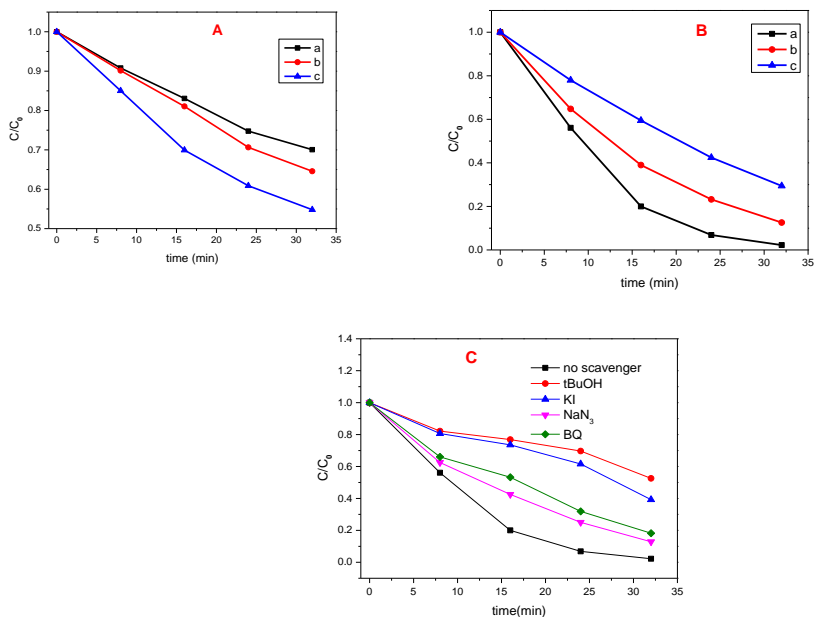


Figure 7. Concentration Vs time plot showing the degradation of BPA with (A) a) T_5 b) T_7 and c) T_6 sample and B) a) TS_5 b) TS_6 and TS_7 sample C) with various scavengers under visible light irradiation.

5.3.1 Measurement of hydroxyl radical content through fluorescence spectra

Fluorescence spectra of T_7 and TS_7 samples were measured at regular interval of time after visible light irradiation and the same are shown in Figure 8 A and B. The PL intensity proportional to the hydroxyl radical generation indicates the formation of hydroxyterephthalate. The non-fluorescent terephthalic acid reacts with $\bullet\text{OH}$ to form a fluorescent hydroxyterephthalate at 423nm which can be assessed by the PL intensity. The PL intensity noted at regular

interval of time. From Figure 8A, it is clear that initially the PL intensity is nil, and after 8 min irradiation under visible light PL intensity increased. As the irradiation time increased from 8 min to 32 min the PL intensity was found to be increased. This could be due to the production of large amount of $\bullet\text{OH}$ during the reaction. Thus, as the catalyst in aqueous solution undergo visible light irradiation, $\bullet\text{OH}$ produced which was responsible for photocatalytic degradation BPA during the reaction.

The lower PL intensity for T6 sample corresponds to lower production of $\bullet\text{OH}$ and lower photo catalytic degradation efficiency. The proposed degradation mechanism is shown in the Figure 8 C.

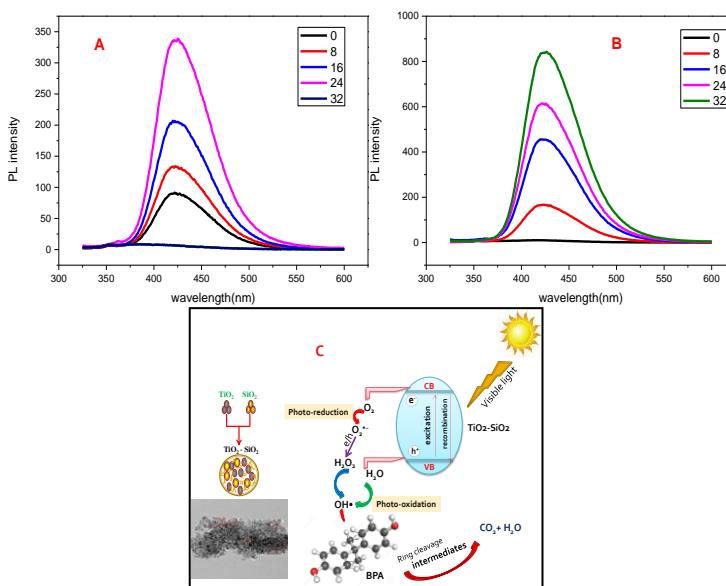


Figure 8. Photoluminescence (PL) spectra of produced hydroxyterephthalic acid in the presence of A) T₇ and B) TS₇ after visible irradiation at regular intervals of time C) Pictorial representation of the proposed degradation mechanism

5.3.2. Photodegradation intermediates and pathways

BPA degradation pathways are proposed on the basis of LC-MS analysis. Previous works in this area suggested that the degradation pathway of BPA by $\bullet\text{OH}$ be classified as: (1) BPA was degraded through hydroxylation, producing hydroxylated and multi-hydroxylated intermediates [7, 65] and (2) $\bullet\text{OH}$ react with aromatic rings by electrophilic substitution due to its electrophilic character [66]. The proposed degradation pathway of the oxidation of BPA is presented in Fig. 9. Herein, the product ion at m/z 227 is identified as the deprotonated molecule $[(M - H)^-]$ of BPA, and other product ions are identified as the deprotonated molecule of intermediates. Initially, BPA molecules are attacked by radicals at the 3-position of the phenyl ring to produce hydroxyl-BPA, which can be easily oxidized into aliphatic compounds containing carboxylic groups along with the cleavage of benzene rings. The carbon atoms at the para-positions with the highest frontier electron density are the most likely sites to be attacked by $\bullet\text{OH}$, leading to the decomposition of BPA into phenol or its derivatives. The ring-rupturing products are presumably further oxidized to produce carboxylic acids, which are finally transformed into CO_2 and H_2O .

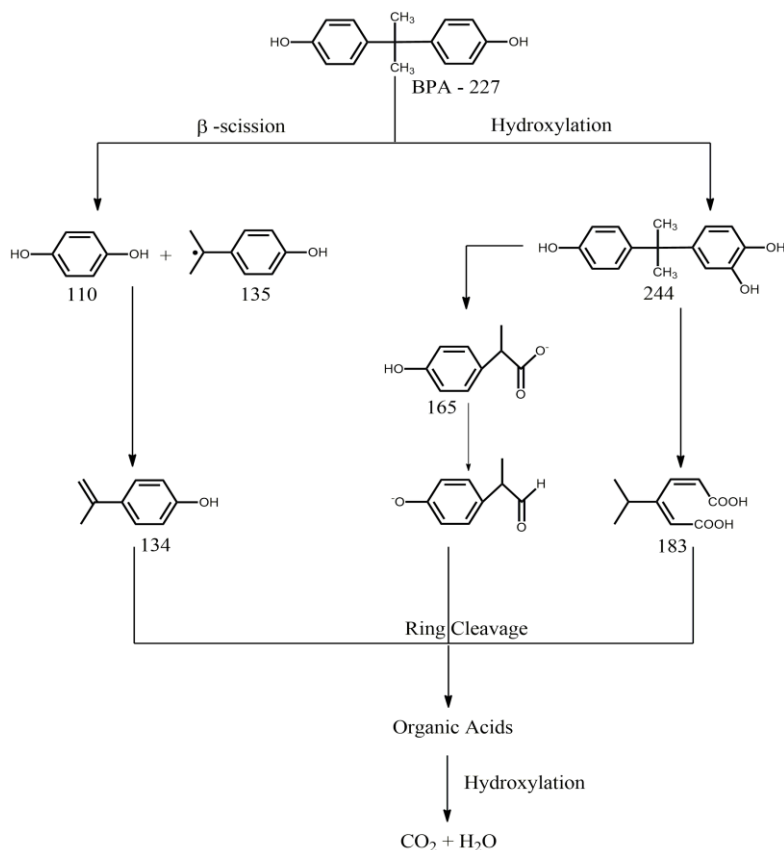


Figure 9. Proposed BPA degradation pathway by TS₇ catalyst under visible light irradiation

5.3.3. TOC measurement

A plot of relative organic carbon content as a function of time is shown in the Figure 10 A which was conducted to analyse the amount of total organic carbon present in the degraded medium after each time interval. It has been concluded that the TOC calculated in the solution was found to be decreased as time increases. The TS₇ sample has lower TOC compared to T₇ at the same exposure period.

5.3.4. Kinetic study

The kinetics of BPA degradation can be mainly studied by pseudo-first-order equation. According to Langmuir–Hinshelwood model, when the initial concentration, C_0 is very small the following pseudo-first-order rate equation can be used.

$$\ln \frac{C_0}{C} = k_1 t \quad (4)$$

where k_1 is pseudo first order rate constant (min^{-1}) and C is the concentration at time t . A plot of $\ln \frac{C_0}{C}$ vs t gives the value of k_1 . Figure 10 B corresponds to the fitted curves of T_7 and TS_7 samples. A good linear relationship exists between $\ln \frac{C_0}{C}$ vs t with a good regression constant value of 0.985 and 0.985 for T_7 and TS_7 samples respectively. The reaction rate constants k_1 for various photocatalysts were determined from the slope of the fitted curves by means of linear regression. The rate constant for TS_7 photocatalyst is highest i.e. 0.1214 min^{-1} compared to T_7 which has rate constant 0.0192 min^{-1} showing that TS_7 is a better catalyst than T_7 . From the Figure 10 it has been concluded that the BPA degradation followed the pseudo first order kinetic model.

Reusability is another important characteristic of a photocatalyst in industrial processes because use for longer periods of time leads to a substantial decrease in the cost of the process. The degradation of BPA with titania-silica hybrid was repeated 5 times,

and the results (Figure 10 C) indicated that the adsorbent showed good activity, even after 5 repeated recycles

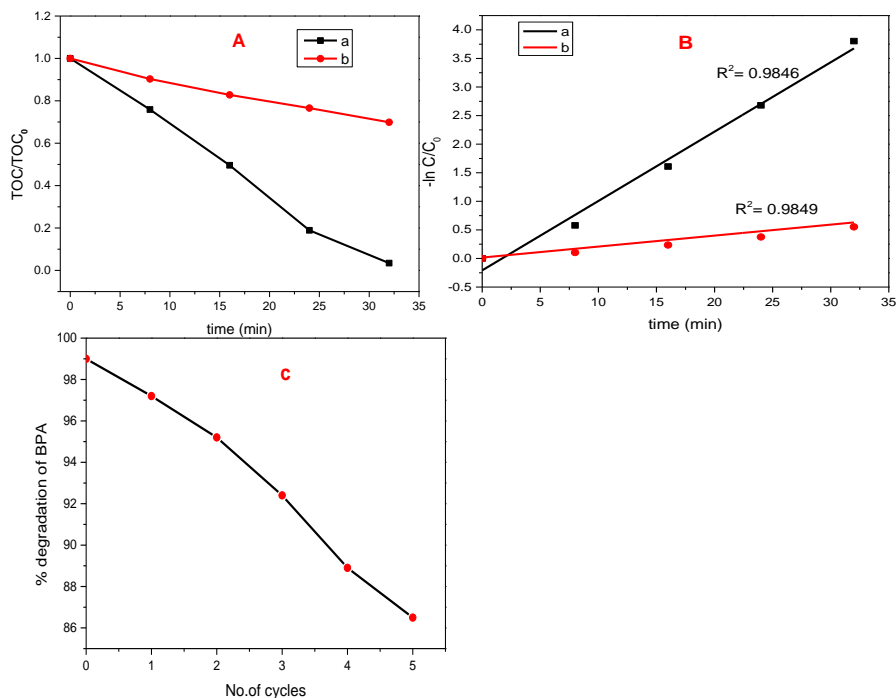


Figure 10. A) Relative organic carbon content as a function of time plot after visible light irradiation B) Pseudo 1st order Kinetic plots of a) T₇ and TS₇ sample C) Reusability of hybrid nanocomposite, % degradation of BPA Vs number of cycles of hybrid nanocomposite.

5.4 Conclusions

1. Mesoporous Titania (TiO₂) and Titania-silica (TiO₂ – SiO₂) nanocomposites have been synthesized through a simple hydrothermal sol-gel route and the synthesized materials

characterized through techniques such as XRD, FTIR, DRS, FESEM, HRTEM, BET and XPS.

2. The phase transition from anatase to rutile is inhibited at high temperature (700°C) for TS₇ catalyst confirms the high temperature anatase phase stability and lower crystallite size of TiO₂ - SiO₂ samples compared to TiO₂ samples which is confirmed from XRD, FESEM and TEM analysis.
3. The band gap energy of the TiO₂ - SiO₂ samples calculated from Tauc plot is lower than TiO₂ samples. The red shift in the absorption spectra of TS₇ sample from UV to visible region results an enhancement in the photocatalytic activity.
4. The surface area and pore volume of the TiO₂ - SiO₂ composites were determined using BET analysis and achieved very high surface area of 495 m²g⁻¹ and high pore volume 0.9535 cm³ g⁻¹ for TS₇.
5. The prepared TiO₂ - SiO₂ composites rapidly degrade the endocrine disrupting compound Bisphenol A (BPA) under visible light within 32 min and the degradation efficiency of TiO₂ - SiO₂ had been compared with bare Titania catalysts.
6. The relationship between the calcination temperature and photocatalytic activity of the material is established. Among the prepared catalysts TS₇ was found to be the best photocatalyst for the oxidation of BPA under the specified conditions and the

TOC analysis for degradation of BPA was in good agreement with the results obtained from HPLC studies.

7. Various radical scavengers were introduced to understand the role of reactive species produced during degradation of BPA and found that the major contribution was from $\bullet\text{OH}$ radicals. The presence of $\bullet\text{OH}$ and its quantification has been done by using fluorescence technique and the results support the chemical examination and based on the results, a comprehensive route is proposed for the degradation of BPA.
8. The degradation of BPA followed pseudo first order kinetics and the higher photocatalytic activity of the TS₇ was mainly due to factors like absorption characteristics, high temperature anatase phase stability, lower particle size, meso pores with high surface area, lower degree of electron hole recombination, and higher production of $\bullet\text{OH}$.

Part B

5.5 Cotton fabric coated with HMDS-GPTMS modified Titania Silica nanocomposite for oil water separation

Some of the earlier works conducted for the oil water separation using different materials are summarised in Table 4.

Table 4. Previous works at a glance

Material	Results	Reference
SiO ₂ nanoparticles modified with (heptadecafluoro-1,1,2,2-tetradecyl) trimethoxysilane (HFTMS) cotton fabric	WCA 170°, oil-water separation efficiency > 97% after single cycle	[67]
Polyaniline and fluorinated alkyl silane to the polyester fabric	WCA slowly decreased from 156° to 146° after 30 separation cycles, durable under severe environments	[49]
Fluoroalkylsilane modified TiO ₂ cotton fabric	WCA 160°, UV light durability for 24 h, super-hydrophobicity retained for at least 5 cycles oil– water separation	[68]
Superhydrophobic bi model SiO ₂ NPs coated fabric	WCA 158°, oil-water separation efficiency 90% after single cycle.	[69]
Organically modified silica- PDMS coated cotton fabric	WCA 160°, oil-water separation efficiency 98.5% after 10 cycles, good abrasion resistance, chemical stability for 24 h	[70]

5.5.1 Result and discussion

The surface of $\text{TiO}_2\text{-SiO}_2$ system is functionalized by HMDS through the replacement of numerous hydrophilic OH groups present on the surface of $\text{TiO}_2\text{-SiO}_2$ with hydrophobic $-\text{CH}_3$ groups to form $-\text{OSi}(\text{CH}_3)_3$. Hydrophobic gels were made super hydrophobic with excess HMDS and GPTMS which facilitate the miscibility of the hybrid in the matrix as well as provide good adherence to the fabric.

The water contact angle (WCA) on the coated fabric was measured using sessile drop method and the mean value of the contact angles was taken and shown in the Figure 11. The WCA on the coated fabric was found to be $161.5^\circ \pm 1.02^\circ$ indicates that the hydrophilic surface of the bare fabric was modified to super-hydrophobic after coating. The Coated Fabric (CF) completely repelled water as soon as water droplets falls on the surface.

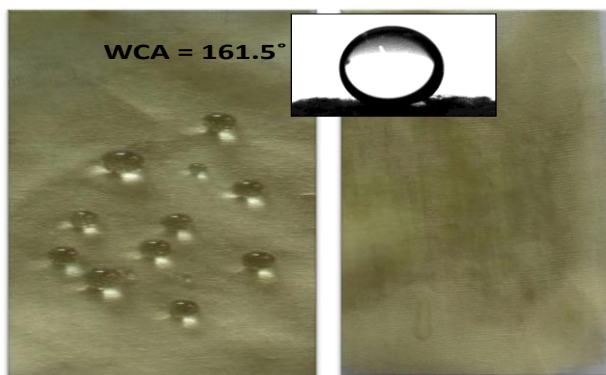


Figure 11. Photographic image of coated and uncoated fabric with water drops on it

To understand the chemical modification of the cotton fabric upon coating and also the functional groups present, ATR spectroscopic studies were carried out. Figure 12 shows the ATR spectra of CF and Uncoated Fabric (UF). As expected, common peaks were observed for the stretching vibrational modes of pure cotton fabric in both spectra. In addition to this, a peak at 968 cm^{-1} which was assigned for the stretching and bending modes of Ti-O-Si also seen in the spectra. Besides, two characteristic peaks are observed at 1131 and 1180 cm^{-1} , which strongly indicates the presence of Si-CH₃ bonds on CF and is a clear evidence of super-hydrophobicity. Two intense peaks at 2858 and 2912 cm^{-1} are assigned to the C-H stretching of the CH₂ groups. Also, after coating an intense peak located at 2965 cm^{-1} owing to the C-H stretching of CH₃ group on CF. The broad band in the range 3600 cm^{-1} attributed to Si-OH groups and also Ti-OH groups with absorbed water molecules. The surface morphologies of CF and UF were displayed in Figure 13. A hierarchical surface structure was observed for CF which is a very essential requirement for a surface to have super-hydrophobic properties. It is seen from the figures that the surfaces of CF are rougher than the UF. The UF showed a smooth surface. The combination of the nanoscale roughness of the aggregated clusters and the inherent micro-scale roughness of the bare fabric could be the main reason for the super-hydrophobicity of the CF [71].

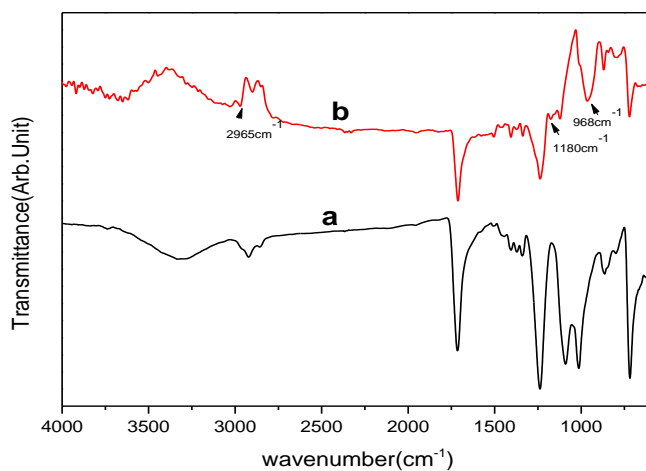


Figure 12. ATR spectra of a) uncoated b) coated fabric.

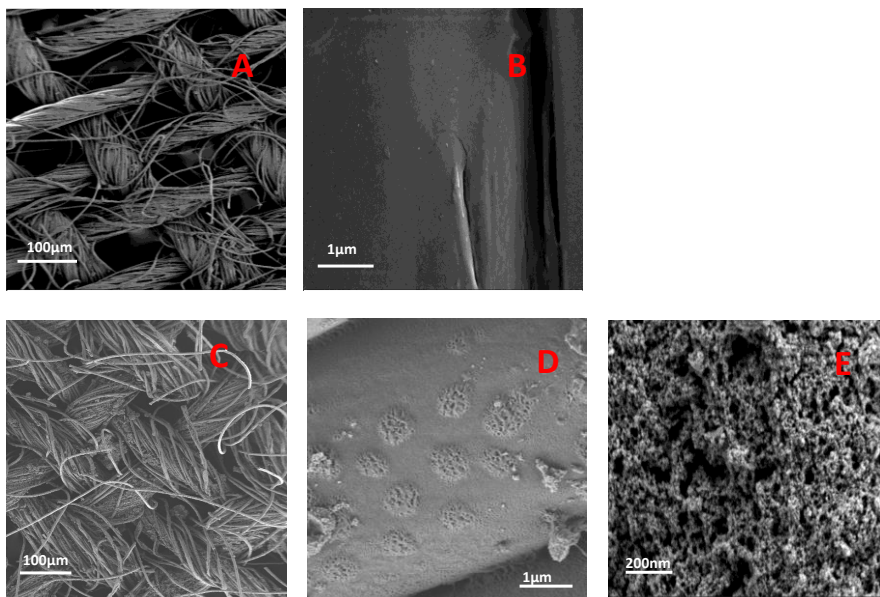


Figure. 13. FESEM image of A & B uncoated and C, D & E coated fabric

5.4.2. Durability of the super-hydrophobic fabric

The chemical as well as mechanical stability of the coated fabric is an important criterion for practical applications of super-hydrophobic coatings. The WCA after immersing in acidic (0.5M HCl), salty (3 wt % NaCl solution) and alkaline (0.5 M NaOH) solutions for every 24 hours were shown in the Figure 14 A and B. It was observed that even though the CF immersed in harsh environmental condition for 72 h, there was only a slight variation in WCA from the initial value. The same test was repeated under UV irradiation to 72 hours and the contact angles of the samples were measured every 24 h. The WCA result (Figure 14 B) confirms that UV light exposure would not affect the stability of coating suggesting superior UV durability. Thus, the results of the study indicate that the CF has very good chemical stability.

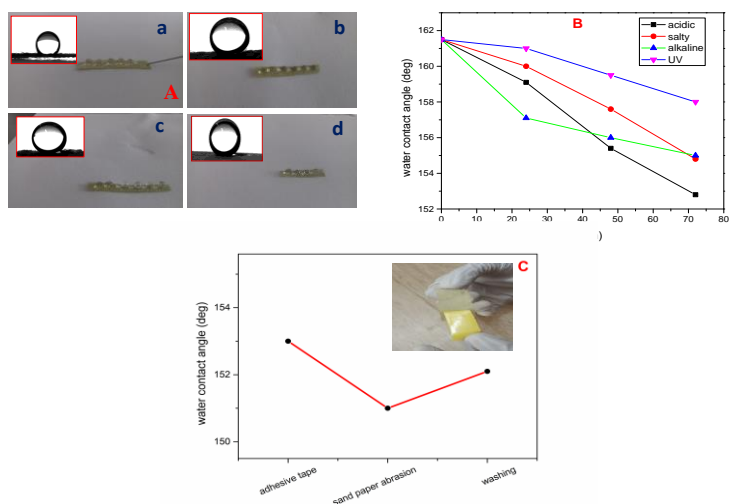


Figure 14 A) Image of coated fabric immersed in a) acidic b) alkaline c) salty solution and d) UV irradiation after 72 h B) corresponding contact angle for every 24 h C) mechanical durability Vs contact angle after repeated cycles (inset: adhesive test photograph)

The tear test with an adhesive tape was conducted for 15 cycles (Figure 14 C) and even after 15 cycles the surface coating exhibited super-hydrophobicity with only a slight change in WCA. The WCA measured after 10 times repetition of abrasion test was $150.8^{\circ} \pm 1^{\circ}$ which was shown in Figure 14 C signifying the presence of a stable coating on the fabric. The mechanical properties of the CF and UF were done after conducting 3 trials. The average tensile strength of CF and UF obtained was $28.3 \pm 0.562 \text{ N/mm}^2$ and $10.2 \pm 0.658 \text{ N/mm}^2$ respectively. Three times increase in tensile strength was observed for CF compared to UF. The value of Young's modulus recorded for UF and CF and was $0.51 \pm 0.478 \text{ N/mm}^2$ and $2.53 \pm 0.625 \text{ N/mm}^2$ and five times increase in Young's modulus has been recorded upon coating. Thus, mechanical properties of the CF have improved. The presence of GPTMS makes good adhesive force to the fabric due to the strong covalent type bonding between the fabric and the polymer. The reusability of the fabric after washing is very important and the durability examined after repeated washings show no drastic change in contact angle (Figure 14 C).

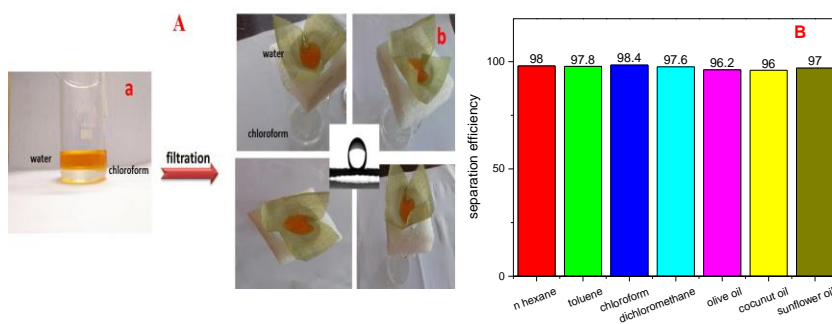


Figure 15 A) image of oil- water separation experiment a) before separation b) after separation B) separation efficiency of different oils after 15 cycles of separation

5.4.3. Separation of oil–water mixtures.

Further evaluated the oil–water separation properties of the coated fabric using oils with different densities. After proper mixing (1:1 volume ratio), the oil -water mixture was poured onto the surface of CF and the colourless oil collected in the beaker without any external force. The CF allows oil into it and water remained on the fabric, which is evident from the appearance of the orange colour of methyl orange dye on the material surface. The Figure 15 A shows the optical image of oil-water mixture before experiment and after experiment. For the efficient oil-water separation, the super-hydrophobic filter used for separation should only allow oil and repel water. The separation efficiency (K_s) was calculated according to the following Equation [31].

$$\text{Separation efficiency, } K_s = \frac{m_t}{m} \times 100$$

where m is the amount of water taken initially in the oil–water mixture and m_t is the amount of water collected after the separation process. Separation of different types of oil-water mixtures was allowed through this CF. Figure 15 B indicates that the separation efficiency of CF using different types of oils after 15 cycles of filtration possess a separation efficiency around 98 %. The WCA measured after separation process was $156^\circ \pm 0.98^\circ$ suggests that a reasonably good super-hydrophobicity exists even after 15 cycles. The coated fabric could be a promising material for large areas such as in self-cleaning, removal of various contaminants in aquatic environment etc.

5.6 Conclusions

Super-hydrophobic GPTMS/HMDS modified $\text{TiO}_2/\text{SiO}_2$ coated cotton fabric developed through dip coating method having WCA of $161.5^\circ \pm 1.02^\circ$. The material was characterized by using ATR and FESEM techniques. The fabricated CF can successfully separate oil-water mixtures. A separation efficiency of 98 % after 15 cycles of filtration process was achieved. The coated fabric could replace conventional toxic fluorine based super-hydrophobic coatings. In addition to this the CF exhibit very good mechanical and chemical durability. Under harsh environmental conditions such as acidic, salty, and alkaline, the CF exhibit superior durability and substantial stability against UV light. Also, the CF possesses better tensile strength and Young's modulus compared to UF indicating adherent nature of coating on fabric. Moreover, the results of abrasion test, and tear test using adhesion tape after 15 repetition tests suggesting the super-hydrophobicity of coated surface. Besides, washing durability test were conducted for the practical application of CF and after 15 cycles of washing the coated fabric found to be robust in nature. Furthermore, the CF could be very useful in large areas such as in self-cleaning, removal of various contaminants presents in aquatic environment etc.

You never fail until you stop trying.

Albert Einstein

References

- [1] H. Khojasteh, M. Salavati-Niasari, F.S. Sangsefidi, Photocatalytic evaluation of RGO/TiO₂NWs/Pd-Ag nanocomposite as an improved catalyst for efficient dye degradation, *Journal of Alloys and Compounds*, 746 (2018) 611-618.
- [2] C.-Y. Wang, X. Zhang, H.-B. Qiu, W.-K. Wang, G.-X. Huang, J. Jiang, H.-Q. Yu, Photocatalytic degradation of bisphenol A by oxygen-rich and highly visible-light responsive Bi₁₂O₁₇Cl₂ nanobelts, *Applied Catalysis B: Environmental*, 200 (2017) 659-665.
- [3] V. Repousi, A. Petala, Z. Frontistis, M. Antonopoulou, I. Konstantinou, D.I. Kondarides, D. Mantzavinos, Photocatalytic degradation of bisphenol A over Rh/TiO₂ suspensions in different water matrices, *Catalysis Today*, 284 (2017) 59-66.
- [4] R. Fagan, D.E. McCormack, D.D. Dionysiou, S.C. Pillai, A review of solar and visible light active TiO₂ photocatalysis for treating bacteria, cyanotoxins and contaminants of emerging concern, *Materials Science in Semiconductor Processing*, 42 (2016) 2-14.
- [5] J.-H. Kang, D. Aasi, Y. Katayama, Bisphenol A in the aquatic environment and its endocrine-disruptive effects on aquatic organisms, *Critical reviews in toxicology*, 37 (2007) 607-625.
- [6] B. Darsinou, Z. Frontistis, M. Antonopoulou, I. Konstantinou, D. Mantzavinos, Sono-activated persulfate oxidation of bisphenol A: kinetics, pathways and the controversial role of temperature, *Chemical Engineering Journal*, 280 (2015) 623-633.
- [7] W. Li, P.-x. Wu, Y. Zhu, Z.-j. Huang, Y.-h. Lu, Y.-w. Li, Z. Dang, N.-w. Zhu, Catalytic degradation of bisphenol A by CoMnAl mixed metal oxides catalyzed peroxymonosulfate: performance and mechanism, *Chemical Engineering Journal*, 279 (2015) 93-102.
- [8] C. Erler, J. Novak, Bisphenol A exposure: human risk and health policy, *Journal of pediatric nursing*, 25 (2010) 400-407.
- [9] Z. Fang, Y. Hu, W. Zhang, X. Ruan, Shell-free three-dimensional graphene-based monoliths for the aqueous adsorption of organic pollutants, *Chemical Engineering Journal*, 316 (2017) 24-32.

- [10] E.B. Simsek, Solvothermal synthesized boron doped TiO₂ catalysts: photocatalytic degradation of endocrine disrupting compounds and pharmaceuticals under visible light irradiation, *Applied Catalysis B: Environmental*, 200 (2017) 309-322.
- [11] C. Wang, H. Zhang, F. Li, L. Zhu, Degradation and mineralization of bisphenol A by mesoporous Bi₂WO₆ under simulated solar light irradiation, *Environmental science & technology*, 44 (2010) 6843-6848.
- [12] G. Zhan, D.D. Dionysiou, C. Zhao, Photocatalytic Degradation of Organic Contaminants in Water: Process Optimization and Degradation Pathways, *Photocatalysis: Applications*, DOI (2016) 1.
- [13] C.S. Turchi, D.F. Ollis, Photocatalytic degradation of organic water contaminants: mechanisms involving hydroxyl radical attack, *Journal of catalysis*, 122 (1990) 178-192.
- [14] D. Lawless, N. Serpone, D. Meisel, Role of hydroxyl radicals and trapped holes in photocatalysis. A pulse radiolysis study, *The Journal of Physical Chemistry*, 95 (1991) 5166-5170.
- [15] X. Pan, M.-Q. Yang, X. Fu, N. Zhang, Y.-J. Xu, Defective TiO₂ with oxygen vacancies: synthesis, properties and photocatalytic applications, *Nanoscale*, 5 (2013) 3601-3614.
- [16] Y. Wang, Q. Wang, X. Zhan, F. Wang, M. Safdar, J. He, Visible light driven type II heterostructures and their enhanced photocatalysis properties: a review, *Nanoscale*, 5 (2013) 8326-8339.
- [17] J. Ran, J. Zhang, J. Yu, M. Jaroniec, S.Z. Qiao, Earth-abundant cocatalysts for semiconductor-based photocatalytic water splitting, *Chemical Society Reviews*, 43 (2014) 7787-7812.
- [18] W. Hu, W. Zhou, K. Zhang, X. Zhang, L. Wang, B. Jiang, G. Tian, D. Zhao, H. Fu, Facile strategy for controllable synthesis of stable mesoporous black TiO₂ hollow spheres with efficient solar-driven photocatalytic hydrogen evolution, *Journal of Materials Chemistry A*, 4 (2016) 7495-7502.
- [19] W. Zhou, W. Li, J.-Q. Wang, Y. Qu, Y. Yang, Y. Xie, K. Zhang, L. Wang, H. Fu, D. Zhao, Ordered mesoporous black TiO₂ as highly efficient hydrogen evolution photocatalyst, *Journal of the American Chemical Society*, 136 (2014) 9280-9283.

- [20] W. Zhou, F. Sun, K. Pan, G. Tian, B. Jiang, Z. Ren, C. Tian, H. Fu, Well-ordered large-pore mesoporous anatase TiO₂ with remarkably high thermal stability and improved crystallinity: preparation, characterization, and photocatalytic performance, *Advanced Functional Materials*, 21 (2011) 1922-1930.
- [21] J. He, X. Zeng, S. Lan, I.M. Lo, Reusable magnetic Ag/Fe, N-TiO₂/Fe₃O₄@ SiO₂ composite for simultaneous photocatalytic disinfection of *E. coli* and degradation of bisphenol A in sewage under visible light, *Chemosphere*, 217 (2019) 869-878.
- [22] M. Alvaro, C. Aprile, M. Benitez, E. Carbonell, H. García, Photocatalytic activity of structured mesoporous TiO₂ materials, *The Journal of Physical Chemistry B*, 110 (2006) 6661-6665.
- [23] H. Shibata, T. Ohkubo, H. Kohno, P. Rangsunvigit, H. Sakai, M. Abe, Preparation and photocatalytic activity of titania particulate film with mesostructured silica as binder, *Journal of Photochemistry and Photobiology A: Chemistry*, 181 (2006) 357-362.
- [24] L. Zhang, Z. Xing, H. Zhang, Z. Li, X. Wu, X. Zhang, Y. Zhang, W. Zhou, High thermostable ordered mesoporous SiO₂-TiO₂ coated circulating-bed biofilm reactor for unpredictable photocatalytic and biocatalytic performance, *Applied Catalysis B: Environmental*, 180 (2016) 521-529.
- [25] C. Xie, Z. Xu, Q. Yang, B. Xue, Y. Du, J. Zhang, Enhanced photocatalytic activity of titania-silica mixed oxide prepared via basic hydrolyzation, *Materials Science and Engineering: B*, 112 (2004) 34-41.
- [26] C.-S. Kim, J.-W. Shin, S.-H. An, H.-D. Jang, T.-O. Kim, Photodegradation of volatile organic compounds using zirconium-doped TiO₂/SiO₂ visible light photocatalysts, *Chemical engineering journal*, 204 (2012) 40-47.
- [27] P. Cheng, M. Zheng, Y. Jin, Q. Huang, M. Gu, Preparation and characterization of silica-doped titania photocatalyst through sol-gel method, *Materials Letters*, 57 (2003) 2989-2994.
- [28] Y. Yang, F. Su, S. Zhang, W. Guo, X. Yuan, Y. Guo, Fabrication of metallic platinum doped ordered mesoporous titania-silica materials with excellent simulated sunlight and visible light photocatalytic

- activity, *Colloids and Surfaces A: Physicochemical and Engineering Aspects*, 415 (2012) 399-405.
- [29] J. Zhu, B. Liu, L. Li, Z. Zeng, W. Zhao, G. Wang, X. Guan, Simple and green fabrication of a superhydrophobic surface by one-step immersion for continuous oil/water separation, *The Journal of Physical Chemistry A*, 120 (2016) 5617-5623.
- [30] Y. Yu, H. Chen, Y. Liu, V.S. Craig, Z. Lai, Selective separation of oil and water with mesh membranes by capillarity, *Advances in colloid and interface science*, 235 (2016) 46-55.
- [31] J. Wang, Y. Chen, Oil-water separation capability of superhydrophobic fabrics fabricated via combining polydopamine adhesion with lotus-leaf-like structure, *Journal of Applied Polymer Science*, 132 (2015).
- [32] G. Wang, Z. Zeng, H. Wang, L. Zhang, X. Sun, Y. He, L. Li, X. Wu, T. Ren, Q. Xue, Low drag porous ship with superhydrophobic and superoleophilic surface for oil spills cleanup, *ACS applied materials & interfaces*, 7 (2015) 26184-26194.
- [33] B. Dubansky, A. Whitehead, J.T. Miller, C.D. Rice, F. Galvez, Multitissue molecular, genomic, and developmental effects of the Deepwater Horizon oil spill on resident Gulf killifish (*Fundulus grandis*), *Environmental Science & Technology*, 47 (2013) 5074-5082.
- [34] Z. Xue, Y. Cao, N. Liu, L. Feng, L. Jiang, Special wettable materials for oil/water separation, *Journal of Materials Chemistry A*, 2 (2014) 2445-2460.
- [35] T.F. Guerin, Heavy equipment maintenance wastes and environmental management in the mining industry, *Journal of environmental management*, 66 (2002) 185-199.
- [36] P.-C. Chen, Z.-K. Xu, Mineral-coated polymer membranes with superhydrophilicity and underwater superoleophobicity for effective oil/water separation, *Scientific reports*, 3 (2013) 2776.
- [37] L.K. Wang, Y.-T. Hung, N.K. Shamas, *Handbook of Environmental Engineering: Advanced Physicochemical Treatment Processes; Volume 4*, Humana Press 2006.

- [38] R.K. Gupta, G.J. Dunderdale, M.W. England, A. Hozumi, Oil/water separation techniques: a review of recent progresses and future directions, *Journal of Materials Chemistry A*, 5 (2017) 16025-16058.
- [39] Z. Wang, Y. Xu, Y. Liu, L. Shao, A novel mussel-inspired strategy toward superhydrophobic surfaces for self-driven crude oil spill cleanup, *Journal of Materials Chemistry A*, 3 (2015) 12171-12178.
- [40] J. Hong, W.K. Bae, H. Lee, S. Oh, K. Char, F. Caruso, J. Cho, Tunable Superhydrophobic and Optical Properties of Colloidal Films Coated with Block-Copolymer-Micelles/Micelle-Multilayers, *Advanced materials*, 19 (2007) 4364-4369.
- [41] S. Yang, S. Chen, Y. Tian, C. Feng, L. Chen, Facile transformation of a native polystyrene (PS) film into a stable superhydrophobic surface via sol-gel process, *Chemistry of Materials*, 20 (2008) 1233-1235.
- [42] X.X. Zhang, S. Cai, D. You, L.H. Yan, H.B. Lv, X.D. Yuan, B. Jiang, Template-free sol-gel preparation of superhydrophobic ORMOSIL films for double-wavelength broadband antireflective coatings, *Advanced Functional Materials*, 23 (2013) 4361-4365.
- [43] D. Angelova, I. Uzunov, S. Uzunova, A. Gigova, L. Minchev, Kinetics of oil and oil products adsorption by carbonized rice husks, *Chemical Engineering Journal*, 172 (2011) 306-311.
- [44] P.S. Brown, B. Bhushan, Bioinspired materials for water supply and management: water collection, water purification and separation of water from oil, *Philosophical Transactions of the Royal Society A: Mathematical, Physical and Engineering Sciences*, 374 (2016) 20160135.
- [45] Y. Cao, X. Zhang, L. Tao, K. Li, Z. Xue, L. Feng, Y. Wei, Mussel-inspired chemistry and michael addition reaction for efficient oil/water separation, *ACS applied materials & interfaces*, 5 (2013) 4438-4442.
- [46] Z. Chu, Y. Feng, S. Seeger, Oil/water separation with selective superantwetting/superwetting surface materials, *Angewandte Chemie International Edition*, 54 (2015) 2328-2338.

- [47] F. Liu, M. Ma, D. Zang, Z. Gao, C. Wang, Fabrication of superhydrophobic/superoleophilic cotton for application in the field of water/oil separation, *Carbohydrate polymers*, 103 (2014) 480-487.
- [48] Z. Xu, K. Miyazaki, T. Hori, Fabrication of polydopamine-coated superhydrophobic fabrics for oil/water separation and self-cleaning, *Applied Surface Science*, 370 (2016) 243-251.
- [49] H. Zhou, H. Wang, H. Niu, A. Gestos, T. Lin, Robust, self-healing superamphiphobic fabrics prepared by two-step coating of fluoro-containing polymer, fluoroalkyl silane, and modified silica nanoparticles, *Advanced Functional Materials*, 23 (2013) 1664-1670.
- [50] M.E. Yazdanshenas, M. Shateri-Khalilabad, One-step synthesis of superhydrophobic coating on cotton fabric by ultrasound irradiation, *Industrial & Engineering Chemistry Research*, 52 (2013) 12846-12854.
- [51] I. Das, G. De, Zirconia based superhydrophobic coatings on cotton fabrics exhibiting excellent durability for versatile use, *Scientific reports*, 5 (2015) 18503.
- [52] M.A. Shirgholami, M.S. Khalil-Abad, R. Khajavi, M.E. Yazdanshenas, Fabrication of superhydrophobic polymethylsilsesquioxane nanostructures on cotton textiles by a solution-immersion process, *Journal of colloid and interface science*, 359 (2011) 530-535.
- [53] K. Sasaki, M. Tenjimbayashi, K. Manabe, S. Shiratori, Asymmetric superhydrophobic/superhydrophilic cotton fabrics designed by spraying polymer and nanoparticles, *ACS applied materials & interfaces*, 8 (2015) 651-659.
- [54] X. Zhang, J. Zhang, Z. Ren, X. Li, X. Zhang, D. Zhu, T. Wang, T. Tian, B. Yang, Morphology and wettability control of silicon cone arrays using colloidal lithography, *Langmuir*, 25 (2009) 7375-7382.
- [55] S. Srinivasan, V.K. Praveen, R. Philip, A. Ajayaghosh, Bioinspired Superhydrophobic Coatings of Carbon Nanotubes and Linear π Systems Based on the "Bottom-up" Self-Assembly Approach, *Angewandte Chemie International Edition*, 47 (2008) 5750-5754.
- [56] L. Zhao, J. Yu, B. Cheng, Preparation and characterization of SiO₂/TiO₂ composite microspheres with microporous SiO₂

- core/mesoporous TiO₂ shell, *Journal of Solid State Chemistry*, 178 (2005) 1818-1824.
- [57] A. Hilonga, J.-K. Kim, P.B. Sarawade, H.T. Kim, Titania-silica composites with less aggregated particles, *Powder Technology*, 196 (2009) 286-291.
- [58] L. Pinho, M.J. Mosquera, Titania-silica nanocomposite photocatalysts with application in stone self-cleaning, *The Journal of Physical Chemistry C*, 115 (2011) 22851-22862.
- [59] C.M. Whang, C.S. Yeo, Y.H. Kim, Preparation and Characterization of Sol-Gel Derived SiO₂-TiO₂-PDMS Composite Films, *BULLETIN-KOREAN CHEMICAL SOCIETY*, 22 (2001) 1366-1370.
- [60] J. Kavil, A. Alshahrie, P. Periyat, CdS sensitized TiO₂ nano heterostructures as sunlight driven photocatalyst, *Nano-Structures & Nano-Objects*, 16 (2018) 24-30.
- [61] T. Lopez, P. Bosch, F. Tzompantzi, R. Gomez, J. Navarrete, E. Lopez-Salinas, M. Llanos, Effect of sulfation methods on TiO₂-SiO₂ sol-gel catalyst acidity, *Applied Catalysis A: General*, 197 (2000) 107-117.
- [62] F. Mazloom, M. Ghiyasiyan-Arani, R. Monsef, M. Salavati-Niasari, Photocatalytic degradation of diverse organic dyes by sol-gel synthesized Cd₂V₂O₇ nanostructures, *Journal of Materials Science: Materials in Electronics*, 29 (2018) 18120-18127.
- [63] R. Monsef, M. Ghiyasiyan-Arani, M. Salavati-Niasari, Application of ultrasound-aided method for the synthesis of NdVO₄ nano-photocatalyst and investigation of eliminate dye in contaminant water, *Ultrasonics sonochemistry*, 42 (2018) 201-211.
- [64] S. Gao, C. Guo, J. Lv, Q. Wang, Y. Zhang, S. Hou, J. Gao, J. Xu, A novel 3D hollow magnetic Fe₃O₄/BiOI heterojunction with enhanced photocatalytic performance for bisphenol A degradation, *Chemical Engineering Journal*, 307 (2017) 1055-1065.
- [65] D. Zhou, F. Wu, N. Deng, W. Xiang, Photooxidation of bisphenol A (BPA) in water in the presence of ferric and carboxylate salts, *Water Research*, 38 (2004) 4107-4116.

- [66] M. Deborde, S. Rabouan, P. Mazellier, J.-P. Duguet, B. Legube, Oxidation of bisphenol A by ozone in aqueous solution, *Water research*, 42 (2008) 4299-4308.
- [67] J. Liang, Y. Zhou, G. Jiang, R. Wang, X. Wang, R. Hu, X. Xi, Transformation of hydrophilic cotton fabrics into superhydrophobic surfaces for oil/water separation, *Journal of the Textile Institute*, 104 (2013) 305-311.
- [68] J. Huang, S. Li, M. Ge, L. Wang, T. Xing, G. Chen, X. Liu, S.S. Al-Deyab, K. Zhang, T. Chen, Robust superhydrophobic TiO₂@ fabrics for UV shielding, self-cleaning and oil–water separation, *Journal of Materials Chemistry A*, 3 (2015) 2825-2832.
- [69] U. Zulfiqar, S.Z. Hussain, M. Awais, M.M.J. Khan, I. Hussain, S.W. Husain, T. Subhani, In-situ synthesis of bi-modal hydrophobic silica nanoparticles for oil-water separation, *Colloids and Surfaces A: Physicochemical and Engineering Aspects*, 508 (2016) 301-308.
- [70] C. Cao, M. Ge, J. Huang, S. Li, S. Deng, S. Zhang, Z. Chen, K. Zhang, S.S. Al-Deyab, Y. Lai, Robust fluorine-free superhydrophobic PDMS–ormosil@ fabrics for highly effective self-cleaning and efficient oil–water separation, *Journal of Materials Chemistry A*, 4 (2016) 12179-12187.
- [71] D. Caschera, B. Cortese, A. Mezzi, M. Brucale, G.M. Ingo, G. Gigli, G. Padeletti, Ultra hydrophobic/superhydrophilic modified cotton textiles through functionalized diamond-like carbon coatings for self-cleaning applications, *Langmuir*, 29 (2013) 2775-2783.



HMDS–GPTMS Modified Titania Silica Nanocomposite: A New Material for Oil–Water Separation

P. K. Jaseela¹ · K. O. Shamsheera¹ · Abraham Joseph¹

Received: 4 September 2019 / Accepted: 26 November 2019
© Springer Science+Business Media, LLC, part of Springer Nature 2019

Abstract

A simple and feasible method is proposed for the fabrication of a super-hydrophobic coating on cotton fabric via sol–gel process. The wettability of the coating was investigated by water contact angle measurement (WCA). WCA of coated fabric reached up to $161.5 \pm 1.02^\circ$. The tensile strength and Young's modulus and mechanical properties of coated fabric is quite promising than uncoated fabric. Moreover, the coated fabric can effectively separate oil–water mixtures through an ordinary filtering process with a separation efficiency of 99%. After 15 cycles of separation the contact angle changes to $155.6 \pm 0.98^\circ$ only and material maintained its super-hydrophobic property. The durability of the coating was evaluated by exposing the specimen at harsh environments like acidic, alkaline, saline, and ultraviolet irradiation was conducted. The tear test was evaluated using the adhesive tape test, abrasion resistance test apart from washing stability and these results suggested that the coating was sufficiently stable. The coated fabric free of fluorine and chlorine can be effectively utilized in various fields.

Keywords Oil water separation · WCA · GPTMS · HMDS

1 Introduction

Mimicking the hierarchical micro/nanoscale morphologies of lotus leaves and butterfly wings that possess super-hydrophobic property (surfaces with a water contact angle greater than 150°) has led to the fabrication of numerous artificial super-hydrophobic surfaces. Various strategies have been proposed for imparting hierarchical surface to substrates, such as template methods, colloidal self-assembly, sol–gel processing, electro-spinning, layer-by-layer deposition, lithography and others [1–4]. The dip coating method is considered as superior method in comparison to others as it is inexpensive, simple, and offers an easy adjustment of chemical composition required for super-hydrophobic behaviour. Super-hydrophobic materials have a wide range of applications [5–9]. In this work we focussed on a serious environmental issue that cause serious threat to living system due to water contamination by oil which resulted from oil production, oil delivery, oil refining industries and petrochemical operations. Millions of tons of refined oil and

crude oil leak into the sea every year, which is responsible for pollution of natural aquatic environment and ecological damage [10–16]. Therefore, it is of great significance to explore a simple, economical and effective method for the separation and collection of oil from oil–water mixture [17]. Super hydrophobic cotton as filter material has been used recently [18]. Many findings have also been reported on the preparation of super-hydrophobic surfaces and its applications in oil–water separation [19–23]. Although these coatings on cotton fabrics offer high oil–water separation efficiency, the use of fluorinated and chlorinated compounds during its preparation limits its direct use. Halogenated compounds are more expensive, toxic, non-biodegradable and easily reactive with other materials and sometimes produces halo acids [24]. Therefore, it is necessary to obtain fluorine and chlorine free coated fabrics with super-hydrophobic and super-oleophilic properties.

In recent years widespread applications have been emerged for titania as well as silica-based hybrids [25–29]. Silica or titania are best choices to fabricate super-hydrophobic surfaces [4, 30, 31] due to their low toxicity, controllable structure and promising thermal stability, strength and durability under drast environmental conditions [32–34]. Some of the materials with poor hydrophobicity allow both water and oil to pass and hence non-effective for oil–water

✉ Abraham Joseph
drabrahamj@gmail.com

¹ Department of Chemistry, University of Calicut, Calicut University P O, Malappuram, Kerala, India



ORIGINAL ARTICLE

Mesoporous Titania-Silica nanocomposite as an effective material for the degradation of Bisphenol A under visible light



P.K. Jaseela, K.O. Shamsheera, Abraham Joseph*

Department of Chemistry, University of Calicut, Calicut University P O, Kerala, India

Received 24 March 2020; revised 14 May 2020; accepted 17 May 2020
Available online 22 May 2020

KEYWORDS

TiO₂-SiO₂;
Photocatalysis;
Bisphenol A;
TOC

Abstract A simple and very effective method is proposed for the removal of Bisphenol A (BPA) under visible light using mesoporous TiO₂-SiO₂ nanocomposite. The material was characterized using FTIR, XRD, DRS, XPS, FESEM, HRTEM, and BET techniques. The photo degradation efficiency of TiO₂-SiO₂ compared with bare TiO₂. The effect of calcination temperature on the photo-degradation of the materials is also studied. The radical intermediates formed during the degradation of BPA were followed with different radical scavengers. The solution after reaction is subjected to TOC (Total Organic Carbon content) and LCMS analysis to determine the mineralization rate and degradation products exist in the solution. Kinetic studies were revealed that the degradation process follow pseudo first order kinetics.

© 2020 Published by Elsevier B.V. on behalf of King Saud University. This is an open access article under the CC BY-NC-ND license (<http://creativecommons.org/licenses/by-nc-nd/4.0/>).

1. Introduction

The degradation of pollutants under visible light using a semiconductor material synthesised by an easy route have been a hot research subject at any point of time. Materials like TiO₂, CdSe, WO₃, Bi₂WO₆, Bi₂O₃, NiTiO₃, ZnO and carbon dots, C₃N₄, Boron nitride quantum dots etc. have already reported as active materials for the degradation of dyes other organic pollutants including microbial contaminants and

antibiotic pollutants, water splitting, hydrogen production solar cells etc. [1–5]. Among these, TiO₂ has a unique position in the field mainly due to its high photo-activity and stability, low cost, and its benign nature. The spectrum of activity of TiO₂ includes degradation of organic pollutants [6] treatment of endocrine disrupting compounds (EDCs) and emerging contaminants [7]. Bisphenol A (2, 2-bis (4-hydroxyphenyl) propane, BPA) is a representative xenoestrogens typically used in the manufacturing of numerous chemical products [8] and is suspected to several adverse effects including endocrine disruption [9]. Huge quantity of BPA directly discharged into water sources from different industrial sectors. In 2010, the United States Environmental Protection Agency (EPA) reported that over one million pounds of BPA were released into the environment annually, and the possible hazards to foetuses, infants and young children were identified by the United States Food and Drug Administration (FDA) [6]. This

* Corresponding author.

E-mail address: drabrahamj@gmail.com (A. Joseph).

Peer review under responsibility of King Saud University.



Production and hosting by Elsevier

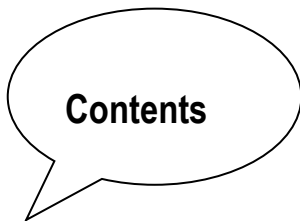
<https://doi.org/10.1016/j.jscs.2020.05.004>

1319-6103 © 2020 Published by Elsevier B.V. on behalf of King Saud University.

This is an open access article under the CC BY-NC-ND license (<http://creativecommons.org/licenses/by-nc-nd/4.0/>).

Chapter 6

SUMMARY AND SCOPE OF FUTURE WORK



6.1	Introduction
6.2	Summary
6.3	Scope of future work

Chapter 6 illustrates the relevance of the research work carried out and outlines future scope and aims to enhance the potential of Titania hybrids for a number of applications...

6.1 Introduction

This research work has been done on titanium-based hybrids, in particular in the area of anti-corrosion and wastewater treatment applications. We have successfully created titania and their hybrids as an efficient adsorbent, photocatalyst, superhydrophobic coating on cotton fabric to eliminate contaminants from water resources, and anticorrosive protective coating.

6.2. Summary

1. First objective of the study was to fabricate environmentally benign coatings to replace environmentally hazardous chromate conversion coatings on mild steel for corrosion protection. In this regard titania, titania–poly vinyl alcohol (PVA) hybrid, thiourea doped titania–poly vinyl alcohol (PVA) hybrid nanocomposite anticorrosion coating on mild steel has been successfully developed via sol–gel dip-coating method. The adopted method was a simple, facile and eco-friendly. The characterization of the coatings was done using different analytical techniques. The corrosion protection ability of these sol–gel coatings were evaluated by weight loss, impedance spectroscopic studies (EIS), and polarization measurement (PDS) in HCl and NaCl media. Among these coatings thiourea doped titania–poly vinyl alcohol (PVA) hybrid was found to be the best choice. Moreover, the modified coating on metal offers attractive protection efficiency on extending the exposure period in HCl and NaCl media for several days, which is much

better than conventional sol–gel coating which losses efficiency day by day. The protective layer consists of a compact structure of hybrid PVA–titania and electron rich thiourea molecules on the surface of the metal offering significant physical barrier against the attack of corrosive species from HCl and NaCl.

2. The second objective was to develop some materials for water pollution remediation applications. For this we have developed the synthesis of mesoporous inorganic – organic hybrid TiO₂ - PVA. It has remarkable adsorption selectivity for methylene blue (MB), from the mixture of methylene blue and methyl orange (MO) in aqueous environment. The hybrid can be utilized as an adsorbent to remove Acridine Orange (AO) and Methylene blue (MB) dye from aqueous environment. The material was selective for cationic dyes. MB adsorption on nanocomposite was investigated under various experimental conditions, adsorption kinetics and isotherms were studied. The recyclability of the sorbent for over 10 cycles could be achieved in acid solution with good activity.
3. The third objective was to study the photocatalytic properties of the titania composite for the degradation of endocrine disrupting contaminant BPA present in water under visible light. Various radical scavengers were introduced to understand the role of reactive species and found that the major contribution was from •OH radicals. To confirm this fluorescence technique was done and the results support the

chemical examination and based on the results a comprehensive route is proposed for the degradation of BPA.

4. The fourth objective of the study was to develop a super-hydrophobic surface using these hybrid materials by coating on cotton fabric via sol-gel process for the removal of oils from water. To attain this Titania-Silica hybrid was modified with GPTMS and HMDS in order to make fluorine and chlorine free coated fabric. The mechanical and chemical durability of the coating was evaluated and coating was robust in all conditions.

6.3. Scope of future work

This work can be further extended for diverse practical utilizations like.

1. Anticorrosion coatings have been produced without the use of adhesive primers such as epoxy resins. It is possible to develop coatings with such BPA free primers, which could certainly improve the durability of the coatings. In addition, we can implement a hydrophobic polymer like PDMS in to titania matrix and that will definitely enhance the anticorrosion property. We have developed coatings for mild steel substrates this can be utilized for other metals like Al.
2. In order to make the adsorbent more efficient and separable, the hybrid can be made into magnetic with ferric oxide. Titania hybrid can be utilized properly and extended for the removal of other pollutants especially for radioactive elements.

3. The photocatalytic activity of titania hybrids can be extended to the degradation other relevant pollutants and the material can be deposited on different matrix for further applications such as self-cleaning.
4. Property of coatings on cotton fabric from superhydrophobic to superoleophobic can be tuned to suit the needs. This will allow oils to be collected from bulk waste water resources. It was concluded that titania hybrids have enormous potential in different fields.

Scientific discovery and scientific knowledge have been achieved only by those who have gone in pursuit of it without any practical purpose whatsoever in view.

Max Planck

LIST OF PUBLICATIONS

	<p><i>Development of Flower Like Hierarchical Thiourea Loaded Titania–Poly Vinyl Alcohol Nano Composite Coatings for the Corrosion Protection of Mild Steel in Hydrochloric Acid</i>, P.K. Jaseela, A. Joseph, J. Inorg. Organomet. Polym. Mater. 28 (4) (2018) 1-15(Springer)</p>
	<p><i>Selective adsorption of methylene blue (MB) dye from aqueous mixture of MB and methyl orange (MO) using mesoporous titania (TiO₂)–poly vinyl alcohol (PVA) nanocomposite</i>, P K. Jaseela, J. Garvasis, A. Joseph, J. Mol. Liq., 286 (2019) 110908 (Elsevier)</p>
	<p><i>HMDS-GPTMS modified Titania Silica nanocomposite-A new material for Oil-Water separation</i>, P.K. Jaseela, A. Joseph, J. Inorg. Organomet. Polym. Mater. (2019) 1-8(Springer)</p>
	<p><i>Mesoporous Titania-Silica nanocomposite as an effective material for the degradation of Bisphenol A under visible light</i>, P.K. Jaseela, K.O. Shamsheera, J. Saudi Chem. Soc. (2020)(Elsevier)</p>

 <p>Arabian Journal of Chemistry</p>	<p><i>Excellent protection of mild steel in sodium chloride solution for a substantial period of time using a hybrid nanocoating of Poly Vinyl Alcohol and Titania, P K Jaseela, Linda Williams, K O Shamsheera and Abraham Joseph, Arab.J.Chem.,(Elsevier)</i></p>
 <p>MATERIALS CHEMISTRY AND PHYSICS</p>	<p><i>Efficient removal of Congo red from aqueous solutions using phytogenic aluminumsulfate nano coagulant. J. Garvasis, A.R. Prasad, K.O. Shamsheera, P.K. Jaseela, A. Joseph, J.Mate. Chem.Phy., (2020) 123040(Elsevier)</i></p>
 <p>chemicaldata COLLECTIONS</p>	<p><i>Development of self-assembled monolayer of stearic acid grafted chitosan on mild steel and inhibition of corrosion in hydrochloric acid, K.O. Shamsheera, A.R.Prasad, P.K. Jaseela, A. Joseph, Chemical Data Collections, (2020) 100402(Elsevier)</i></p>

PRESENTATIONS

1. Presentation on paper entitled “Poly vinyl alcohol modified titania Sol-Gel coatings- a novel inorganic – organic hybrid for the protection of mild steel in acid environment” in the TEQIP II sponsored International Conference on Advances in Biological, Chemical and Physical Sciences (ABCPS’2017) held at Bharathidasan Institute of Technology (BIT) Campus, Anna University, Tiruchirappalli during March 13th – 15th , 2017[ISBN No:978-93-80622-24-8]
2. Presentation on “Development of Thiourea Loaded Titania (TiO₂) - Poly Vinyl Alcohol (PVA) Nanocomposite as Protective Coating for Mild Steel in NaCl Solution”in the MESMAC international conference organised by MES Mampad college, Mampad, Malappuram, Kerala, in association with Kerala State Higher Educational Council on 15, 16 & 17 January 2019.
3. Presentation on “Titania –Silica Hybrid Photocatalyst For The Degradation Of Methylene Blue Dye Under Visible Light” in National Conference on Advances in Green Chemistry and its applicationsorganised by Sri Ramakrishna College of Arts and Science, Coimbatore, on 30th January 2020.